Applications of InP-on-Silicon Microdisks in All-Optical Signal Processing

Toepassingen in optische signaalverwerking van microschijven in InP op silicium

Rajesh Kumar

Promotor: prof. dr. ir. G. Morthier
Proefschrift ingediend tot het behalen van de graad van
Doctor in de Ingenieurswetenschappen: Fotonica

Vakgroep Informatietechnologie
Voorzitter: prof. dr. ir. D. De Zutter
Faculteit Ingenieurswetenschappen en Architectuur
Academiejaar 2011 - 2012

UNIVERSITEIT
GENT

ISBN 978-90-8578-533-0
NUR 959
Wettelijk depot: D/2012/10.500/59

Promotor:

Prof. Dr. Ir. Geert Morthier

Examencommissie:

Prof. Dr. Ir. Daniël De Zutter (voorzitter)	Universiteit Gent, INTEC
Prof. Dr. Ir. Geert Morthier (promotor)	Universiteit Gent, INTEC
Prof. Dr. Ir. Oded Raz	Technische Universiteit Eindhoven
Dr. Ir. Guy Van der Sande	Vrije Universiteit Brussel
Prof. Dr. Ir. Patrick De Visschere	Universiteit Gent, ELIS
Prof. Dr. Ir. Gunther Roelkens	Universiteit Gent, INTEC
Prof. Dr. Ir. Dries Van Thourhout(secretaris)	Universiteit Gent, INTEC

Universiteit Gent
Faculteit Ingenieurswetenschappen en Architectuur

Vakgroep Informatietechnologie
Sint-Pietersnieuwstraat 41, B-9000 Gent, België

Tel.: +32-9-264.99.59
Fax.: +32-9-331.35.93

Dit werk kwam tot stand in het kader
van het EU FP7 Project HISTORIC.

Dankwoord

It is not easy to cover all the persons who have directly or indirectly helped me to accomplish my PhD work. However, I am making an attempt to thank at least those with whome I had strong association while carrying out my PhD research work. First and foremost, my highest regards to Geert. I can not imagine that this thesis work would have been accomplished without his active guidance and support. Geert has not been merely a promotor but a real GURU. I learnt a lot from him and I will always be indebted to him. He paid full attention for the research work and guided me even when being abroad. Not to mention, he was always available to discuss the progress and gave directions to proceed further well in time. Gunther actively helped me during the course of thesis work. He always provided critical feedback on the results obtained. He put very sincere efforts so that everything goes smooth when I worked in TU Eindhoven. He co-ordinated exceptionally well whenever I visited COBRA clean room of TU Eindhoven. Thanks a lot Gunter!. Dries has worked a lot behind the scenes. From the beginning of my PhD, he had been providing valuable inputs. He made available the chips for the exciting experiments I did in later half of my PhD. Many thanks to you Dries!. On my very first day in the photonics research group, Roel said to me that the doors of his office will always be open to me. And indeed it happened. I discussed many things with him. My sincere thanks to Roel. Any SOI design work can not be complete (at least when you begin your PhD in the group here) unless helped by Wim and Peter Dumon. My thanks to both of them for their help. Wim also deserves very special thanks for the intellectual humour embedded in his e-mails. Technical staff in UGent clean room always played important role, particularly Liesbet and Steven. I highly appreciate their graciousness.

I want to extend my sincere thanks to jury members of my PhD for their important feedback. I wish to thank all the people involved in HISTORIC project from different groups and different countries. Meint Smit and his team deserves special thanks for help and co-operation extended to me during the COBRA clean-room visits. I am also thankful to Harm for the discussions when I did

joint experiments with Oded in TU Eindhoven. Oded has been an excellent collaborator and I enjoyed doing joint experiments with him. My sincere thanks to Oded.

"There is no free lunch"but I always had free dinners :-) while visiting TU Eindhoven. I am indebted to Abhinav for that. Other than free indian dinners, he helped me a lot with practical arrangements. He and his many good friends (difficult to list them all) made me feel like being in Ghent (or Delhi).

My ex-colleague Liu deserves special mention and special thanks. Working with him was absolutely fantastic. Thijs and Pauline have been excellent colleagues and friends....with Thijs I discussed several things while he worked on WADIMOS project. With Pauline, it was not only the research work which I enjoyed but also she helped in many ways (particularly when things were in french.). Tour of Paris after a project meeting with some friends under her lead role :-), I recall just as one such an example. Jens (from IBM Zurich) joins the league for training me in skiing. Thanks Jens!!

A PhD life is more than just doing research. In Ghent, all those opportunities exist. Drinks after the group meetings, get togethers of photonics days, going to bars and pubs in Ghent, city festival of Ghent...etc..... etc....., all made me always feel awesome. Social life becomes even more important when you are abroad. In a multicultural group, I never missed that. Indian gang of the group-Sukumar, Samir, Aditya, Adil, Shibnath...and so on...all have been a source of cheerfulness in the weekdays as well as in the week-ends. Stevan, Shahram, Gunay deserve special mention for their help on many occasions. I enjoyed discussions with newly (not so new now..)joined group members (Andrea, Zhechao, Ananth and many more...). I acknowledge Honghui and Yannick for many useful discussions. For the party people (Alf, Sa, As, Os, Ka, Kr, Alb, Cr....) I will always be thankful. The great officemates : Thijs, Eva, Diedrik, Peter DH, Thomas, Sukumar, Honghui, thanks to all of you for the lively environment you provided all these years.

Finally my deep gratitude to my parents for their faith in me, and teachers who encouraged and inspired me to excel in my life. Jai Ho!!

Gent, September 2012
Rajesh Kumar

Table of Contents

List of Figures

List of Acronyms

A

AOFF	All-optical Flip-flop
ASE	Amplified Spontaneous Emission
AWG	Arrayed Waveguide Grating

B

BCB	Benzocyclobutene
BER	Bit error rate
BERT	Bit error rate tester
BOX	Buried OXide
BPSK	Binary Phase Shift Keying

C

CMOS	Complementary Metal Oxide Semiconductor
CG	Common Ground
CW light	Continuous Wave light
CW mode	Clockwise mode
CCW mode	Counterclockwise
CMP	Chemical Mechanical Polishing

D

DFF	Data Flip-flop
DPSK	Differential Phase Shift Keying
DQPSK	Differential Quadrature Phase Shift Keying
DUV	Deep Ultra Violet
DVS-BCB	Divinylsiloxane-Benzocyclobutene

E

EDFA	Erbium Doped Fiber Amplifier

F

FIB	Focused Ion Beam
FSR	Free Spectral Range
FWHM	Full Width at Half Maximum
FWM	Four Wave Mixing

G

Gbps	Giga bits per second
GSG	Ground Signal Ground

H

HSPD	High Speed Photodiode

I

IM	Intensity Modulation
I/O	Input/Output
IC	Integrated Circuit

L

LNMOD	Lithium Niobate Modulator

M

MZI	Mach-Zehnder Interferometer

N

NOLM	Nonlinear Optical Loop Mirror
NRZ	Non-return-to-zero

O

OBPF	Optical Band Pass filter
OEO	Optical-Electrical-Optical
ONoC	Optical Network-on-Chip
OOK	On Off Key
ORAM	Optical Random Access Memory
OS	Optical Switch

P

PIC	Photonic Integrated Circuit
PRBS	Pseudo Random Bit Sequences

Q

QAM	Quadrature Amplitude Modulation
Q factor	Quality factor
QPSK	Quadrature Phase Shift Keying

R

RAM	Random Access Memory
RF	Radio Frequency
RZ	Return-to-zero

S

SEM	Scanning Electron Microscope
SOA	Semiconductor Optical Amplifier
SOI	Silicon-On-Insulator
SRFF	Set-reset Flip-flop

T

TDM	Time Domain Multiplexing
TE	Transverse Electric
TIA	Transimpedance Amplifier
TL	Tunable Laser

TPA	Two Photon Absorption

V

VOA	Variable Optical Attenuator

W

WDM	Wavelength Division Multiplexing

X

XGM	Cross Gain Modulation
XPM	Cross Phase Modulation

Nederlandse samenvatting –Summary in Dutch–

In de huidige tijd is het moeilijk om zich het leven zonder communicatie voor te stellen. In de voorbije decennia is de afhankelijkheid van optische communicatie steeds maar toegenomen. Optische communicatie heeft ingang gevonden (en is zelfs noodzakelijk) bij zowel korte- als lange-afstandscommunicatie. Ook on-chip communicatie en computing toepassingen steunen meer en meer op het gebruik van optica en fotonica.

Groeiende behoeftes om grote hoeveelheden data te transporteren, een steeds diepere penetratie van multimedia in ons dagelijks leven, de behoefte aan snelle processoren voor computers en een snel expanderende e-commercie sector hebben tot een ongeziene vraag geleid naar een nieuwe generatie van snellere en kleinere (on-chip) componenten met laag vermogenverbruik. Omwille van deze vraag is een breder gamma van nieuwe optische oplossingen vereist. Verschillende optische en fotonische platformen hebben als basis gediend om de nieuwe componenten te ontwikkelen. Deze platformen omvatten o.a. InP, silicium, silica, polymeer of een combinatie van deze materialen. Onder al deze platformen wordt het siliciumplatform beschouwd als het meest belovende. De voornaamste reden is dat het siliciumplatform toelaat om de optische componenten op goedkope manier te fabriceren gebruik makend van de standaard halfgeleiderfabricatietechnieken (CMOS) en om deze componenten te integreren met micro-electronische chips. Silicium fotonische chips kunnen zorgen voor een goedkope en hoogperformante implementatie van optische modulatie en signaalverwerking. Maar het genereren van een optisch signaal zelf, gebruik makend van een kleine, elektrisch gepompte silicium chip, is momenteel praktisch onmogelijk. Deze fundamentele beperking is te wijten aan het indirecte bandendiagram van silicium. Aan de andere kant is het InP platform wel geschikt voor het genereren, transporteren, verwerken en detecteren van optische signalen, maar het is een duur platform. Een veelbelovende aanpak voor het maken van multifunctionele fotonische chips is evenwel om silicium te gebruiken voor de routeringspaden en het te combineren met InP voor de andere optische functionaliteiten en om de CMOS fabricatieprocessen

ook voor InP te gebruiken. Deze combinatie laat toe om een brede waaier aan mogelijke optische functionaliteiten te implementeren en heeft het voordeel dat de fabricatie relatief goedkoop is. Dit is dan ook de belangrijkste motivatie geweest voor het uitvoeren van het werk beschreven in dit doctoraat. De optische functionaliteiten worden gerealiseerd in III-V materiaal terwijl de SOI golfgeleiders dienen als transportmedium voor het licht. De III-V componenten hebben de vorm van microschijven omwillen van hun potentieel laag vermogenverbruik en hun potentieel kleine voetafdruk. In het onderzoekswerk hier beschreven is de uitbuiting van twee belangrijke fenomenen in microschijven - laserwerking en het bestaan van resonanties in de transmissiekarakteristieken - essentieel voor de gerealiseerde optische functionaliteiten. In dit hoofdstuk wordt een korte samenvatting van de bekomen resultaten gegeven.

Optische flip-flops: De optische flip-flops die onderzocht werden zijn gebaseerd op op microschijflasers in CW werking. In theorie kan men verschillende werkingsregimes onderscheiden bij deze lasers: bidirectionele werking, alternerende oscillaties en unidirectionele (bistabiele) werking. In de praktijk wordt de bistabiliteit niet gemakkelijk waargenomen omdat er koppeling is tussen de mode in wijzerzin en deze in tegenwijzerzin. Deze koppeling vindt haar oorsprong voornamelijk in de verstrooiing tgv. de oppervlakteruwheid van de zijwanden van de microschijf. Door het gebruik van een geöptimiseerd recept voor het etsen van microschijven met gladde zijwanden werd evenwel bistabiliteit bekomen in microschijflasers met een diameter van slechts 7.5μm. De flip-flop werking werd bekomen door het schakelen tussen de wijzerzin- en tegenwijzerzinmode, bij een stroom van 3.5 mA voor de microschijflaser, waarbij deze laatste in bistabiel regime werkte. Het schakelen werd geïnduceerd door de injectie van korte optische pulsen in de laser, pulsen met een golflengte die nagenoeg gelijk was aan de golflengte van de laserende mode. De flip-flop werkte in CW regime met een elektrische vermogenconsumptie van slechts een paar mW en liet schakelen toe in 60 ps met behulp van schakelpulsen met een energie van 1.8 fJ. Dit is de enige totnogtoe gerapporteerde elektrisch-gepompte en CW-opererende optische flip-flop gerealiseerd in III-V-op-silicium.

Optische poorten: Optische poortwerking vormt een tweede fundamentele functionaliteit die met behulp van III-V-op-Si microschijven kan geïmplementeerd worden. Voor deze toepassing dienen de schijven ook niet noodzakelijk van stroom voorzien te worden. De resonanties in de transmissie van de microschijfresonatoren kunnen gemanipuleerd worden in een zgn. pomp-probe configuratie. De manipulatie van de transmissieresonanties vindt trouwens ook toepassing in bv. golflengteconversie, tijdsdomeindemultiplexering en formatconversie van optische data.

Werking als optische poort werd gerealiseerd in microschijfresonatoren met een probebundel afgestemd op één van de resonanties en een pompbundel afgestemd op een andere resonantie. De transmissiekarakteristiek van de microschijf werd veranderd doordat de pompbundel, met hoog vermogen, via absorptie vrije ladingdragers creëert in de microschijf, hetgeen leidt tot een verschijving van de transmissienullen naar kortere golflengtes. Door gebruik te maken van een korte-pulstrein als pomp wordt afwisselend een hoog of laag uitgangsvermogen bij de probegolflengte bekomen tgv. een periodische verschuiving van de resonantie rond de probegolflengte. Wanneer de probegolflengte iets korter is dan de golflengte waarbij een transmissienul optreedt, zal in afwezigheid van een pomppuls het uitgangsvermogen hoog zijn en de poort dus open, terwijl in aanwezigheid van een pomppuls het uitgangsvermogen laag zal zijn en de poort dus gesloten. In een eerste reeks experimenten werd poortwerking bij 10GHz gerealiseerd in een microschijf van 10 m diameter, en mits het aanleggen van een negatieve spanning van 1 Volt. Het gemiddeld vermogen van pomp- en probebundel in de SOI golfgeleider was 4 mW en 170 μ W respectievelijk. De stijg- en daaltijd voor de poortuitgang waren 85 en 41.5 ps respectievelijk. In een tweede serie experimenten, ditmaal met een component die volledig in een 200 mm CMOS pilootlijn werd gefabriceerd, werd de performantie nog verbeterd. De poortwerking werd gerealiseerd bij 10GHz met een microschijf met diameter 7.5 μm en ditmaal zonder toepassing van enige elektrische spanning of stroom. Het gemiddeld vermogen van pomp en probebundel in de SOI golfgeleider was 1.5 mW en 375 μW respectievelijk en stijg- en daaltijd waren 18.6 en 26.4ps respectievelijk. Een dergelijke snelle werking impliceert dat er potentieel is om deze componenten te laten werken voorbij 20 GHz.

Optische golflengteconversie: 'Bias'-loze optische golflengteconversie kan gerealiseerd worden in een pomp-probe configuratie door de pulstrein voor de pomp te vervangen door optische data. De informatie omvat in de data bij één resonantiegolflengte kan dan worden gecopieerd naar de probebundel bij een andere resonantiegolflengte. Het gebruik van kleinere microschijven met een grotere 'vrij spectraal bereik' ('free spectral range') kan zelfs de golflengteconversie toelaten van de ene telecomband naar de andere, bv. van de C- naar de L-band. Optische golflengteconversie werd gedemonstreerd van 1550.1nm naar 1580.9 nm voor 10 Gbit/s PRBS NRZ data. Foutvrije werking met een vermogenspenalty van ongeveer 3.5 dB werd bekomen.

Optische tijdsdomeindemultiplexering: Deze toepassing is gebaseerd op het feit dat optische data al of niet bij de resonantiegolflengte liggen afhankelijk van het vermogen van de optische klok. In essentie is de optische klok de pomp

en vormen de optische data de probebundel. Indien de optische data naar de microschijf gestuurd worden, dan zal aan de uitgang het vermogen hoog of laag zijn wanneer de klok (bij een resonantiegolflengte) een hoog dan wel laag vermogen heeft. Op basis van dit principe werd optische demultiplexering van 10 Gbit/s NRZ data gedemonstreerd, dit zowel voor een 5 GHz als een 2.5 GHz klok. Het is verder ook vermeldenswaardig dat ook deze experimenten gedaan werden zonder toepassing van elektrische bias, net zoals bij de optische poorten en de golflengteconversie.

Optische data formatconversie: De optische functionaliteiten die in de vorige paragrafen besproken werden kunnen nuttig zijn voor zowel on-chip als off-chip communicatie. Optische data formatconversie van NRZ naar RZ daarentegen is waarschijnlijk alleen interessant voor lange-afstands-communicatie en dus off-chip communicatie.
Het principe waarop de format conversie gebaseerd is, is gelijkaaardig aan dat van de optische tijdsdomeinmultiplexering. Alleen is bij formatconversie de pulsduur van de optische klokpulsen korter dan de duur van een bit. De optische data blijven gekoppeld in de microschijf zolang het vermogen van de optische klok laag is. Wanneer het vermogen van de klok hoog is worden de data niet meer in de schijf gekoppeld voor de duur van de klok. Op die manier is het vermogen aan de uitgang van de busgolfgeleider enkel hoog wanneer zowel de data als de klok een hoog vermogen hebben. Wegens het verschil in tijdsduur tussen de klok en de data bit is de tijdsduur van de databit aan de uitgang korter dan de initiele tijdsduur. Dit is een soort pulsinkorting van de databit. Dit fenomeen resulteert in conversie van NRZ naar RZ. Gebruikmakend van dit principe werd biasvrije en foutvrije formatconversie (van NRZ naar RZ) bekomen van 10 Gbit/s data met een vermogenpenalty van ongeveer ~3.6 dB.

English summary

In the present era, its difficult to imagine life without communication. There has been increased reliance on optical communication in the past few decades. Optical communication has made its presence (and even has become necessary) for short distance as well as long distance communication. On-chip communication and computing applications are relying more and more on the use of optics and photonics.

Growing needs to transport large amount of data, penetration of multimedia into our daily lives, need of fast processors for computers and a rapidly expanding e-commerce sector has triggered an unprecedented demand for the new generation of faster, smaller (on-chip) and low power components and devices. Due to these demands, a wide range of new optical solutions are required. Several optics and photonics based platforms have been used to investigate the new devices and components. These platforms include, but are not limited to, InP, silicon, silica, polymer, or a combination of these platforms. But out of these, silicon has been considered the most promising platform so far. The main reason for this is the fact that the silicon platform allows optical devices to be made cheaply using standard semiconductor fabrication (CMOS) techniques and integrated with microelectronic chips. The silicon photonic chips can provide the cheap and high performance solutions for modulation and processing of optical signals. But the generation of an optical signal using a small silicon chip in an efficient way is still far from reality. This fundamental limitation is due to the indirect band gap of silicon. On the other hand, the InP based photonics platform is capable of signal generation, transportation, processing and detection but is very costly. Using InP for the optical functionalities while using silicon for the routing paths, and adopting the CMOS fabrication processes for InP is a promising way ahead for having fully- and multi-function photonic chips. This combination will provide the advantage of a range of optical functionalities while still having cheaper fabrication. Such an advantage has been a key motivation for carrying out the research work presented here. The optical functionalities are realized in III-V material while the SOI waveguides served as the light transportation medium. The III-V devices are in the form of microdisks due to their potential for low foot-prints and low power con-

sumption. In the research work presented here, the exploitation of two main phenomena in microdisks - lasing and transmission resonance characteristics - has been at the heart of the optical functionalities realized. In this chapter, a brief summary of the obtained results is presented.

All-optical flip-flops: The all-optical flip-flops (AOFFs) investigated here are based on a continuous wave microdisk laser. In theory; different operating regimes namely bidirectional, alternate oscillations and unidirectional (bistable) are the typical characteristics of microring/disk lasers. In practice it is not easy to obtain the bistability in microdisk/ring lasers due to the mode coupling between clockwise and counterclockwise mode. The coupling between clockwise and counterclockwise modes arises mainly due to the backscattering from rough sidewall of a microdisk. An optimized recipe was used to fabricate the microdisks with smooth side walls leading to obtain the bistability in a microdisk laser of only 7.5 μm diameter.

The flip-flop operation was obtained by switching the mode from clockwise to counterclockwise and vice-versa when the microdisk laser was biased in bistable regime at 3.5 mA of injection current. The switching between clockwise and counterclockwise mode was triggered by injection of external optical pulses into the microdisk laser. The triggering pulses were closely matched in wavelength to the lasing longitudinal mode. The AOFF worked in continuous-wave regime with an electrical power consumption of only a few mW and allowed switching in 60 ps with pulses of energy 1.8 fJ. This is the only electrically-pumped and CW laser based AOFF built on III-V-on-silicon platform.

All-optical gates: All-optical gating phenomenon is another dimension for obtaining a range of functionalities in III-V-on-silicon microdisks. For gating phenomenon, the microdisks do not need to be biased necessarily . The transmission resonance characteristics of the microdisk resonators can be manipulated in real time in a pump-probe configuration. The manipulation of transmission resonances can provide not only the gating functions but also functionalities such as wavelength conversion, time domain demultiplexing and all-optical format conversion of optical data.

All-optical gating operation was achieved in microdisk resonators with the probe beam tuned at one of the resonances and the pump at another. The transmission characteristic of the microdisk was altered by having the pump intensity higher than that of the probe beam. When pump light was injected into the microdisk at another resonance of the microdisk, free carriers were generated which caused a blue shift in the transmission dip. Using a pulse train as a pump resulted in high or low output of the probe beam due to a periodic shifting of the resonance around the probe wavelength. When the probe wave-

length was slightly blue tuned off the transmission dip, then in the absence of the pump pulse, the output was high and the gate was in the open state while in the presence of the pump pulse the output was low and the gate was in the closed state. In the first series of experiments, the gating at 10 GHz was realized in a microdisk of 10 μm diameter with an application of a reverse bias of one volt. The average power of pump and probe in the SOI waveguide was 4 mW and 170 μW respectively. The rise time and fall time for the gate output was 8.5 ps and 41.5 ps respectively. In the second series of experiments for which the devices used were completely fabricated in a 200 mm CMOS pilot line, the performance of the gating was improved. The gating phenomenon was realized at 10 GHz in a 7.5 μm diameter microdisk without application of any electrical bias. The average pump and probe power in the SOI waveguide was 1.5 mW and 375 μW respectively. The rise and fall time of the gate output were recorded to be 18.6 ps and 26.4 ps respectively. Such a fast response implies the potential of these devices for bias-free operation beyond 20 GHz.

All-optical bias-free wavelength conversion: All-optical and bias-free wavelength conversion can be realized in a pump-probe configuration by replacing the pump pulse train with optical data. The information contained in the data at one resonance wavelength can be copied to another wavelength provided that the target wavelength is at another transmission resonance of the microdisk resonator. Use of smaller microdisks which have larger free spectral range can facilitate the wavelength conversion from one telecom band to another, e.g. from C to L band of telecom. All-optical wavelength conversion from 1550.1 nm to 1580.9 nm was done for 10 Gbits/s PRBS NRZ data. An error-free operation was obtained with a power penalty of $\sim$ 3.5 dB.

All-optical time domain demultiplexing: All-optical time domain demultiplexing is based on the phenomenon of optical data becoming on- or off-resonance as a function of the power level of the optical clock. In essence, the optical data is a probe signal and the optical clock is a pump signal. If the optical data is coupled to the microdisk, then the output of the microdisk will be high/low when the on-resonance clock signal has high/low level respectively. Based on this principle, proof-of-concept demonstration of all-optical demultiplexing of 10 Gbits/s NRZ data was done. Two sets of optical clock frequency, one at 5 GHz and another at 2.5 GHz were used. It is worth mentioning here that these experiments were also done without using any electrical bias like for the all-optical gating and wavelength conversion.

All-optical data format conversion: The optical functionalities presented in the previous paragraphs can be useful for both on- and off-chip communica-

tion. The all-optical data format conversion from NRZ-to-RZ is most likely to find applications only in long distance communication and hence has off-chip communication applications.

The principle of all-optical format conversion from NRZ-OOK to RZ-OOK is similar to that used for all-optical time domain demultiplexing. But in case of format conversion, the temporal pulse width of the optical clock is shorter than the temporal duration of a single bit. The optical data remains coupled into the microdisk when the power level of the optical clock is low. When the power level of the optical clock is high, the optical data becomes off-resonance for the duration of the clock pulse. In this way, the output from the microdisk becomes high only when both optical data as well as the optical clock are high. Due to the difference in the temporal pulse width of the clock and the data bit; at the output, the temporal width of the data bit becomes shorter than its initial temporal width. This is effectively the pulse carving of the data bit in the time domain. This phenomenon results in format conversion from NRZ to RZ. Using this principle, all-optical bias-free and error-free (BER $\sim 10^{-12}$) format conversion of 10Gbits/s data from NRZ to RZ was obtained with a power penalty of $\sim$ 3.6 dB.

1 Introduction

In the 20th century the optical fiber communication systems brought a revolution in the information transportation from one part of the world to another at an unprecedented speed. These optical fiber based communication systems are named as long haul transmission systems. At the heart of this revolution are three important inventions. These are: (a) invention of a semiconductor laser [1], (b) development of low-loss optical fiber [2] and (c)invention of an erbium-doped fiber amplifier [3]. A semiconductor laser operating in a continuous wave mode has been a reliable source for encoding information in the optical domain. The low-loss optical fiber has been serving as a robust medium of transmission as it not only provides high bandwidth but is also immune to electromagnetic interference. Since the optical fiber has a finite loss, although only 0.1-0.2dB/km at 1550, the optical amplifiers were needed to realize the transoceanic optical networks. The invention of an erbium-doped fiber amplifier was a major breakthrough to realize the fiber-optic networks as we see them today. Before the advent of modern optical communications, the electrical communication systems were widely used for long distance communications. In the electrical communication systems, the signals in the electrical form are sent through the co-axial cables and are bandwidth limited. Along with several other reasons, bandwidth limitation is the primary reason for the electrical communication systems being less preferred and being replaced by the optical communication systems. The devices and components used in the conventional optical

communication systems are discrete, bulky and expensive. The primary reason for these photonic devices being expensive is that they are manufactured using various technologies and different base materials. Therefore, the interest has arised to assemble many photonic components and devices on a single chip which can be used for performing large number of functions. The compact assembly of various photonic components and devices on a single chip is expected to bring down the cost of fabrication and will also result into easy handling in practical situations. The compact assembly of a large number of different photonic components and devices on a single chip has the potential of processing the data at a faster rate, as compared to their electronic counterparts, for on-chip as well as off-chip communication with a reduced power consumption.

In the past three decades there has been a tremendous research effort by the optics and photonics researchers to use the mature complementary metal-oxide semiconductor (CMOS) technology for fabricating the silicon photonic chips for diverse applications. These applications are mainly in the area of long reach as well as short reach communication networks. Although new applications have emerged in the field of bio-photonics, this work is communication network centred and hence bio-photonics will not be discussed here. The prime aim of using the CMOS technology for fabricating the silicon photonic chips is motivated by the cost advantage which silicon electronics industry can offer. Although silicon has a long and successful technological history, the indirect bandgap of silicon has been a limiting factor to realize active functionalities. This has been the driving force for the work being presented here. In this chapter, a brief description of all relevant topics related to the research work presented here will be provided.

1.1 Fiber-optic communications

A fiber based optical communication system mainly consists of a transmitter (modulated laser or light emitting diode), a communication channel (silica fiber), and the photo-receiver (photo-detector). Advanced fiber-optic communication systems include many more components such as amplifiers and repeaters. A serial bit stream in an electrical form is presented to a light source directly (often called direct modulation) or externally (often called external modulation) which results in the generation of a serial bit stream in an optical form. This information in optical form is sent through the optical fiber to the other end, called the receiver end, of the communication system. At the receiver end, the light is fed to a detector and converted back into the electrical form to construct the original bit stream. The research for the fiber based optical communication systems started around the year 1975 [4]. The first gen-

eration of optical communication systems used GaAs semiconductor lasers in the visible region of the electromagnetic spectrum. The first generation systems became commercially available in 1980 [5]. Although these systems could handle only tens of Mbit/s, they allowed a repeater spacing of ~ 10 km. The repeater spacing of the state-of-the-art co-axial copper cable based electrical communication systems was only 1 km in those days. The larger repeater spacing served as the main motivation to prefer the optical communication systems because it reduced the installation and maintenance cost of the repeaters. The second generation of fiber based communication made use of 1.3 μm wavelength region due to the low propagation loss of the fiber (<1 dB/km). Another reason to choose 1.3 μm was the minimum dispersion of the optical fiber in this wavelength region. In the second generation fiber optic communication systems, multimode fiber were used [6] first but were soon replaced by single mode fibers. The third generation fiber-optic communication systems operating at 1.55 μm with a capacity of 2.5 Gbit/s became commercially available in 1990. These systems made use of dispersion shifted fibers which can be designed to have minimum dispersion around 1.55 μm and have a propagation loss of 0.2 dB/km. The third generation had a drawback of making use of repeaters typically separated by 60-70 km. The coherent detection schemes were being developed to minimize these problems because the use of coherent detection system improves the receiver sensitivity resulting into larger separation of repeaters. But the advent of fiber amplifiers led to the postponement of the commercial introduction of coherent detection schemes. The current (fourth) generation of the optical fiber communication systems exploits WDM (wavelength-division multiplexing) and optical amplification for increasing the bit rates and the repeater spacing respectively. In real-life the communication between different end-users happens through a collection of transmission links. The collection of transmission links along with other equipments which provide a means of information exchange and processing is called a network. A network based on fiber-optic transmission lines and electronic/optoelectronic/all-optical information processing devices is called a fiber optical network. Three basic network topologies [7] used for fiber optical networks are the following - (a) Linear-bus configuration, (b) Ring configuration and (c) Star configuration. In a linear bus topology, at one end is the controller while at another is the terminator. The controller and the terminators are basically computers. Any computer that wants to communicate with the main computer must wait till the transmission line becomes available to it. When a terminator uses the network, the information is sent to the controller computer which in turn sends back the response to information down the line of computers until it reaches the terminating computer. In a ring topology, consecutive nodes are connected by point-to-point links to form a single closed path. The information is transmitted from node to

node going around the ring. The nodes have the active devices to recognize the address and the data is forwarded to the next node if it is not addressed to the current node. In a star network, all the nodes are linked to a single point. The central node can be an active or a passive device. The single point is called the central node or the hub. The star topology reduces the chances of a network-failure. It also prevents the passing of data packets through an excessive number of nodes.

1.2 On-chip optical communications

Board-to-board and chip-to-chip communication using optical links and systems have been proposed and are under development but the feasibility of on-chip optical communication is an open research question. The optical communication links on a chip scale are likely to be similar to fiber-optic communication links as used for long distance communication. From a functionality point of view, in a broad sense and at the basic level on-chip data links will mimic the fiber-optic links. The simplified schematic of an on-chip data communication link is shown in figure 1.1. Since there does not exist a reliable on-chip laser suitable for practical applications, it is shown off-the chip but connected to an on-chip modulator. The optical modulator and the electronic circuitry associated to the transmission-end shown here has the same role as in case of fiber-optic transmission links. An electro-optical modulator converts the elec-

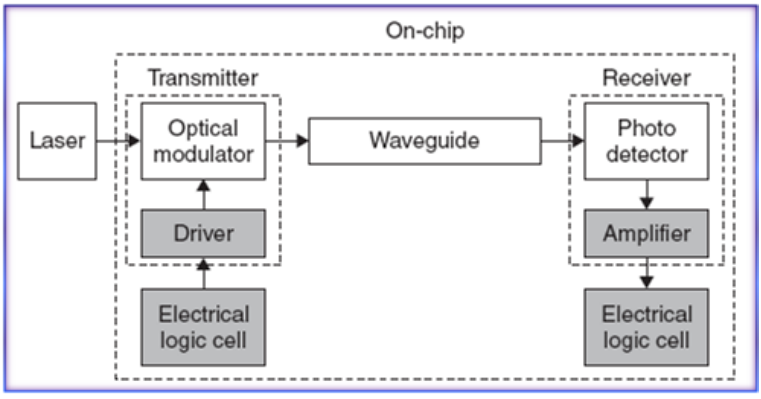

Figure 1.1: Simplified schematic of an on-chip data communication link.

trical data supplied from an electrical driver into a modulated optical signal. There have been several proposals on high speed electro-optical modulators. These are based on either a Mach-Zehnder interferometric configuration or a resonant microcavity structure. The operating principle of these modulators is

based on a change in the refractive index or absorption coefficient of an optical path with the application of an electrical signal.

As a transmission medium an optical waveguide replaces the optical fiber. There are several possible choices of optical waveguides for future applications. Among them, the most prominent ones are silicon-on-silica or SOI [8], silica-on-silica [9], silica-on-silicon [10], InP-on-InP [11], InP-on-silicon [12] and silicon nitride-on-silica [13]. The high index contrast waveguides offer a smaller pitch while low index contrast waveguides offer a low propagation delay [14]. The optical waveguides exhibit a smaller propagation delay as compared to electrical wires. This is clearly an argument in favour of optical waveguides for delay limited on-chip networks. The optical waveguides on a chip need to be separated from each other by an approximate distance of 0.5-3.0 μm to avoid a significant cross-talk. For a given pitch, if the waveguide is too wide, then crosstalk is higher due to the proximity between the sides of the adjacent waveguides. If the waveguide is too narrow, the optical mode becomes less confined resulting into a higher crosstalk due to larger overlap between adjacent optical modes. The optical waveguides have the same promise of wavelength-division multiplexing (WDM) on a chip as an optical fiber for long distance communications.

On the receiver side, the functionality of the photo-diode and the electronic circuitry following it is analogous to that in the fiber-optic communication links. A photo-diode is followed by a trans-impedance amplifier (TIA) stage. The TIA converts the electrical current generated by the photodiode into the voltage which is thresholded by subsequent stages to the digital levels. Of these, the TIA is arguably the most critical component for high-speed performance. The reason being the fact that it has to cope with a generally large photo-diode capacitance situated at its input.

The research is being carried out for optical Network-on-Chip (ONoC)[15-16]. The need for the on-chip optical networks has been discussed for almost more than two decades [17] but it has not been possible to implement due to the large foot-prints of the necessary components which prevented their integration on a chip. Also, the power consumption of many necessary components was way too high to be good for practical applications. One notable thing regarding the power consumption in ONoC is the fact that the power consumption of an optical interconnect is almost independent of the interconnect length [18]. It is much less as compared to electrical interconnect (around 1/10 in general). The ONoC has been considered to enabling high bandwidth and low contention routing of data using WDM [19]. A micronetwork based on wavelength routing is suggested in [20]. As an example of a ONoC, a brief description of a simple wavelength routed optical network architecture proposed in [21] is presented here (see figure 1.2). A general wavelength routed optical network con-

sists of input/output nodes and multiple stages. The number of stages equals the number of input/output nodes but this rule is not valid when the number of input/output nodes is 2. In figure 1.2 (a) there are four stages corresponding to four input/output nodes while in figure 1.2(b) the number of stages is five as the number of input/output nodes is five. At any stage , all the optical switches within it share the same resonant wavelength (W).

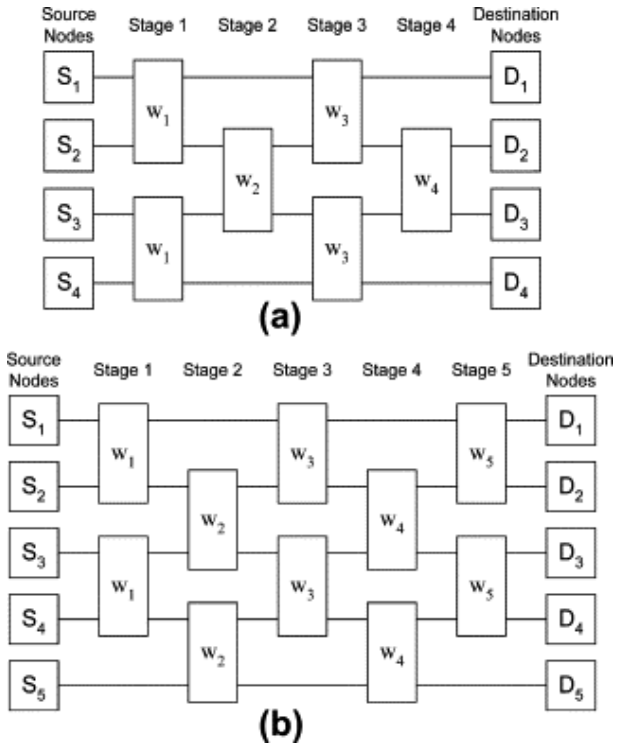

Figure 1.2: Wavelength routed ONoC [21].

1.3 Silicon photonics

The history of silicon photonics can be traced back to the work of Soref and Petermann in the late 1980s and early 1990s [21-24]. Early work in the field of silicon photonics was mostly related to passive optical devices [24-31]. Creation of photonic devices and components by making use of electronic IC industrial processes has been the main motivation for photonics researchers. Another motivation has been the availability of highly-pure silicon-on-insulator (SOI) wafers for the creation of planar lightwave circuits. The high index contrast

between silicon (n ~ 3.45) and SiO_2 (n ~ 1.45) offers strong optical confinement making it possible to scale down the photonic waveguides to hundreds of nanometer. The large index contrast between silicon and silica leads to a high optical intensity . This makes it possible to observe non-linear effects such as Raman and Kerr effect on an SOI chip. These non-linear effects in SOI waveguides have led to amplification [32], lasing [33] wavelength conversion [34] etc. which were perceived to be beyond the reach of silicon photonics. Silicon also has other excellent material properties such as high thermal conductivity, high optical damage threshold and high third-order optical nonlinearities which are important for photonic devices. As compared to silica fiber, the Raman and Kerr effects are 1000 and 100 times stronger in silicon respectively. As can be seen

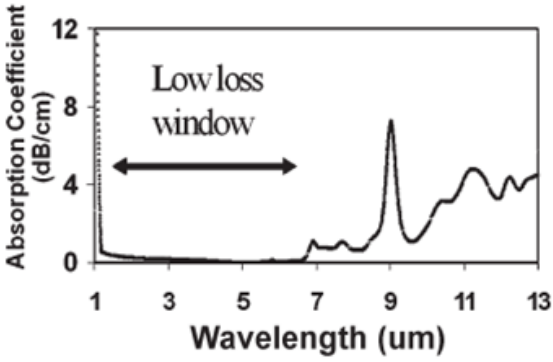

Figure 1.3: Absorption spectrum of silicon [36].

from figure 1.3, the low-loss wavelength window in silicon extends from 1.1 to ~ 7μm [36]. Therefore, the utility of silicon is not limited to the telecommunication band but it can also serve as a good material for nonlinear optical devices in the mid IR range.

One of the main applications of silicon photonics is optical interconnects for CMOS electronics [37]. The optical interconnects are thought to be much better suited than copper interconnects in handeling high data rates (~ 10s of Gbits/s). But for this to become a reality, the optical interconnects must provide a low power solution. Untill now focus has been on the realization of optical functionalities in silicon and very little attention has been paid to the issue of power consumption. Overall an impressive progress has been made in passive as well as active photonic devices based on silicon. Below a brief description of each type (passive and active) is provided.

1.3.1 Passive silicon photonic devices

The basic requirement for on-chip optical communication devices is a low-loss optical waveguide. This waveguide may be used just as a transmission medium or for advanced functionalities such as modulators. Silicon photonic waveguides are able to fulfill this condition. All the passive silicon photonic devices make use of a silicon waveguide. Due to the high index contrast between a silicon waveguide and the medium surrounding it (air or SiO_2), the surface roughness causes a significant scattering loss. In ref. [38], it has been shown that backscattering due to sidewall roughness is one of the most severe limiting factors in state-of-the art SOI nanowires employed in densely integrated photonics. In general, the silicon waveguides are characterized by losses in the range of 0.1-3 dB/cm depending upon the dimensions and the processing conditions. Obviously, the losses are higher in smaller waveguides due to the higher optical intensity at the surface and with an increase in the dimensions the losses decrease as the evanescent tail of the light feels the surface roughness less. There have been two main approaches to reduce the propagation losses of the waveguides. One makes use of optimized waveguide geometry to avoid scattering loss from the waveguide cross-section [39-41] while another is based on post fabrication treatments [42-44] such as wet chemical oxidation and thermal oxidation. The main passive silicon photonic devices based on the waveguides are the following: (i) microrings [45]/disks [46], (ii) delay lines formed by spirals [47], (iii) directional coupler [48], (iv) star couplers [49], (v) multimode interference couplers [50],(vi) arrayed waveguides or phasors [51], (vii) waveguide crossings [52] and (viii) couplers (inverse tapers and the gratings) [53-54] for coupling of light from chip to fiber and vice-versa. One of the most important applications of passive silicon photonic devices is in the form of optical filters used for wavelength multiplexing and de-multiplexing . The AWG was one of the first devices aimed for WDM applications and recently microring and microdisk structures have been investigated extensively for the same applications [55-56]. For the initial characterization of devices formed on a chip, a light in- and out-coupler is necessary. Basically, there are two main approaches adopted for this purpose. One is the inverse taper approach where there is a gradual expansion of a core guided mode into a much larger cladding guided mode. Using this approach, coupling loss uncertainty as low as 0.2dB has been demonstrated from a single-mode fiber to a silicon wire waveguide [57]. The limitation of this approach is that the access fibers need to be aligned at the chip facets and hence the chips can not be used for wafer scale testing. Another approach is the use of grating couplers. This approach has been used for all the work reported here and hence it is described in detail here.

The grating coupler is basically a one dimensional diffraction grating etched into silicon. The light impinging on the grating will diffract under an angle de-

termined by the projected Bragg condition, which is graphically illustrated in Figure 1.4. The z- component of the wave vector belonging to a certain diffraction order is given by

$$\kappa_{z,m} = \beta + m\mathrm{K}$$

Where β is the effective propagation constant of the optical mode in the grating, K is inversely proportional to the grating period Λ and m is the diffraction order. The actual diffraction angle in the superstrate and substrate is determined by taking into account the dispersion relation in these media, for an isotropic medium the dispersion relation is given by

$$\kappa_{sub,sup} = (2\pi/\lambda)n_{sub,sup}$$

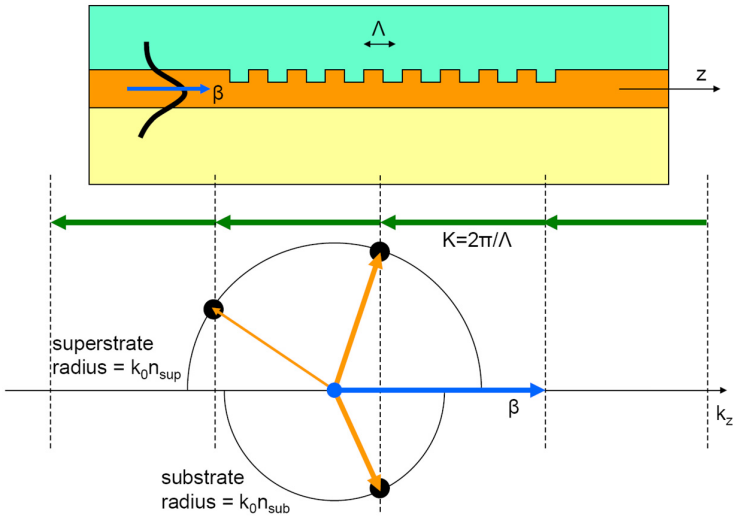

Figure 1.4: Cross-section through a basic diffraction grating structure and the associated Bragg diagram [58].

By a proper design of the grating structure, the diffraction can be limited to a single order. Variation in the grating periods results into a change in diffraction angle. At first sight, one may prefer to position the optical fiber perfectly vertical with respect to the photonic chip. This requires K = β. However, this is not a suitable choice as it allows another diffraction order to exist when exciting the grating from the optical waveguide, namely

$$\kappa_z = \beta - 2\mathrm{K} = -\beta.$$

The equation above implies that the grating structure will provide a strong reflection in the waveguide. While these reflections are as such problematic for

many applications, they also result in a drastically decreased fiber-chip coupling efficiencies. To overcome these problems a slightly detuned configuration in which the grating period is chosen such that the fiber is tilted slightly off-vertical (with 10° off-vertical being a typical number). Given the fact that the mode field diameter of a single mode optical fiber is about 10 μm, the diffracted field profile needs to have comparable dimensions, which implies that a strong (i.e. high index contrast) grating is required.

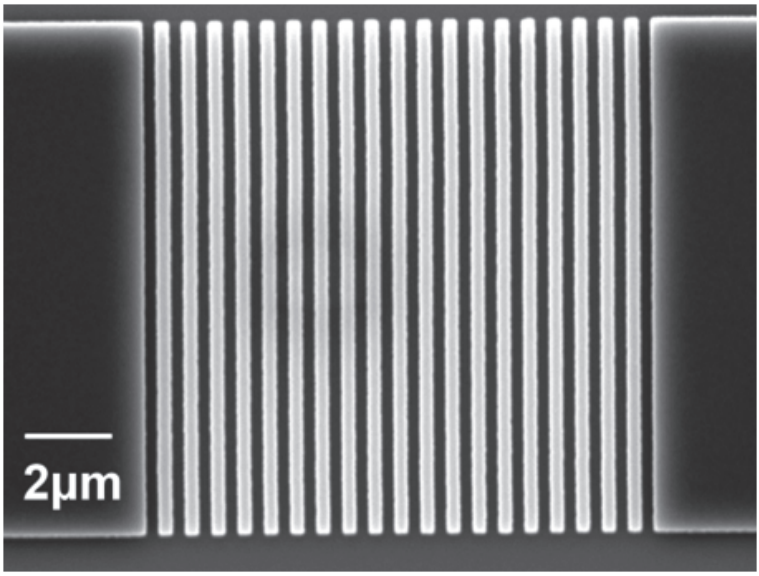

Figure 1.5: SEM image of a grating coupler fabricated at imec.

This kind of gratings can be easily achieved on an SOI platform. Figure 1.5 shows the SEM image of such a grating fabricated at imec.The height of the silicon is 220nm which rests on a 2μm thick BOX (burried oxide) layer. Below the BOX layer is the silicon substrate. The depth of the grating slit into top silicon is 70nm and the fill factor is 50% while the grating period is 630 nm. The complete fabrication process for such grating couplers is done in the 200 mm CMOS pilot line with 193nm DUV lithography. As an illustration of a real fiber-to-chip coupling scenario, figure 1.6 shows the schematic of the fibers aligned to grating couplers at each end of an SOI waveguide for in- and out-coupling of light. The coupling efficiency of fiber-to-chip couplers, as described here, is 30% around 1550 nm. The efficiency of such grating couplers is limited by two factors. First, a uniform grating, as is the case here, creates an approximately exponentially decaying output field along the propagation direction while the fiber has a Gaussian mode profile. This results into mode mismatch between

the fiber and the grating. Secondly, the grating does not only couple light from the SOI waveguide upward towards the fiber but also towards the substrate. The light coupled to the substrate is lost.

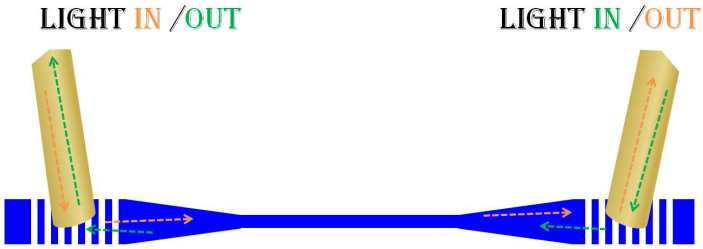

Figure 1.6: Basic configuration of fiber-to-chip-coupler.

1.3.2 Active silicon photonic devices

As discussed in the previous section, silicon photonics has delivered up to the expectations in the area of passive devices. For light modulation many breakthroughs have been achieved, e.g. [59-60]. A remarkable success was achieved at INTEL where researchers invented first GHz speed electro-optic modulators [61]. But a significant progress in active silicon photonic devices such as lasers and amplifiers is still awaited. Over the years, researchers have explored a myriad of ways to generate light emission from silicon, including doping with active rare-earth ions such as erbium [62], riddling silicon with an array of nanoscale holes to create porous silicon, or relying on gain from nonlinear processes such as the Raman effect [33-34]. These schemes, although capable of emitting light and even achieving lasing, either require optical pumping (and thus the presence of another laser) or emit light only weakly, and are therefore not considered as practical or satisfactory solutions [63]. At the root of all these limitations lies the fact that the silicon has an indirect band structure i.e. the conduction and valence band extremes do not occur at the same level of crystal momentum. As a consequence, the probability for a radiative recombination is low which means that the e-h(electron-hole) radiative life time is long (of the order of some milliseconds). During this time both the hole and electron move around and cover a volume of $\sim 10\mu m^3$. If they come across a defect or a trapping center, the carriers may recombine nonradiatively. Typically, the nonradiative recombination lifetime in Si is of the order of some nanoseconds. In addition, there are two more phenomena which limit the use of Si for light amplification. The first one is a nonradiative Auger recombination process. This process is a three particle recombination process in which an excited electron (hole) recombines

with a hole (electron) by releasing the energy to another electron(hole). The second phenomenon is associated with free carrier absorption. Excited carriers may absorb photons and hence deplete the inverted population and at the same time increase the optical loss suffered by the signal beam.

1.4 Fully-functional photonic chips

A fully functional chip needs to be capable of performing passive as well as active functions. As discussed in previous sections, silicon photonics provides robust solutions for passive functionalities. Light generation and processing (such as buffering, wavelength conversion and time domain de/multiplexing etc.) has not yet been realized in silicon with acceptable level of power consumption and performance. In the near future it does not look feasible to realize these function in Si with smaller footprints and low power consumption. Therefore, the photonics community is at a junction where III-V-on-silicon is the most promising road ahead. The III-V/SOI technology has already been used to realize the most advanced devices and most advanced photonic integrated circuits (PICs) [64].

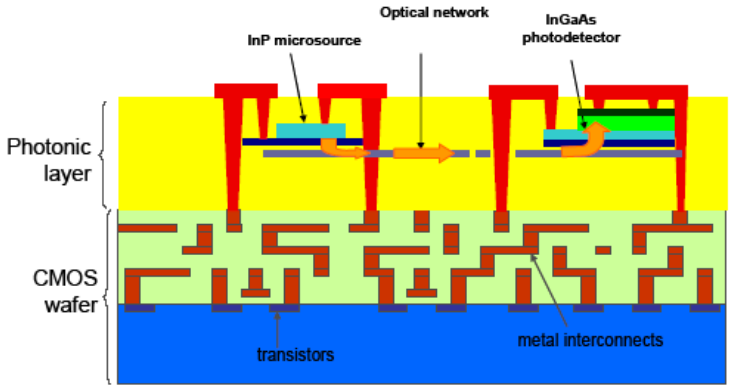

Figure 1.7: Above-IC silicon photonics and III-V-on-silicon integration scheme [65].

Traditionally, the argument for not using III-V-on-silicon in a CMOS pilot line has been that the III-V fabrication process is not CMOS compatible. But recently, at LETI in France, the CMOS pilot line has been used to fabricate III-V-on-silicon devices with satisfactory performance [65]. Devices fabricated included the III-V microdisk lasers, the photodetectors and the wavelength selective circuits on 200 mm wafer scale. Using the III-V-on-silicon microdisk resonators fabricated on the same platform, all-optical wavelength convertors

[66], all-optical de-multiplexers [67], all-optical format convertors [68], tunable microwave photonic filters[69] and electro-optic phase modulators [70] were demonstrated.

A specific process adapting and modifying the standard III-V material process steps to comply with a CMOS environment was developed, using the so-called above-IC approach as shown in figure 1.7. In this approach the devices were fabricated at the back-end of line (BEOL) levels keeping the temperature budget limited to 350°C-400°C. To achieve CMOS compatibility, (a) die-to-wafer bonding was developed at the 200mm scale, (b) a dry etching chemistry capable of etching the III-V dice while preserving the Si/SiO_2 based surface was used and (c) CMOS compatible metals (Ti/TiN/AlCu) were used to replace the standard gold based contacts used in optoelectronics.

1.5 Overview of this work

The prime idea behind carrying out this work was to demonstrate the feasibility of multifunctional and fully-functional photonic chips using the III-V-on-silicon photonics platform. It was envisaged that the III-V-on-silicon platform will be a CMOS compatible platform in the near future. At present III-V material based device fabrication is not widely accepted to be CMOS compatible, but processes can be developed in which III-V-on-silicon will become CMOS compatible. The microdisk was chosen as a building block because it can be fabricated with a small foot-print and different photonic functionalities are possible in it with lower power consumption. Based on the different functionalities tested separately, a functional digital photonic circuit can be constructed. For example, a 4X1 mux/demux with latching memory. This is illustrated in figure 1.8. In this figure τ represents the optical delay and optical flip-flops represent the photonic memory.

Chapter 2 gives a generic and brief overview of designs and fabrication processes used to fabricate III-V microdisks on top an SOI waveguide circuit. In remaining chapters, the versatility of single microdisks for different optical functionalities is investigated. These functionalities can find applications in on-chip as well as off-chip communication networks. Using a microdisk laser, an all-optical flip-flop operation was shown with a switching energy as small as 1.8 fJ. This has been a great success with a potential for realization of all-optical random access memories. All the challenges faced for the realization of all-optical flip-flops and the results obtained are presented in chapter 3. Chapter 4 is devoted to all-optical gating based on the concept of one light beam controlling another. The success of this gating approach was extended for the realization of bias-free all-optical wavelength conversion. In chapter 5, all-optical time domain demultiplexing and format conversion from non-return-to-zero (NRZ)to

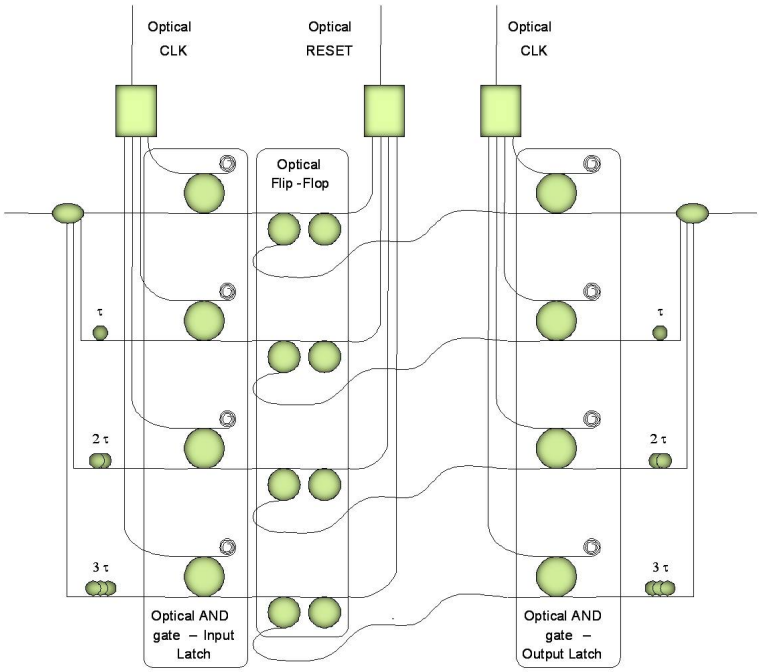

Figure 1.8: Illustration of a digital photonic circuit.

return-to-zero (RZ) is presented. The format conversion was mainly aimed at applications in long haul communication network nodes. Chapter 6 is aimed at providing the detailed view of complex designs constructed by integrating microdisks for complex functions such data flip-flops and shift registers. Chapter 7 highlights the future scope of this work and draws the conclusions of the whole work.

1.6 Publications

The results obtained within this work have been published in several international journals and were presented at various international conferences. The work presented in international conferences included several invited talks. The work on all-optical flip-flops was widely covered in popular scientific media. The following list gives an overview.

Publications in international journals

1. J. Lloret, R. Kumar, S. Sales, F. Ramos, G. Morthier, P. Mechet, T. Spuesens, D. Van Thourhout, N. Olivier, J.-M. Fedeli and J. Capmany. *Ultra-compact electro-optic phase modulator based on III-V-on-silicon microdisk resonator.* Optics Letters, 37(12):2379–2381, June 2012.

2. R. Kumar, T. Spuesens, P. Mechet, N. Olivier, J.-M. Fedeli, P. Regreny, G. Roelkens, D. Van Thourhout and G. Morthier. *10Gbit/s all-optical NRZ-OOK to RZ-OOK format conversion in an ultra-small III-V-on-silicon microdisk fabricated in a CMOS pilot line.* Optics Express, 19(24):24647–24656, November 2011.

3. R. Kumar, T. Spuesens, P. Mechet, P. Kumar, O. Raz, N. Olivier, J.-M. Fedli, P. Regreny, G. Roelkens, R. Baets, D. Van Thourhout and G. Morthier. *Ultra-fast and bias-free all-optical wavelength conversion using III-V-on-silicon Technology.* Optics Letters, 36(13):2450–2452, July 2011.

4. H.D. Jung, R. Kumar, P. Regreny, H.J.S. Dorren, T. Koonen, and O. Raz. *Analog modulation characteristics of InP membrane microdisc laser for in-building networks".* Electronics Letters, 47(2):121–123, January 2011.

5. D. Van Thourhout, T. Spuesens, S. Salvaraja, L. Liu, G. Roelkens, R. Kumar, G. Morthier, P.R -Romeo, F. Mandorlo, O. Raz, C. Kopp and L. Grenouillet. *Nanophotonic devices for optical interconnect.* IEEE J. Sel. Top. Quantum Electron.,**invited**, 16(5):1363–1375, Sept./Oct. 2010.

6. R. Kumar, L. Liu, G. Roelkens, E.-J. Geluk, T. de Vries, F. Karouta, P. Regreny, D. Van Thourhout, R. Baets and G. Morthier. *10GHz all-optical gate based on a III-V/SOI microdisk.* IEEE Photonics Technology Letters, 22(13):981–983, July 2010.

7. L. Liu, R. Kumar, K. Huybrecht, T. Spuesens, G. Roelkens, E.-J. Geluk, T. de Vries, P. Regreny, D. Van Thourhout, R. Baets and G. Morthier. *An ultra-small, low-power, all-optical flip-flop memory on a silicon chip.* Nature Photonics, 4(3):182–187, March 2010.

Publications in international conferences

8. G. Roelkens, S. Keyvaninia, S. Stankovic, M. Tassaert, N. Hattasan, A. Gassenq, P. De Heyn, Y. De Koninck, P. Mechet, R. Kumar, M. Muneeb, D. Vermeulen, G. Morthier, R. Baets and D. Van Thourhout. *III-V-on-silicon membrane photonics for near-infrared and mid-infrared applications.* In proceedings of European Conference on Integrated Optics (ECIO) 2012 (invited), Spain, 2012.

9. R. Kumar, T. Spuesens, P. Mechet, N. Olivier, J.-M. Fedeli, P. Regreny, G. Roelkens, D. Van Thourhout and G. Morthier. *10Gbit/s bias-free and error-free all-optical NRZ-OOK to RZ-OOK format conversion using a III-V-on-silicon microdisk resonator.* In Proceedings of the Optical Fiber Communication Conference and Exposition (OFC) and the National Fiber Optic Engineers Conference (NFOEC) 2012,United States, p.JW2A.77, 2012.

10. R. Kumar, T. Spuesens, P. Mechet, J.-M. Fedeli, N. Olivier, P. Regreny, G. Roelkens, D. Van Thourhout and G. Morthier. *All-optical demultiplexing of 10Gbps data using III-V/SOI microdisk resonators.* In Proceedings of the 2011 Annual Symposium of the IEEE Photonics Benelux Chapter, Belgium, p.89–91, 2011.

11. G. Morthier, P. Mechet, R. Kumar, G. Roelkens, T. Spuesens, T. De Vries, E.J. Geluk, P. Regreny, R. Baets and D. Van Thourhout. *Progress in heterogeneously integrated silicon-InP laser diodes for on-chip all-optical networks and signal processing.* In Proceedings of Frontiers in Optics 2011, **invited**, United States, p.FWBB4, 2011.

12. G. Roelkens, S. Stankovic, S. Keyvaninia, P. Mechet, R. Kumar, T. Spuesens, G. Morthier, R. Baets, D. Van Thourhout, M. Lamponi, G. Duan, Y. Halioua, F. Raineri and R. Raj. *Laser sources on a heterogeneous III-V/silicon platform.* In proceedings of IEEE Photonics Confrence (IPC)2011, **invited**, United States, p.WA2, 2011.

13. R. Kumar, T. Spuesens, P. Mechet, J.-M. Fedeli, N. Olivier, P. Regreny, G. Roelkens, D. Van Thourhout and G. Morthier. *Proof-of-concept demonstration of an all-optical de-multiplexer using III-V/SOI microdisk resonator fabricated in a CMOS pilot line.* In proceedings of IEEE Photonics Confrence (IPC)2011, United States, p.MR2, 2011.

14. R. Kumar, T. Spuesens, P. Mechet, P. Regreny, J.-M. Fedeli, N. Olivier, G. Roelkens, D. Van Thourhout and G. Morthier. *All-optical de-multiplexing using III-V/SOI microdisk resonators.* In Proceedings of European Semiconductor Laser Workshop (ESLW) 2011, Switzerland, p.C2, 2011.

15. R. Kumar, T. Spuesens, P. Mechet, P. Regreny, N. Olivier, J.-M. Fedeli, G. Roelkens, D. Van Thourhout and G. Morthier. *10Gbps bias-free all-optical wavelength conversion using InP-microdisk resonators heterogeneously integrated onto SOI.* In proceedings of European Confrence on Optical Communication (ECOC)2011, Switzerland, p.We.9.LeSaleve.3, 2011.

16. O. Raz, H.J.S. Dorren, R. Kumar, G. Morthier, P. Regreny and P.R. -Romeo. *50 fJ-per-bit, high speed, directly modulated light sources for On-chip optical data communications*. In Proceedings of the Optical Fiber Communication Conference and Exposition (OFC) and the National Fiber Optic Engineers Conference (NFOEC) 2011,United States, p.OMM5, 2011.

17. P. Mechet, L. Liu, R. Kumar, K. Huybrechts, T. Spuesens, G. Roelkens, E.-J. Geluk , T. De Vries , P. Regreny , D. Van Thourhout, R. Baets and G. Morthier. *Heterogeneously integrated microdisk lasers for optical interconnects and optical logic*. In Proceedings of SPIE Photonics West 2011, **invited**, Vol.7913, United States, p.791319, 2011.

18. O. Raz, H.D. Jung, R. Kumar, P. Regreny, T. Koonen and H.J.S. Dorren. *Integrated InP membrane light sources for analog CMOS photonic transmitters*. In Proceedings of the 2010 Annual Symposium of the IEEE Photonics Benelux Chapter, The Netherlands, p.177–180, 2010.

19. R. Kumar, P. Kumar, G. Roelkens, L. Liu, P. Regreny, T. de Vries, D. Van Thourhout, R. Baets and G. Morthier. *Performance analysis of III-V/SOI microdisk based all-optical gate for on-chip interconnects*. In Proceedings of the 2010 Annual Symposium of the IEEE Photonics Benelux Chapter, The Netherlands, p.129–131, 2010.

20. K. Huybrechts, L. Liu, R. Kumar, T. Spuesens, G. Roelkens, E.J. Geluk, T. de Vries, P. Regreny, D. Van Thourhout, R. Baets and G. Morthier. *All-optical flip-flops using electrically pumped microdisk lasers integrated on silicon*. In Proceedings of IEEE Photonics Society Annual Meeting 2010, **invited**, United States, p.MH1, 2010.

21. O. Raz, L. Liu, R. Kumar, G. Morthier, P. Regreny and H.J.S. Dorren. *A single InP membrane disc cavity for both transmission and detection of 10Gb/s signals in On chip interconnects*. In Proceedings of European Confrence on Optical Communication (ECOC)2010, Italy, p.P2.12, 2010.

22. G. Roelkens, D. Vermeulen, L. Liu, T. Spuesens, R. Kumar, P. Mechet, K. Huybrechts, S. Keyvaninia, S. Stankovic, M. Tassaert, P. De Heyn, K. Komorowska, S. Selvaraja, D. Van Thourhout, G. Morthier, R. Baets and R. Halir. *III-V/silicon photonic integrated circuits for FTTH and optical interconnect*. In Proceedings of the Fifth International Conference on Broadband and Biomedical Communications (IB2Com), **invited**, 2010.

23. J. Hofrichter, O. Raz, F. Horst, N. Chrysos, C. Minkenberg, T. de Vries, H.J.S. Dorren, R. Kumar, L. Liu and B.-J. Offrein. *A fast and comprehensive microdisc laser model applied to all-optical wavelength conversion*. In

Proceedings of the Integrated Photonics Research, Silicon and Nano Photonics (IPR), Photonics in Switching (PS) 2010, United States, p.PTuA2.pdf, 2010.

24. G. Morthier, L. Liu, R. Kumar, P. Mechet, K. Huybrechts, G. Roelkens, T. Spuesens, T. de Vries, E.-J. Geluk, P. Regreny, R. Baets and D. Van Thourhout. *Heterogeneous InP on SOI integration for the realization of all-optical logic devices*. In Proceedings of Integrated Photonics Research, Silicon and Nano Photonics (IPR), Photonics in Switching (PS) 2010, **invited**, United States, p.IWF2.pdf, 2010.

25. J. Hofrichter, F. Horst, N. Chrysos, C. Minkenberg, R. Kumar, L. Liu, G. Morthier, T. de Vries and B.-J. Offrein. *Digital all-optical signal processing using microdisk lasers*. In Proceedings of Integrated Photonics Research, Silicon and Nano Photonics (IPR), Photonics in Switching (PS)2010, United States, p.PTuA3.pdf, 2010.

26. G. Morthier, R. Kumar, F. Raineri, R. Raj, J. Hofrichter, N. Chrysos, B.-J. Offrein, R. Zhang, J. van der Tol, O. Raz and H.J.S Dorren. *Overview of the EU FP7-project HISTORIC*. In Proceedings of SPIE - Silicon Photonics and Photonic Integrated Circuits II, **invited**, Vol.7719, Belgium, p.771908, 2010.

27. K. Huybrechts, L. Liu, R. Kumar, T. Spuesens, G. Roelkens, E.-J. Geluk, T. de Vries, M. Smit, P. Regreny, P.R. -Romeo, D. Van Thourhout, R. Baets and G. Morthier. *Digital photonics using InP microdisk lasers heterogeneously integrated on Silicon-on-Insulator*. In Proceedings of European Conference on Integrated Optics (ECIO) 2010, **invited**, United Kingdom, p.WeF1, 2010.

28. O. Raz, L. Liu, R. Kumar, G. Morthier, D. Van Thourhout, P. Regreny, P.R.-Romeo, T. de Vries and H.J.S. Dorren. *Compact, low power and low threshold electrically pumped micro disc lasers for 20Gb/s non return to zero all optical wavelength conversion*. In Proceedings of the Optical Fiber Communication Conference and Exposition (OFC) and the National Fiber Optic Engineers Conference (NFOEC) 2010, United States, p.OMQ5, 2010.

29. R. Kumar, K. Huybrechts, L. Liu, T. Spuesens, G. Roelkens, E.-J. Geluk, T. de Vries, P. Regreny, D. Van Thourhout, R. Baets and G. Morthier. *An ultra-small, low-power all-optical flip-flop memory on a silicon chip*. In Proceedings of the Optical Fiber Communication Conference and Exposition (OFC) and the National Fiber Optic Engineers Conference (NFOEC) 2010, United States, p.OTuN7. 2010.

30. R. Kumar, L. Liu, G. Roelkens, E.-J. Geluk, T. de Vries, P. Regreny, D. Van Thourhout, R. Baets and G. Morthier. *10GHz all-optical gate on a silicon chip*. In Proceedings of the Optical Fiber Communication Conference and Exposition (OFC) and the National Fiber Optic Engineers Conference (NFOEC) 2010, United States, p.JWA44, 2010.

31. R. Kumar, L. Liu, G. Roelkens, G. Morthier and R. Baets. *Simple and accurate measurements to characterize microdisk lasers for all-optical flip-flop operation*. In Proceedings of the 2009 Annual Symposium of the IEEE Photonics Benelux Chapter, Belgium, p.81–84, 2009.

Publications in national conferences

32. R. Kumar and G. Morthier. *Photonic integrated circuits using III-V/SOI microresonators*. In Proceedings of 11th UGent-FirW PhD Symposium, p.132, Ghent, Belgium, 2010.

Research higlights and news coverage

33. Article [1] on format conversion apperaed in the Virtual Journal of Ultrafast Science, Vol.11(1), January 2012.

34. Article [2] on wavelength conversion apperaed in the Virtual Journal of Ultrafast Science, Vol.10(8), August 2011.

35. Research highlights : *Microdisk lasers on silicon for high-speed switching* in IEEE Photonics Society News Letter, Vol.24(3), June 2010.

36. News : Optical RAM - Imec's optical flip-flop paves the way for low-power, all-optical telecommunications. In IEEE Spectrum, February 2010.

37. News : IMEC shines laser on optical RAM. In Electronics Weekly, Januray 2010.

References

[**1**] T.H. Maiman. *Stimulated optical radiation in ruby.* Nature, 187(4736):493-494, 1960.

[**2**] K. C. Kao and G. A.Hockham. *Dielectric-fibre surfacewaveguides for optical frequencies.* Proceedings of the Institution of Electrical Engineers-London, 113(7):1151-1158, 1966.

[**3**] R.J. Mears, L. Reekie, I.M. Jauncey and D.N. Payne. *Low-noise erbium-doped fibre amplifier operating at 1.54ţm.* Electronics Letters, 23(19):1026-1028, 1987.

[**4**] G.P. Agrawal. *Fiber-optic communication systems.* Chapter 1, Second edition, John Wiley & Sons, 2002.

[**5**] R.J. Sanferrare. *Terrestrial Lightwave Systems.* AT&T Technical Journal, 66(1):95-107, 1987.

[**6**] D. Gloge, A. Albanese, C.A. Burrus, E.L. Chinnock, J.A. Copeland, A.G. Dentai, T.P. Lee, T. Li and K. Ogawa. *High-Speed Digital Lightwave Communication Using LEDs and PIN Photodiodes at 1.3μm.* Bell System Technical Journal, 59(8):1365-1382, 1980.

[**7**] G. Keiser. *Optical fiber communication.* Chapter 12, Third edition, McGraw-Hill international editions, 2000.

[**8**] P. Dumon, W. Bogaerts, V. Wiaux, J. Wouters, S. Beckx, J.Van Campenhout, D. Taillaert, B. Luyssaert, P. Bienstman, D. Van Thourhout and R. Baets.*Low-loss SOI photonic wires and ring resonators fabricated with deep UV lithography* . Photonics Technoloy Letters, 16(5):1328-1330, 2004.

[**9**] Q. Lai, J.S. Gu, M.K. Smit, J. Schmid and H. Melchior. *Simple technologies for fabrication of low-loss silica waveguides.* Electronics Letters, 28(11):1000-1001, 1992.

[**10**] J. F. Bauters, M.J.R. Heck, D. John, M.-C. Tien, A. Leinse, R.G. Heideman, D.J. Blumenthal and J.E. Bowers. *Ultra-low loss silica-based waveguides with millimeter bend radius.* European Conference on Optical Communication (ECOC), paper We.8.E.6, 2010.

[**11**] S.Dupont, A. Beaurain, P. Miska, M. Zegaoui, J.-P. Vilcot, H.W. Li, M. Constant, D. Decoster and J. Chazelas. *Low-loss InGaAsP/InP submicron optical waveguides fabricated by ICP etching.* Electronics Letters, 40(14):865-866, 2004.

[**12**] J. van der Tol, R. Zhang, J. Pello, F. Bordas, G. Roelkens, H. Ambrosius, P. Thijs, F. Karouta and M. Smit. *Photonic integration in Indium-Phosphide membranes on silicon.* IET Optoelectronics, 5(5):218-225, 2011.

[**13**] J.F. Bauters, M.J.R. Heck, D.D. John, J.S. Barton, C.M. Bruinink, A. Leinse, R.G. Heideman, D.J. Blumenthal and J.E. Bowers. *Planar waveguides with less than 0.1 dB/m propagation loss fabricated with wafer bonding.* Optics Express 19(24): 24090-24101, 2011.

[**14**] M. Haurylau, H. Chen, J. Zhang., G. Chen, N.A. Nelson, D.H. Albonesi, E.G. Friedman and P.M. Fauchet. *On-chip Optical Interconnect Roadmap: Challenges and Critical Directions.* IEEE International Conference on Group IV Photonics, paper WA1(plenary), 2005.

[**15**] Optical Network-on-Chip Bibliography on the web address: *http://www.ee.ust.hk*

[**16**] D. Van Thourhout, I.O'Connor, A. Scandurra, L. Liu, W. Bogaerts, S. Selvaraja and G. Roelkens. *Nanophotonic Devices for Optical Networks-on-Chip.* OSA Conference on Lasers and Electro-Optics (CLEO), paper CMAA2, 2009.

[**17**] R.G. Beausoleil. *Large-scale integrated photonics for high-performance interconnects.* ACM Journal on Emerging Technologies in Computing Systems,7(2):6-1 to 6-54, 2011.

[**18**] G. Chen, H. Chen, M. Haurylau, N. Nelson, D. Albonesi, P.M. Fauchet and E.G. Friedman. *Electrical and optical on-chip interconnects in scaled microprocessors.* The international Symposium on Circuits and systems, 3:2514-2517, 2005.

[**19**] I. O'Connor. *Unconventional interconnects: optical solutions for system-level interconnect.* The international workshop system level interconnect, 79-88, 2004.

[**20**] M. Briere, B. Girodias, Y. Bouchebaba, G. Nicolescu, F. Mieyeville, F. Gaffiot, I. O'Connor. *System level assessment of an optical NoC in an MPSoC platform.* Design, Automation & Test in Europe Conference & Exhibition, 1-6, 2007.

[**21**] L. Zhang, M. Yang, Y. Jiang and E. Regentova. *Architectures and routing schemes for optical network-on-chips.* Computers and Electrical Engineering, 35, 856-877, 2009.

[**22**] R. Soref and J. Lorenzo. *All-silicon active and passive guided-wave components for λ= 1.3 and 1.6 ţm.* IEEE Journal of Quantum Electronics, QE-22(6):873-879, 1986.

[**23**] R. A. Soref and B.R. Bennett. *Kramers-Kronig analysis of E-O switching in silicon.* Proceedings of SPIE Integrated Optical Circuit Engineering, 704:32-37, 1986.

[**24**] B. Schuppert, J. Schmidtchen and K. Petermann. *Optical channel waveguides in silicon diffused from GeSi alloy.* Electronics Letters, 25(22):1500-1502, 1989.

[**25**] R.A. Soref, J. Schmidtchen and K. Petermann. *Large single-mode rib waveguides in GeSi and Si-on-SiO2.* IEEE Journal of Quantum Electronics, 27(8):1971-1974, 1991.

[**26**] P. D. Trinh, S. Yegnanarayanan and B. Jalali. *Integrated optical directional couplers in silicon-on-insulator.* Electronics Letters 31(24):2097-2098, 1995.

[**27**] U. Fischer, T. Zinke and K. Petermann. *Integrated optical waveguide switches in SOI.* Proceedings of IEEE Interantional SOI Conference, 141-142, 1995.

[**28**] T. T. H. Eng, S.S.Y. Sin, S.C.Kan and G.K.L. Wong. *Surface micromachined movable SOI optical waveguides.* Proceedings of International Conference on Solid-State Sensers and Actuators,1:348-350, 1995.

[**29**] C. Z. Zhao, G.Z.Li, E.K. Liu, Y. Gao and X.D.Liu. *Silicon on insulator Mach-Zehnder waveguide interferometers operating at 1.3 ţm.* Applied Physics Letters, 67(17):2448-2449, 1995.

[**30**] P. D. Trinh, S. Yegnanarayanan and B. Jalali. *5X9 integrated optical star coupler in silicon-on-insulator technology,* IEEE Photonics Technology Letters 8(6):794-796, 1996.

[**31**] P. D. Trinh, S. Yegnanarayanan, F. Coppinger and B. Jalali. *Silicon on-insulator (SOI) phased-array wavelength multi-demultiplexer with extremely low-polarization sensitivity.* IEEE Photonics Technology Letters, 9(7):940-942, 1997.

[**32**] R. Espinola, J. Dadap, R. Osgood Jr., S. McNab and Y. Vlasov. *Raman amplification in ultrasmall silicon-on-insulator wire waveguides.* Optics Express, 12(16):3713-3718, 2004.

[**33**] O. Boyraz and B. Jalali. *Demonstration of a silicon Raman laser*. Optics Express, 12(21):5269-5273, 2004.

[**34**] H. Rong, R. Jones, A. Liu, O. Cohen, D. Hak, A. Fang and M. Paniccia. *A continuous-wave Raman silicon laser*. Nature, 433:725-728, 2005.

[**35**] B. G. Lee, A. Biberman, A.C. Turner-Foster, M.A. Foster, M. Lipson, A.L. Gaeta and K. Bergman. *Demonstration of broadband wavelength conversion at 40 Gb/s in silicon waveguides*, IEEE Photonics Technology Letters, 21(3):182-184, 2009.

[**36**] B. Jalali and S. Fathpour. *Silicon Photonics*. IEEE Journal of Lightwave Technology 24(12);4600-4615, 2006.

[**37**] D. A. B. Miller. *Optical interconnects to silicon*. IEEE Journal of Selected Topics in Quantum Electronics, 6(6): 1312-1317, 2000.

[**38**] F. Morichetti, A. Canciamilla, C. Ferrari, M. Torregiani, A. Melloni and M. Martinelli. *Roughness induced backscattering in optical silicon waveguides*. Physical Review Letters, 104(3):33902-1 to 33902-4, 2010.

[**39**] S. Steven, W.G. Michael, L. Donna, C.W. Richard and M.L. Theodore. *Hybrid multi-mode/single-mode waveguides for low loss*. Integrated Photonics Research (IPR), paper IThE5, 2004.

[**40**] P. Dong, W. Qian, S. Liao, H. Liang, C.-C.Kung, N.-N.Feng, R. Shafiiha, J.Fong, D. Feng, A.V. Krishnamoorthy and M. Asghari. *Low loss shallow-ridge silicon waveguides*. Optics Express, 18(14):14474-14479, 2010.

[**41**] E. Cassan, S. Laval, S. Lardenois and A. Koster. *On-Chip optical Interconnects with compact and low-loss light distribution in silicon-on-insulator rib waveguides*. IEEE Journal of Selected Topics in Quantum Electronics, 9(2):460-464, 2003.

[**42**] K. K. Lee, D.R. Lim, L.C. Kimerling, J. Shin and F. Cerrina. *Fabrication of ultralow-loss Si/SiO2 waveguides by roughness reduction*. Optics Letters, 26(23):1888-1890, 2001.

[**43**] D. K. Sparacin, S.J. Spector and L.C. Kimerling. *Silicon waveguide sidewall smoothing by wet chemical oxidation*. Journal of Lightwave Technology, 23(8):2455-2461, 2005.

[**44**] J. Takahashi, T. Tsuchizawa, T. Watanabe and S. Itabashi. *Oxidation-induced improvement in the sidewall morphology and cross-sectional profile of silicon wire waveguides*. Journal of Vacuum Science & Technology B, 22(5):2522-2525, 2004.

[**45**] Q. Xu, D. Fattal and R.G. Beausoleil. *Silicon microring resonators with 1.5 μm radius.* Optics Express, 16(6):4309-4315, 2008.

[**46**] M. Soltani, S. Yegnanarayanan and A. Adibi. *Ultra-high Q planar silicon microdisk resonators for chip-scale silicon photonics.* Optics Express , 15(8):4694-4704, 2007.

[**47**] W. Bogaerts, S. Selvaraja, P. Dumon, J. Brouckaert, K. De Vos, D. Van Thourhout and R. Baets. *Silicon-on-insulator spectral filters fabricated with CMOS technology.* IEEE Journal of Selected Topics in Quantum Electronics, 16(1):33-44, 2010.

[**48**] P. D. Trinh, S. Yegnanarayanan and B. Jalali. *Integrated optical directional couplers in silicon-on-insulator.* Electronics Letters, 31(24):2097-2098, 1995.

[**49**] G. B. Cao, L.J. Dai, Y.J. Wang, J. Jiang, H. Yang and F. Zhang. *Compact integrated star coupler on silicon-on-insulator.* IEEE Photonics Technology Letters, 17(12):2616-2618, 2005.

[**50**] R. Halir, A. Ortega-Moñux, Í. Molina-Fernández, J.G. Wangüemert-Pérez,P. Cheben, D.-X. Xu, B. Lamontagne and S. Janz. *Compact high-performance multimode interference couplers in silicon-on-insulator.* IEEE Photonics Technology Letters, 21(21):1600-1602, 2009.

[**51**] P. Dumon, W. Bogaerts, D. Van Thourhout, D. Taillaert, R. Baets, J. Wouters, S. Beckx and P. Jaenen. *Compact wavelength router based on a Silicon-on-insulator arrayed waveguide grating pigtailed to a fiber.* Optics Express, 4(2):664-669, 2006.

[**52**] W. Bogaerts, P. Dumon, D. Van Thourhout and R. Baets. *Low-loss, low-crosstalk crossings for SOI nanophotonic waveguides.* Optics Letters, 32(19):2801-2803, 2007.

[**53**] A. Barkai, A. Liu, D. Kim, R. Cohen, N. Elek, H.-H. Chang, B.H. Malik, R. Gabay, R. Jones, M. Paniccia and N. Izhaky. *Double-stage taper for coupling between SOI waveguides and single-mode fiber.* IEEE/OSA Journal of Lightwave Technology, 26(24):3860-3865, 2008.

[**54**] D. Taillaert, P. Bienstman, R. Baets. *Compact efficient broadband grating coupler for silicon-on-insulator waveguides.* Optics Letters, 29(23):2749-2751, 2004.

[**55**] T. Tsuchizawa, K. Yamada, H. Fukuda, T. Watanabe, J. Takahashi, M. Takahashi, T. Shoji, E. Tamechika, S. Itabashi and H. Morita. *Microphotonic*

devices based on silicon microfabrication technology. IEEE Journal of Selected Topics in Quantum Electronics, 11(1):232-240, 2005.

[**56**] P. Koonath, T. Indukuri and B. Jalali. *Add-drop filters utilizing vertically-coupled microdisk resonators in silicon.* Applied Physics Letters, 86(9): 091102(1)-091102(3), 2005.

[**57**] S. McNab, N. Moll and Y. Vlasov. *Ultra-low loss photonic integrated circuit with membrane-type photonic crystal waveguides.* Optics Express, 11(22): 2927-2939, 2003.

[**58**] G. Roelkens, D. Vermeulen, S. Selvaraja, R. Halir, W. Bogaerts and D. Van Thourhout. *Grating-based optical fiber interfaces for silicon-on-insulator photonic integrated circuits.* EEE Journal of Selected Topics in Quantum Electronics, 17(13):571-580, 2011.

[**59**] B. Schmidt, Q. Xu, J. Shakya, S. Manipatruni and M. Lipson. *Compact electro-optic modulator on silicon-oninsulator substrates using cavities with ultrasmall modal volumes.* Optics Express, 15(6):3140-3148, 2007.

[**60**] Q. Xu, B. Schmidt, S. Pradhan and M. Lipson. *Micrometre-scale silicon electro-optic modulator.* Nature 435:325-327, 2005.

[**61**] A. Liu, R. Jones, L. Liao, D. Samara-Rubio, D. Rubin, O. Cohen, R. Nicolaescu and Mario Paniccia. *A high-speed silicon optical modulator based on a metal-oxide-semiconductor capacitor.* Nature, 427:615-618, 2004.

[**62**] A.W. Elshaari, S.F. Preble, C. Cress, R. Raffaelle and M.A. Abushagur. *Towards a low-Q erbium doped silicon laser.* Frontiers in Optics (FiO), paper FThW5, 2008.

[**63**] O. Graydon. *View from... Group IV Photonics: Hope from hybrids.* Nature Photonics, 5:718-719, 2011.

[**64**] D. Liang and J. Bowers. *Recent progress in lasers on silicon,* Nature Photonics, 4:511-517, 2010.

[**65**] J.-M.Feledli, L. Liu, L. Grenouillet, D. Bordel, F. Mandorlo, N.Olivier, T. Spuesens, P. Regreny, P. Grosse, P. Rojo-Romeo, R. Orobtchouk, D. Van Thourhout. *Towards optical networks-on-chip with 200mm hybrid technology.* Optical Fiber Communication Conference and Exposition/National Fiber Optic Engineers Conference(OFCNFOEC), paper OMM3, 2011.

[**66**] R. Kumar, T. Spuesens, P. Mechet, P. Kumar, O.Raz, N. Olivier, J.- M. Fedeli, G. Roelkens, R. Baets, D. Van Thourhout and G. Morthier. *Ultra-fast and*

bias-free all-optical wavelength conversion using III-V-on-silicon technology. Optics Letters, 36(13):2450-2452, 2011.

[**67**] R. Kumar, T. Spuesens, P. Mechet, J.-M. Fedeli, N. Olivier, P. Regreny, G. Roelkens, D. Van Thourhout and G. Morthier. *Proof-of-concept demonstration of an all-optical de-multiplexer using III-V/SOI microdisk resonator fabricated in a CMOS pilot line*. IEEE Photonics Conference, paper MR2, 2011.

[**68**] R. Kumar, T. Spuesens, P. Mechet, N. Olivier, J.-M. Fedeli, P. Regreny, G. Roelkens, D. Van Thourhout and G. Morthier. *10Gbit/s all-optical NRZ-OOK to RZ-OOK format conversion in an ultra-small III-V-on-silicon microdisk fabricated in a CMOS pilot line*. Optics Express, 19(24):24647-24656, 2011.

[**69**] J.Lloret, G. Morthier, F. Ramos, S. Sales, D. Van Thourhout, T. Spuesens, N. Olivier, J.-M.Fedeli and J. Capmany. *Broadband microwave photonic fully tunable filter using a single heterogeneously integrated III-V/SOI-microdisk-based phase shifter*. Optics Express, 20(11):10796-10806, 2012.

[**70**] J. Lloret, R. Kumar, S. Sales, F. Ramos, G. Morthier, P. Mechet, T. Spuesens, D. Van Thourhout, N. Olivier, J.-M. Fedeli and J. Capmany. *Ultra-compact electro-optic phase modulator based on III-V-on-silicon microdisk resonator*. Accepted for publication in Optics Letters.

2

Design and fabrication of III-V-on-silicon microdisk based photonic integrated circuits

2.1 Introduction

As elaborated in section 1.4 of chapter 1, for the realization of fully-functional chips III-V-on-silicon technology is the most promising way ahead [1]. III-V materials are capable of providing all the active functionalities such as amplification, lasing, modulation, gating and memory etc. and SOI waveguides are most suitable as the transmission channels and the routing paths. A robust technology is required to transfer the III-V material on the silicon platform. In the last decade two main technologies have been used extensively to integrate III-V on silicon. These are: (1) Direct bonding technology [2-3] and (2) Adhesive bonding technology [4-5]. Recently, a new way -direct growth- of integrating III-V on silicon has also been considered and is under investigation in different research groups [6-9]. Since the microdisks used for the functionalities reported here were fabricated using either direct bonding technology or adhesive bonding technology, a brief description of both of these will be given in section 2.4. In section 2.2, a description of the epitaxial structure of the III-V material is provided. Later on, the structure of the fully fabricated microdisk is discussed. Sec-

tion 2.3 highlights the fabrication technology aspects of SOI waveguide circuits while section 2.5 provides an overview of III-V processing steps to fabricate microdisks.

2.2 Design of III-V-on-silicon microdisks

The base material used for fabricating the microdisks is the InP, a III-V group material. The material growth was done at INL (L'Institut des Nanotechnologies de Lyon) in France using solid source molecular beam epitaxy (SSMB) on a two inch wafer at 490 °C. One of the difficulties in fabricating the microdisk is to form an ohmic contact at the p-type layer of the junction. Normally it can be done by using a heavily p-doped layer, but these layers are highly absorbing and hence not suitable for thin membranes. To overcome this problem, a tunnel junction based design is used which allows to have two n-type contacts. The tunnel junction consists of two very thin (20 nm), highly doped layers (10^{19} cm^{-3}) and is reverse biased [10]. The use of a tunnel junction makes it possible to have a low electrical resistivity and acceptable optical losses. The total

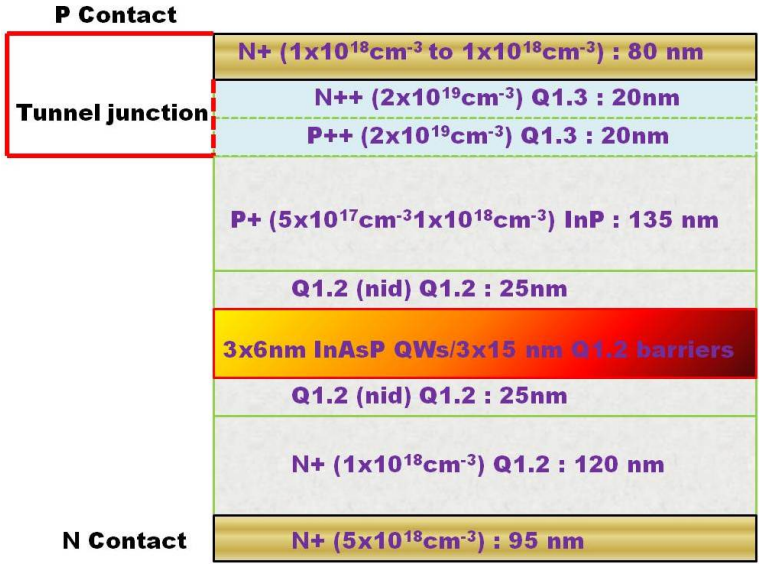

Figure 2.1: Epitaxial structure of InP based material.

thickness of the epitaxial membrane is 583 nm. A schematic of the epitaxial membrane is shown in figure 2.1 which gives the details of the other parts of the membrane. Most important is the fact that three compressively strained quantum wells are meant to provide transverse electric (TE) gain [10-11]. In figure

2.2, a schematic of the structure of a III-V microdisk [12] integrated on top of an SOI waveguide circuit is drawn. The bonding layer (of BCB/silica) and the metal contacts meant for the electrical injection are also shown in this figure.

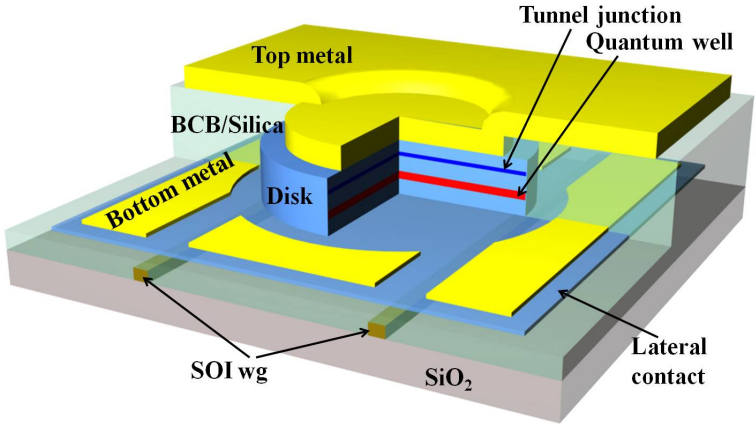

Figure 2.2: Structure of a III-V-on-silicon microdisk [12].

To make the designs of III-V-on-silicon microdisk based PICs, the PICAZZO and IPKISS softwares [13] are used extensively. These are in-house developed softwares of INTEC Photonics, Ghent University (Belgium). The SOI waveguide circuits are designed using PICAZZO while the mask layers to define the III-V microdisks and the metalization for electrical contacts are designed using IPKISS. As an illustration, the virtual fabrication diagram of an SOI waveguide circuit generated from a .gds file is shown in figure 2.3 (top). It can be seen from this figure that the grating couplers for in- and out- coupling of light to/from the SOI waveguide are shown at the ends of the waveguides. Details about the grating couplers have been provided in the previous chapter (section 1.3). Since high-index contrast is needed for high optical confinement factor of light in the III-V microdisk, a part of the silicon is replaced by silica. This is the area where the III-V material will remain after the complete fabrication. The same is visible in the top part of the figure 2.3 indicated by the blue color. In the same figure at the bottom side the snap shot of the .gds file is shown which shows the microdisk design on top of an SOI waveguide. In this figure a microdisk coupled to a single waveguide is shown but as the complexity level of the PICs increases, the microdisks coupled to the waveguides from two or more sides are needed. This will be elaborated in chapter 6 while describing the design of the complex PICs such as data flip-flops and shift registers. The GSG (ground-signal-ground) electrical contact pads at a pitch of 150 μm are designed to enable high-speed electrical probing. This kind of electrical pads are not necessary for static (dc)

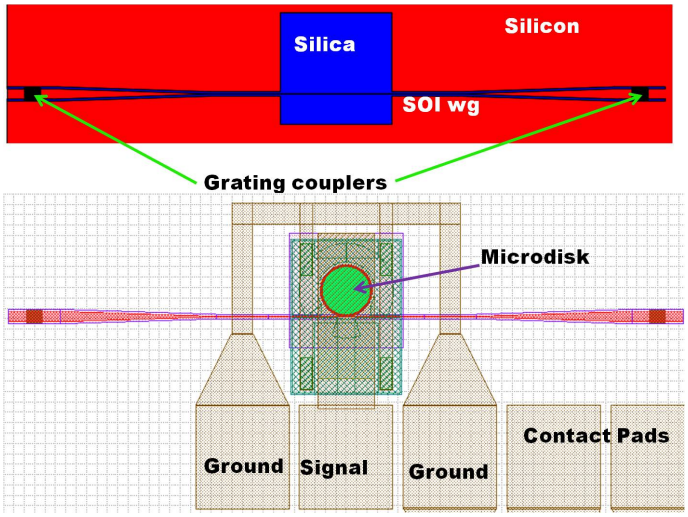

Figure 2.3: Design of a III-V-on-silicon microdisk.

electrical probing of the microdisks but are needed when a high speed electrical signal is needed to drive the microdisk. For example, the high-speed electrical signal is required (a) for direct modulation of microdisk lasers [14] and (b) when using microdisk as an electro-optic modulator [15]. In figure 2.4, the design layers for III-V microdisk fabrication and metalization are presented in a sequential order.

2.3 SOI optical waveguide circuit technology

The wafers of the SOI optical waveguide circuits are fabricated using the ePIXfab platform [16]. These wafers are diced to get dies when required. For the fabrication of SOI optical waveguide circuits, the starting material system is an SOI wafer with crystalline silicon of 220 nm thickness on 2 μm buried oxide. The SOI wafers are of 200 mm diameter and are purchased from SOITEC [17]. The process of SOI waveguide circuit fabrication is light and dark field in LETI and IMEC, respectively. In the case of a light field based process, the silicon waveguide is surrounded by silica while in the case of a dark field the silicon waveguides have trenches of silica surrounded by silicon. The waveguides are defined using 193 nm deep ultra violet (DUV) lithography. Generally the waveguide width is in the range of 450-600 nm for the devices using the telecommunication wavelength. The height of the SOI waveguide is 220 nm. These dimensions are optimized for the SOI waveguides to be single mode in the telecommunication wavelength band around 1550 nm. As an illustration, a SOI waveguide

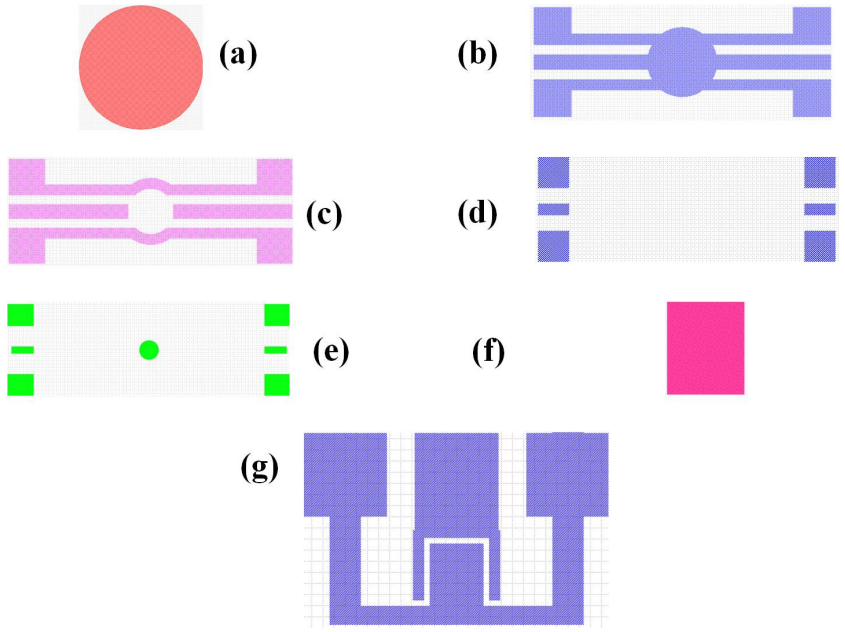

Figure 2.4: Design layers of a III-V microdisk : (a) disk definition, (b) island, (c) Bottom metal, (d) bottom via, (e) top via, (f) top metal and (g) electrical contact pads.

fabricated at imec is shown in figure 2.5. More information about the fabrication process of SOI photonic wire waveguides can be found from references [18-19].

2.4 Bonding technology for III-V-on-silicon

For the integration of two different material systems direct molecular bonding or adhesive bonding techniques have been used extensively in the past decade. Direct molecular bonding [20] relies on the van der Waals interaction between both surfaces. As this is a short-range force, sub-nm rms roughness of the surfaces is required [21]. This can be obtained on unprocessed SOI wafers using chemical mechanical polishing (CMP) which is also the preferred way to fabricate SOI layer stacks. In case of adhesive bonding, one of the main advantages is that the surface quality required for bonding is less stringent as the polymer wets the surface and fills the troughs of the surface. For the devices investigated in this work both the bonding technologies were used. For the microdisks used for flip-flop operation and biased optical gating, DVS-BCB polymer based adhesive bonding was used. While for the devices used for bias-free all-optical

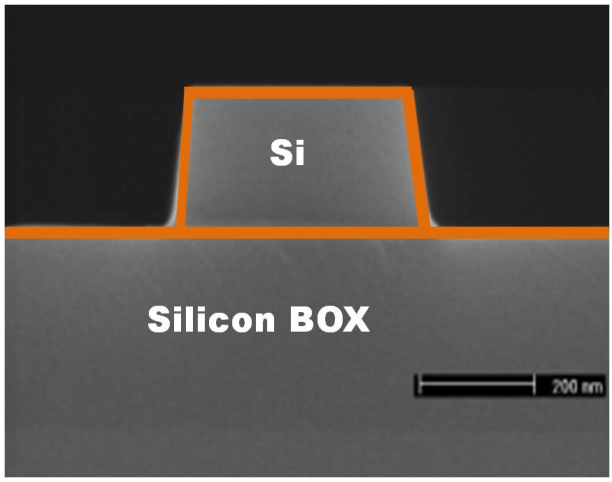

Figure 2.5: Silicon-on-insulator waveguide fabricated at imec.

gating, wavelength conversion, de-multiplexing and format conversion, direct bonding was used and the complete fabrication run was done in a 200 mm CMOS pilot line at LETI in France. The next two subsection are devoted for the description of each of these bonding processes.

2.4.1 Adhesive bonding

The bird's eye view of adhesive bonding between a III-V die and an SOI die is drawn in figure 2.6 (a). In order to achieve a good bond, the die surface needs to be very clean, since the inclusion of particles at the bonding interface can result in large unbonded areas. Therefore, cleaning of the SOI die as well as the III-V die is of paramount importance. The hydrocarbon contamination of an SOI die can be removed by immersing the sample in a Piranha solution, a warm mixture of $3H_2SO_4 : 1H_2O_2$. In a second step, particles can be removed by using a Standard Clean 1 solution. This solution is a mixture of NH_4OH, H_2O_2 and H_2O. After surface cleaning, the commercially available adhesion promoter AP3000 is applied by spin coating. The cleaning of the InP/InGaAsP dies can best be done by removing a pair of sacrificial InP/InGaAs layers by selective wet etching using the etchants $3HCl : H_2O$ and $1H_2SO_4 : 3H_2O_2 : 1H_2O$, respectively. This etch lifts-off foreign particles and etches down and lifts off InP/InGaAsP particles, created by the cleaving or dicing of the dies. No adhesion promoter is applied to the III-V surface, as this would require spin coating of the individual cleaved dies, which is very time intensive and leads to the formation of an edge bead. After surface cleaning, the DVS-BCB is deposited on the SOI die

surface by spin coating. Although most of the mesitylene solvent already evaporates during the spin-coating process, some solvent may still be remaining in the spin-coated film, which is evaporated by a thermal treatment at 150 °C for one minute. This thermal treatment also causes a reflow of the DVS-BCB, which improves its planarizing properties. In the next step, both samples are brought into contact. Attachment is done at 150 °C, as DVS-BCB has about the lowest viscosity at this temperature [22] and keeping the DVS-BCB at this temperature does not significantly increase the degree of polymerization for at least an hour. The attachment of the III-V die onto the SOI waveguide circuit can be done in clean room air, by using tweezers to attach the die to the host substrate. After attachment of the III-V die, the DVS-BCB film has to be cured. The curing has to be performed in an atmosphere containing less than 100 ppm oxygen, to prevent the oxidation of the DVS-BCB. In order to do so, nitrogen is purged through the curing chamber. After bonding of the InP/InGaAsP die, the InP substrate needs

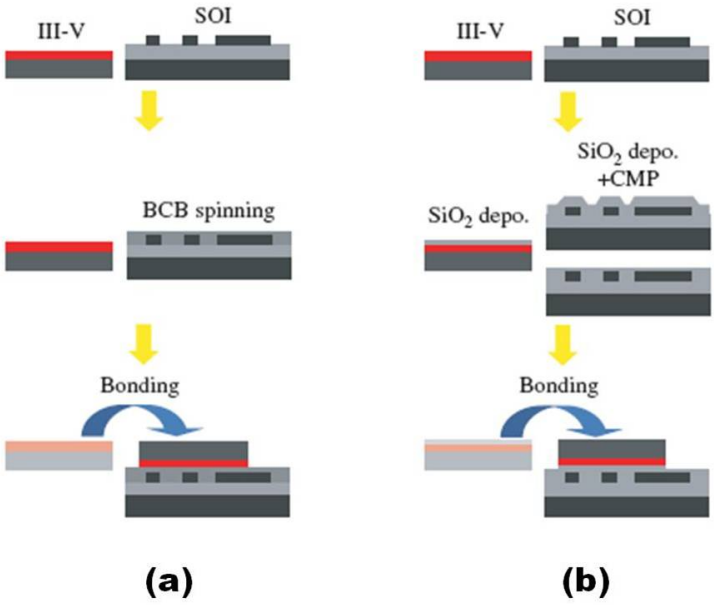

Figure 2.6: Sketch of (a) BCB adhesive bonding and (b) SiO_2 direct bonding. The sketch is adapted from [23].

to be removed so that InP/InGaAsP epitaxial layers can be accessed and processed. The InP substrate can be removed by complete wet chemical etching or by using a combination of mechanical grinding and wet chemical etching. Complete chemical etching can be done using a mixture of HCl and H_2O. For a good compromise between etch rate and etching quality a mixture of 3HCl

: $1H_2O$ is used. An InGaAs etch stop layer can be used, which shows nearly complete etching selectivity to InP. However, the drawback of complete chemical etching using a HCl : H_2O etching solution is the arising of unetched ramps at two sides of the cleaved InP die. Since no isotropic but selective etching solution for InP is known, a combination of isotropic non-selective etching and anisotropic selective etching can be used to avoid the formation of the ramps. A combination of HNO_3 : HCl and 3HCl : H_2O is a good choice to avoid the formation of the ramps. Good timing for changing the etch bath is needed in order to prevent the etching of the InP/InGaAsP epitaxial layers by the non-selective HNO_3 : HCl etchant.

2.4.2 Direct bonding

The process of direct bonding of III-V material on a SOI wafer is depicted in figure 2.6(b). The description given in this section is based on the process flow as is done at LETI [24] in a 200 mm CMOS pilot line. In this process, the unpatterned III-V wafer is integrated on top of a processed SOI wafer by means of SiO_2/SiO_2 bonding. The thickness of SiO_2 above the Si waveguide is adjusted to be 100 nm. In the next step CMP is performed. Following the CMP, the SOI wafers are cleaned in a RCA solution, which is performed in a specific equipment - the FSI Magellan. The InP heterostructure is directly covered by a 10 nm thick SiO_2 layer compatible with direct bonding (means a roughness < 0.5 nm RMS) deposited by plasma-enhanced chemical vapor deposition (PECVD). In order to prevent the undesirable outgassing from the oxide layer during subsequent heat treatments, the wafers are annealed at a temperature higher than the subsequent processing temperature after SiO_2 deposition. After annealing, the InP wafer is first cleaned in acetone and ethanol, followed by a DI water rinse and blow-dried in nitrogen. The O_2 plasma treatment is then performed in order to activate the surface by creating a high density of hydroxyl groups (-OH). The wafers are then brought in contact at room temperature to perform the bonding. Since the III-V structures are fabricated after bonding, no tight alignment is needed at this stage. Finally, the bonded pair is annealed at 200°C for three hours. A selective wet etching in 3HCl : $1H_2O$ and $1H_2SO_4$: $1H_2O_2$: $10H_2O$ is done to remove the InP substrate and InGaAs etch stop layer, respectively. After this, the III-V material bonded on silicon becomes ready for further processing of devices in III-V.

2.5 Post bonding InP processing

For the BCB bonded samples, the InP processing was done partly in the UGent clean room and partly in the COBRA (Technical University of Eindhoven) clean

room. For molecularly bonded samples , the InP processing was done completely at LETI in France. A description of this can be found in reference [24]. I was not involved in fabrication done at LETI. In the following section, a description of the InP processing, as done in the UGent clean room and the COBRA clean is provided. I was involved only in post bonding InP processing at UGent clean room and COBRA clean room.

2.5.1 Microdisk definition

In order to define the microdisks, a hard mask of SiO_2 with a thickness of 200 nm is deposited on top of the bonded samples. The contact lithography is used in combination with a silica etching . Positive-tone photoresists are used in this work (AZ5214 or HPR 504), which also can be used for image reversal, using a flood exposure. After spin coating of photoresist, typically at 3000 RPM (rotations per minute), the chip is pre-baked at 100 °C. Then, the glass mask plate - containing the microdisk patterns in chromium - is aligned with respect to the sample in the mask aligner tool (Karl Suss MA-6). After alignment using the complementary markers in the chromium plate with respect to the SOI markers, the mask plate is pushed against the photoresist and the sample is illuminated, with 320 nm wavelength. After an additional post bake at 110 °C, the photoresist is developed. This is followed by stripping of the photoresist by oxygen plasma. In the next step, the oxide hard mask is removed using a reactive-ion etching (RIE) process.

2.5.2 InP etching

Inductively coupled plasma (ICP) etching is used to etch the InP material so that it leaves a thin (around 90 nm) bottom contact layer. This is the most crucial step for the fabrication of InP microdisks and an optimized recipe is required as the total thickness of the InP material is only 583 nm. During InP etching the ICP machine is operated with an RF power of 110 W and maintains a pressure of 23 mTorr. In total normally eight cycles of etching are required to etch around 480 nm deep into the InP. In order to have an idea of the etch rates, the process of etching is completed in two or three steps. After 4-5 cycles, the etch depth is measured using a profilometer. Figure 2.7 shows the SEM images after InP etching where in (a) the InP microdisk aligned to the SOI waveguide is shown while in (b) a view of another microdisk covered with the hard mask is shown. In the next step, the hard mask is removed by image reversal lithography and plasma etching. This is followed by island definition. Defining of the islands means that the bottom contact layer of III-V material is removed from all the places except in the vicinity of the microdisks. In order to define islands, lithography is followed by RIE to remove III-V material.

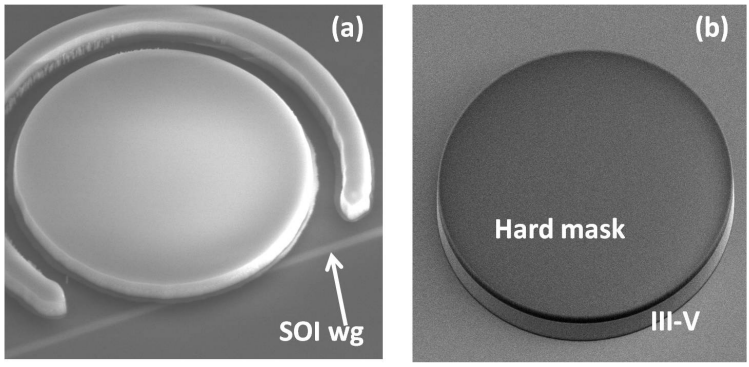

Figure 2.7: SEM image of (a) a microdisk aligned to an SOI waveguide and (b) a microdisk covered with the SiO_2 hard mask.

2.5.3 Contacts definition and Isolation

After island definition, photoresist is spin coated on the chip which is followed by the image reversal lithography. The bottom contact is formed by evaporating the Ti(25 nm)/Pt(50 nm)/Au(100 nm) followed by the metal lift-off. In order to optically isolate the waveguides - both the SOI waveguides and the microdisk resonator-from the absorptive metal contacts, a DVS-BCB polymer is spun over the chip. Undiluted DVS-BCB Cyclotene (3022-35) is used for this purpose. The polymer is spin coated at 5000 RPM. Then, the DVS-BCB is cured in an N_2 atmosphere to avoid oxidation, with the following temperature evolution. First the temperature is increased to 150°C at a rate of 5°C/minute. Then the temperature is increased to 250 °C at a rate of 1.6°C/minute, and kept at that temperature for 60 minutes. Finally, the sample is left to cool down. The shape and position of the top contact via in the DVS-BCB layer is of paramount importance for proper device operation, since it determines where the subsequently deposited metal will be in contact with the microdisk. The most important thing to be taken care of is that no metal contacts should be deposited on top of the whispering-gallery zone, as this would lead to excessive optical absorption. The top and the bottom vias are defined in separate lithography and etching steps, since they require different etch depths. Contact lithography is used in combination with the AZ5124 resist, which is also used as an etch mask. Both the bottom and top vias are etched by ICP-RIE, using a SF_6/O_2 gas mixture (5/40 sccm) at 60 mTorr and 150W RF power and 50W ICP power. To soften the sidewall edges of the deep bottom vias, they are subsequently treated with an RIE step using the same gas flow, but at a high pressure (1000 mTorr) and 100W RF power. After the definition of the bottom via, the next step is to deposit the top contact metal using the image reversal lithography and metal evaporation. The

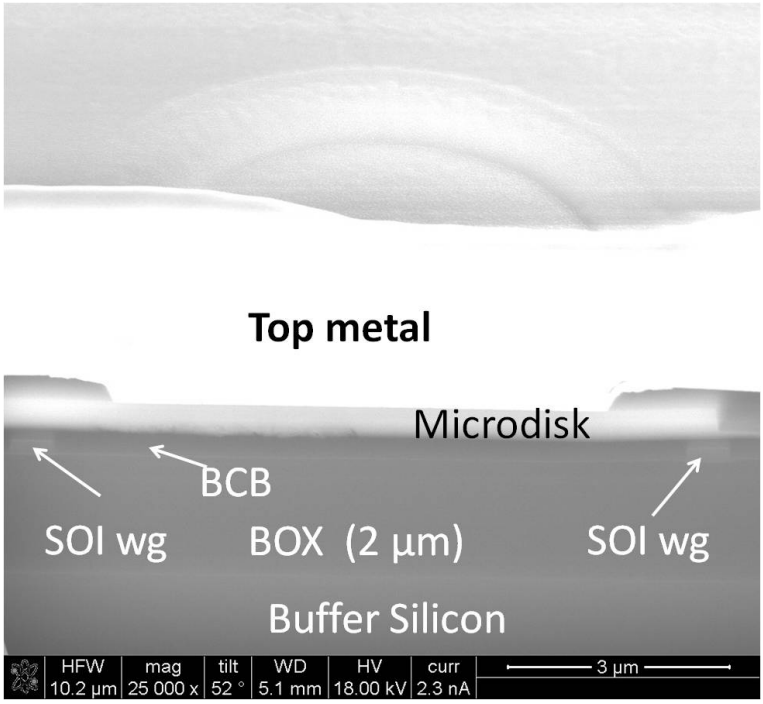

Figure 2.8: FIB-SEM image of a fully fabricated III-V microdisk on an SOI waveguide circuit.

metal combination is Ti(25 nm)/Pt(50 nm)/Au(100 nm). This is followed by the metal lift-off.

2.5.4 Probe pads definition

The final step for making the microdisks ready for electrical injection is the definition of the contact metal for the electrical probing pads. The process to deposit the metal for electrical probe pads is similar to the metal deposition for bottom metal definition and the top metal definition. But the metal combination is different. The Ti(40 nm)/Au(500 nm) is deposited by the evaporation technique using resistance heating.

2.6 Overview of fully fabricated chips

The fabrication process is complete after definition of the electrical probe pads. For an illustration, in figure 2.8, the focussed-ion beam (FIB)-SEM image is

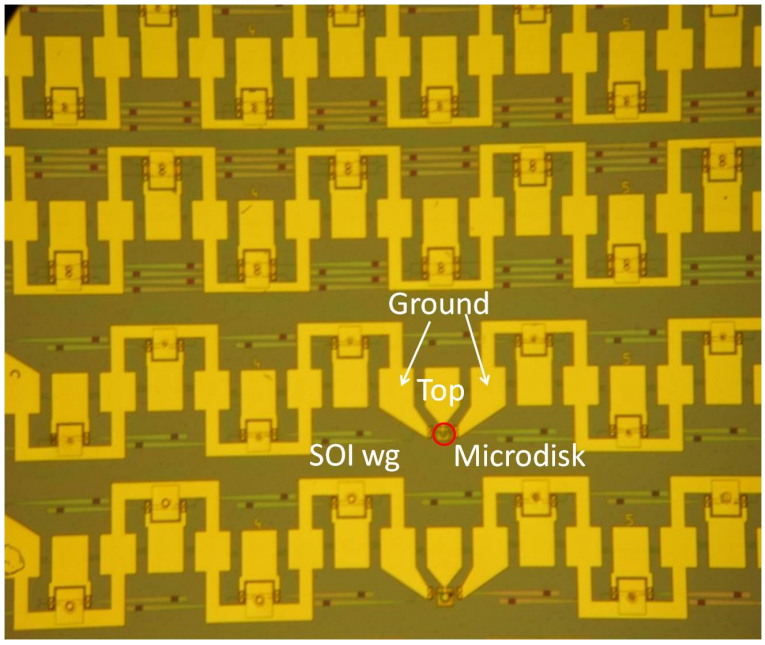

Figure 2.9: Overview of a fully fabricated chip.

shown depicting the fully fabricated III-V microdisk on a SOI waveguide circuit. It also shows the buffer silicon on which SOI waveguide circuits are fabricated. In the next figure, an optical microscope picture of a fully fabricated chip is shown depicting the array of the microdisk based devices. This figure also indicates the location of the electrical contact pads.

2.7 Conclusions

In this chapter, the design, structure and the overview of the fabrication process used for making III-V microdisk based devices and PICs is provided. Adhesive and direct bonding technologies are discussed in view of their importance and necessity for heterogeneous integration of III-V material based active devices on top of passive silicon waveguide based circuits. Details of the microdisks after etching are given, as inspected by the SEM. Details of the fully fabricated devices are also given. These details are obtained by using FIB-SEM and optical microscope.

References

[**1**] D. Liang and J. Bowers. *Recent progress in lasers on silicon.* Nature Photonics, 4:511-517, 2010.

[**2**] T. Maruyama, T. Okumura and S. Arai. *Direct wafer bonding of GaInAsP/InP membrane structure on silicon-on-insulator substrate.* Japanese Journal of Applied Physics, 45(11):8717-8718, 2006.

[**3**] T. R. Chung, L. Yang, N. Hosoda and T. Suga. *Room temperature GaAs-Si and InP-Si wafer direct bonding by the surface activated bonding method.* Nuclear Instruments and Methods in Physics Research B, 121:203-206, 1997.

[**4**] G. Roelkens, J. Brouckaert, D. Van Thourhout, R. Baets, R. Notzel and M. Smit. *Adhesive bonding of InP/InGaAsP dies to processed silicon-on-insulator wafers using DVS-bis-Benzocyclobutene.* Journal of Electrochemical Society, 153(12):G1015-G1019 2006.

[**5**] S. Stankovic, R. Jones, J. Heck, M. Sysak, D. Van Thourhout and G. Roelkens. *Die-to-die adhesive bonding procedure for evanescently-coupled photonic devices.* Electrochemical and Solid-State Letters, 14(8):H326-H329, 2011.

[**6**] T. Orzali, G. Wang, N. Waldron, C. Merckling, O. Richard, H. Bender, W.-E. Wang and M. Caymax. *In situ HCl etching of InP in shallow-trench-isolated structures.* ECS transactions, 41(7): 345-354, 2011.

[**7**] L. Cerutti, J.B. Rodriguez and E. Tournie. *GaSb-based laser, monolithically grown on silicon substrate, emitting at 1.55 μm at room temperature.* IEEE Photonics Technology Letters, 22(8):553-555, 2010.

[**8**] S. Liebich, M. Zimprich, A. Beyer, C. Lange, D.J. Franzbach, S. Chatterjee, N.Hossain, S.J. Sweeney, K. Volz, B.Kunert and W. Stolz. *Laser operation of Ga(NAsP) lattice-matched to (001) silicon substrate.* Applied Physics Letters, 99:071109-1 to 0771109-3, 2011.

[**9**] Z. Wang, C. Junesand, W. Metaferia, H.Chen, S. Lourdudoss and L. Wosinski. *A monolithic integration platform for silicon photonics.* ICO International Conference on Information Photonics, pp.1-2, 2011.

[**10**] T. Spuesens, L. Liu, T. de Vries, P.R.-Romeo, P. Regreny and D. Van Thourhout. *Improved design of an InP-based microdisk laser heterogeneously integrated with SOI.* IEEE International Conference on Group IV Photonics, United States, p.FA3, 2009.

[**11**] D. Van Thourhout, T. Spuesens, S. Selvaraja, L. Liu, G. Roelkens, R. Kumar, G. Morthier, P.R.-Romeo, , F. Mandorlo, O. Raz, C. Kopp and L. Grenouillet. *Nanophotonic devices for optical interconnect.* IEEE Journal of Selected Topics in Quantum Electronics (invited), 16(5):1363-1375, 2010.

[**12**] R. Kumar, L. Liu, G. Roelkens, E.-J.Geluk, T. de Vries, F. Karouta, P. Regreny, D. Van Thourhout, R. Baets and G. Morthier. *10 GHz All-optical gate based on a III-V/SOI microdisk.* IEEE Photonics Technology Letters, 22(13):981-983, 2010.

[**13**] Webaddress : *www.ipkiss.be*

[**14**] O. Raz, H.J.S. Dorren, R. Kumar, G. Morthier, P. Regreny and P.R.-Romeo. *50 fJ-per-bit, high speed, directly modulated light sources for On-chip optical data communications.* The Optical Fiber Communication Conference and Exposition (OFC) and the National Fiber Optic Engineers Conference (NFOEC), paper.OMM5, 2011.

[**15**] L. Liu, J. Van Campenhout, G. Roelkens, R.A. Soref, D. Van Thourhout, P.R.-Romeo, P. Regreny, C. Seassal, J.-M. Fédéli and R. Baets. *Carrier-injection-based electro-optic modulator on silicon-on-insulator with a heterogeneously integrated III-V microdisk cavity.* Optics Letters, 33(21): 2518-2521, 2008.

[**16**] Web address : *http://www.epixfab.eu*

[**17**] Web address : *http://www.soitec.com/en/index.php*

[**18**] W. Bogaerts, R. Baets, P. Dumon, V. Wiaux, S. Beckx, D. Taillaert, B. Luyssaert, J. Van Campenhout, P. Bienstman and D. Van Thourhout. *Nanophotonic waveguides in silicon-on-insulator fabricated with CMOS technology.* Journal of Lightwave Technology (invited), 23(1):401-412, 2005.

[**19**] S. Selvaraja, P. Jaenen, W. Bogaerts, P. Dumon, D. Van Thourhout and R. Baets. *Fabrication of photonic wire and crystal circuits in silicon-on-insulator using 193 nm optical lithography.* Journal of Lightwave Technology, 27(18):4076-4083, 2009.

[**20**] Q.-Y. Tong and U. Gosele. *Semiconductor Wafer Bonding - Science and Technology.* The Electrochemical Society Series, Wiley Interscience, 1999.

[**21**] N. Miki and S.M. Spearing. *Effect of nanoscale surface roughness on the bonding energy of direct-bonded silicon wafers.* Journal of Applied Physics, 94:6800-6806, 2003.

[**22**] F. Niklaus, R.J. Kumar, J. J. McMahon, J. Yu, J.-Q. Lu, T. S. Cale and R. J. Gutmann. *Adhesive wafer bonding using partially cured benzocyclobutene for three-dimensional integration.* Journal of Electrochemical Society, 153(4):G291-G295, 2006.

[**23**] L. Liu, G. Roelkens, J. Van Campenhout, J. Brouckaert, D. Van Thourhout and R. Baets. *III-V/silicon-on-insulator nanophotonic cavities for optical network-on-chip.* Journal of Nanoscience and Nanotechnology (invited), 10(3)1461:1472, 2010.

[**24**] J.-M.Fedeli, L. Liu, L. Grenouillet, D. Bordel, F. Mandorlo, N.Olivier, T. Spuesens, P. Regreny, P. Grosse, P. Rojo-Romeo, R. Orobtchouk, D. Van Thourhout. *Towards optical networks-on-chip with 200mm hybrid technology.* Optical Fiber Communication Conference and Exposition/National Fiber Optic Engineers Conference(OFCNFOEC), paper OMM3, 2011.

3

Microdisk laser as an all-optical flip-flop

Digital subsystems for optical processing are of great importance due to their intrinsic properties such as large bandwidth and immunity to the electromagnetic interference and their potential for achieving high speed with low power consumption. The key basic functionalities for optical processing are logic gates, mux/demux, optical buffers or optical random access memories (ORAMs) and wavelength convertors etc. Out of all these functionalities, optical buffers or ORAMs are the least mature from the point of view of practical applications. This is mainly due to the fact that the devices investigated for optical buffering had large foot-prints [1-2] and many of them operated with high power consumption [3].

Multi-bit ORAM can be constructed by cascading many single all-optical flip-flops. In this chapter, the results on experimentally demonstrated all-optical flip-flops using a single microdisk laser of only 7.5 μm diameter are presented. It is important to mention here that the devices used for experiments were jointly fabricated by Dr. Liu Liu and my self. Also, Dr. Koen Huybrechts helped during dynamic measurements. The chapter begins with a background on the need of an ORAM, highlights the theory of bistability and practical challenges to achieve it in the small dimension microdisks and ends with the conclusions and the discussion of the obtained results.

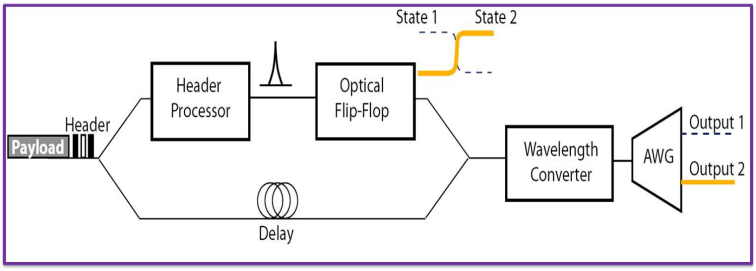

Figure 3.1: Schematic of 1x2 all-optical packet switch showing the all-optical flip-flop needed to store the processed header information [4].

3.1 Need of an all-optical buffer

For fully functional photonic chips for short reach communications, many active functionalities are needed and optical flip-flops or optical buffers are one of them. An example of a fully functional digital photonic circuit is represented by figure 1.8 in chapter 1 in which flip-flops are used as memory elements. At the same time, all-optical packet switching is being considered as the long term solution for the problems arising due to the exponential increase in the data rates in optical telecommunication networks. An all-optical flip-flop memory or ORAM is envisaged as an integral part of an all-optical packet switch [4] as shown in figure 3.1. In this figure, the arrayed waveguide(AWG) forms the demultiplexing unit. Depending upon the information in the header, a pulsed output from the header processing unit changes the state of the flip-flop.

In order to process the header and to resolve the contention in optical networks in the optical domain itself, a good ORAM is required. Unfortunately, a good ORAM which can be competitive or better as compared to an electronic RAM in terms of power consumption, footprint and buffer time does not exist yet. The main requirements to be met by optical buffers are briefly discussed in the next paragraph. The primary reason for the need of an ORAM is the fact that it will eliminate the need of optoelectronic conversions. Optoelectronic conversions are power hungry. This can be understood by an example as presented in reference [5] taking the case of a packet router. An OC-768 16:1 multiplexer-demultiplexer chip set typically dissipates 4.5 W of power [6]. An additional OC-48 8:1 multiplexer-demultiplexer typically dissipates 2.5 W of power [7]. This brings the total power consumption for the chip sets required to demultiplex a 40 Gbits/s data stream into 64 622 Mbits/s data streams to approximately 45 W (per wavelength channel). An equal amount of power is required for multiplexing. Apart from that, a 40 GHz clock recovery circuit typically dissipates 15 W of power [8]. This brings the total power consumption for demultiplexing, multi-

plexing, and clock recovery for a single 40 Gbits/s channel to the order of 100 W. This sounds moderate, but in the case of a thousand-port switch, this adds up to 100,000 W of power, only for optoelectronic conversions.

Optical buffers must meet certain requirements to achieve acceptance [9]. First of all, it is necessary that a buffering approach can impart a delay of at least the length of the packet payload in order to provide contention resolution. It is important for the buffering device to be bit rate scalable to 10 Gbits/s or more to offer an advantage over their electrical counterparts. For acceptable network loads, optical buffers should have the capability to store packets of at least 40 bytes with guard bands no more than several nanoseconds long. Packet payload length is one of the difficult challenges for many buffering approaches, but unless the ratio of the payload length to the overhead of the header and guard-bands is reasonable, optical buffers and packet switches can not be advantageous. In addition, it is desirable to require less header processing for a given amount of payload. In order to accommodate short guard bands, buffers must be able to switch or reset in less than several nanoseconds. There are also other considerations that increase the probability of success of a given optical buffer approach. As usual, low cost is a main issue. Optical packet switches must lower the cost per bit for data transmission to make them advantageous. It is also necessary that optical buffers have low power consumption, low heat dissipation, and a small footprint. For both cost and footprint, it is obviously important that the number and complexity of components included in a given buffer architecture must be kept to a minimum. In order to make the optical buffer more flexible, it is desirable for the buffer to be transparent to packet length and to provide dynamically variable storage time. Apart from these architectural considerations, it is also desirable that the buffer devices impart the least possible dispersion and minimum optical power penalty.

3.2 Laser theory for optical bistability

The possibility of achieving bistability in two mode lasers via gain saturation was first explained mathematically in terms of an idealized model in [10]. In this section, description of bistable operation of a two mode semiconductor laser based upon the mode competition through gain saturation is presented. The notations used here are the same as in [11].

The saturated gain of a given mode in an ideal laser is related to the unsaturated gain through the following relation:

$$g(I) = g[1 - SI]$$

where *I*, *g(I)* and *g* are the mode intensity, saturated gain and unsaturated gain respectively. And $S = \frac{1}{I_{sat}}$ where I_{sat} is the saturation parameter. In case of

two modes, the rate of change of the intensity of one mode depends upon the intensity of the other mode and can be expressed by the equations *(3.1)* and *(3.2)*.

$$\frac{dI_1}{dt} = g_1(I_1, I_2)I_1 = g_1 I_1[1 - S_1 I_1 - C_{12} I_2] \tag{3.1}$$

$$\frac{dI_2}{dt} = g_2(I_1, I_2)I_2 = g_2 I_2[1 - S_2 I_2 - C_{21} I_1] \tag{3.2}$$

In the equations above *S's, C's* and *g's* represent the self-gain saturation coefficient, the cross-gain saturation coefficient and the net gain of each mode respectively. The stability of such a gain-coupled two-mode system can be analyzed in the phase plane (I_1, I_2) by looking at the slope of the trajectory of $I_2(I_1)$ given by

$$\frac{dI_2}{dI_1} = \frac{g_2 I_2[1 - S_2 I_2 - C_{21} I_1]}{g_1 I_1[1 - S_1 I_1 - C_{12} I_2]} \tag{3.3}$$

which is obtained after dividing equation *(3.2)* by *(3.1)*. The trajectories of

$$\frac{dI_2}{dI_1} = 0 \tag{3.4}$$

and

$$\frac{dI_2}{dI_1} = \infty \tag{3.5}$$

cross at a point X (x_1, x_2) such that

$$x_1 = \frac{(C_{12} - S_2)}{(C_{21}C_{12} - S_1 S_2)} \tag{3.6}$$

$$x_2 = \frac{(C_{21} - S_1)}{(C_{21}C_{12} - S_1 S_2)} \tag{3.7}$$

The bistability occurs when the product of cross-gain saturation coefficients exceeds the product of self-gain saturation coefficients i.e. $C_{21}C_{12} > S_1 S_2$. Within the case of bistability, if $x_1 < 0$ and $x_2 > 0$ then mode 1 will oscillate; and mode 2 will oscillate when $x_2 < 0$ and $x_1 > 0$.

A model proposed by Sorel et.al. [12] fits well to describe the occurrence of bistability in case of a microdisk laser. This model takes into account the carrier reservoir, gain saturation and linear coupling between the CW and CCW mode. The linear coupling between CW and CCW modes will be addressed further in the next subsections too. The model proposed by Sorel et.al. has been used to simulate the LI curves of a microdisk laser by Yanick De Koninck [13]. The rate equation model of the microdisk laser described here is the same as presented in the thesis of Dr. Koen Huybrechts [14] which is primarily based on the model proposed by Sorel et. al.[12]. If the electric field associated to the clockwise

mode is denoted as E^+ and that in the counter clockwise direction as E^-, the rate equations can be written as follows :

$$\frac{dE^+}{dt} = \frac{1}{2}(1+j\alpha)\left[G^+ - \frac{1}{\tau_p}\right]E^+ - KE^- \tag{3.8}$$

$$\frac{dE^-}{dt} = \frac{1}{2}(1+j\alpha)\left[G^- - \frac{1}{\tau_p}\right]E^- - KE^+ \tag{3.9}$$

where α is line width enhancement factor accounting for phase-amplitude coupling in the semiconductor medium, G is the modal gain factor which will be described further and K = K_d + jK_c represents an explicit linear coupling rate between the two modes. Here K_d is the dissipative coupling and K_c is the conservative coupling. This coupling describes the effect of scattering due to sidewall roughness of the microdisk and the reflections from different points such as grating couplers, disk-waveguide interface and the fiber facets. The carrier density rate equation can be written as

$$\frac{dN}{dt} = \frac{I}{qV} - \frac{N}{\tau_c} - G^+|E^+|^2 - G^-|E^-|^2 \tag{3.10}$$

where N, I, q, V and τ_c are carrier density, applied current, elementary charge, volume of active region and carrier life time respectively. The gain suppression takes place due to spectral hole burning and carrier heating. In order to account for this effect, a gain suppression is added in the denominator of the expression for the modal gain :

$$G^+ = \frac{\Gamma g_0 v_g (N - N_0)}{1 + \epsilon_s|E^+|^2 + \epsilon_c|E^-|^2} \tag{3.11}$$

$$G^- = \frac{\Gamma g_0 v_g (N - N_0)}{1 + \epsilon_s|E^-|^2 + \epsilon_c|E^+|^2} \tag{3.12}$$

where Γ, g_0, v_g and N_0 represent the mode confinement factor, differential gain, group velocity and 'carrier density at transparency' respectively. The ϵ_s reflects the self-gain suppression while ϵ_c reflects the cross-gain suppression. These expressions can be re-written as follows:

$$G^+ = \Gamma g_0 v_g (N - N_0)(1 - \epsilon_s|E^+|^2 - \epsilon_c|E^-|^2) \tag{3.13}$$

$$G^- = \Gamma g_0 v_g (N - N_0)(1 - \epsilon_s|E^-|^2 - \epsilon_c|E^+|^2) \tag{3.14}$$

It can be proved that ϵ_c = $2\epsilon_s$ [15-16]. The cross-gain suppression ϵ_c will break the symmetry and enforce the unidirectional operation of the laser. The gain suppression is, however, only significant when the photon density is high. At lower powers laser will operate in a bidirectional regime.

From the above equations, we can conclude that there are two main effects in the coupling between the two modes: (a). The linear coupling K due to reflections at the end facets (dissipative) and due to sidewall roughness (conservative). Unidirectional operation is favoured by a lower value of the coupling K. (b). The nonlinear cross-gain suppression prohibits the counterpropagating cavity mode to build up. This effect is necessary for the unidirectional operation and occurs at large values of the photon density. The above equations have been used to implement a simulation tool to study the influence of the laser parameters. More information on this topic is available in the Master thesis of Yanick De Koninck [13]. In Figure 3.2, a typical light-current (L-I) graph of a ring/disk laser structure is depicted. Three different operating regimes can be seen in this figure. The first regime, just after threshold, is the bidirectional regime where the two counterpropagating modes are equally strong. There will be a small notch in their spectrum as the coupling between the two modes will introduce a very small frequency splitting. When the injection current is increased, laser operates a bidirectional regime with alternating oscillations [12, 17]. In this regime, the intensities of the two counterpropagating modes are modulated with harmonic sinusoidal oscillations. The modulation is out-of-phase (or alternate) which means that the power in one mode is high when it is low in the other mode. The graph depicts the maximal and minimal values of the mode intensities. The last regime is the unidirectional regime and the initial conditions determine which of the two modes is dominant [18]. When the laser operates in a unidirectional regime, one can switch the lasing direction (from CW to CCW and vice-versa) by exterally injecting an optical pulse to realize the flip-flop operation.

3.3 Practical challenges to achieve bistability

The main problem for achieving the bistability in a microdisk laser arises from coupling between CW and CCW modes. The coupling between CW and CCW modes depends on the surface roughness of the disk sidewalls, on the coupling between the microdisk and the straight SOI waveguides, on the reflection feedback from the grating couplers, and on the reflection at the interface between disk and straight waveguide. The sidewall surface roughness is the most critical parameter for the coupling between the two contra-propagating modes. The surface roughness on the microdisk sidewall breaks the azimuthal symmetry and results in removal of the degeneracy of CW and CCW modes. Scattered light couples either in to a radiation mode or the counter propagating mode [19]. Excitation of the counter propagating mode by back-reflected light prevents unidirectional or bistable behaviour. A detailed experimental and theoretical analysis by Sorel et.al. in ref. [12] has revealed that conservative scattering acts as a driv-

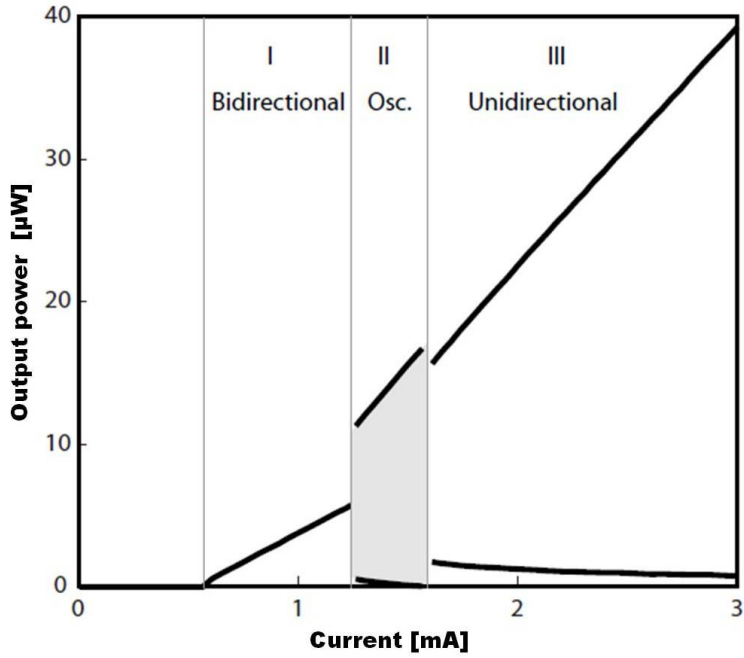

Figure 3.2: A simulated LI curve showing different regimes of a microdisk laser.[13].

ing force for alternate oscillations while dissipative scattering tends to restore either bidirectional or unidirectional regime depending upon the value of conservative scattering. The large roughness of the microdisk sidewall also leads to the high propagation loss making it difficult to achieve lasing with high output power.

Normally the bonding layer (DVS-BCB) thickness is about a few hundred nanometers and the coupling ratio between the microdisk and the waveguide is estimated to be about 1 %. The estimated value for the reflection from grating couplers used is about -22dB. Therefore , the influence of reflections from the grating couplers and from the interface between disk and straight waveguide can be ignored. From the description of the optical field evolution for the CW and CCW modes using coupled wave equations, it can be shown that there is a frequency split in the spectrum of the total optical field due to the mode coupling. The frequency split is normally too small to be seen in an optical spectrum, but it can be seen in an RF-spectrum. On these aspects theoretical investigations have been reported by different authors [19-20]. Also, there have been measurements of propagation loss in microring/disk resonators [21-22] where sidewall surface roughness induced backscattering accounts for either

the most significant or a substantial contribution to the propagation loss. In reference [23], the transmission loss in S_i/S_iO_2 waveguide is measured where again sidewall roughness is the major source of loss. Transmission measurements [24] in passive silicon microdisks have shown lifting of the degeneracy between the clockwise (CW) and the counterclockwise (CCW) propagating whispering gallery modes (WGMs), due to scattering from disk sidewall surface roughness. Experimental investigations were reported on surface roughness induced detrimental effects on the bistability in disk/ring lasers in ref. [25].

3.4 Characterisation of mode coupling

The measurement of the RF-spectrum of mode beating between CW and CCW modes allows to extract the information about the coupling between CW and CCW modes. Assuming $K_c >> K_d$, an analytical expression for K_c and K_d can be derived from the rate equations for CW and CCW mode :

$$\frac{dE^+}{dt} = \frac{1}{2}(1+j\alpha)\left[G - \frac{1}{\tau_p}\right]E^+ + (jK_c + K_d)E^- + F_{se}^+ \tag{3.15}$$

$$\frac{dE^-}{dt} = \frac{1}{2}(1+j\alpha)\left[G - \frac{1}{\tau_p}\right]E^- + (jK_c + K_d)E^+ + F_{se}^- \tag{3.16}$$

Where F_{se}^+ and F_{se}^- represent the spontaneous emission noise in the CW and CCW direction respectively while all other symbols have the same meaning as stated in the previous section. Taking the solutions of above equations as $E^+ = E^+ \exp(j\Omega t)$ and $E^- = E^- \exp(j\Omega t)$and $\Delta G = G - {\tau_p}^{-1}$, above two equations result into the following equations :

$$[j\Omega - \frac{1}{2}(1+j\alpha)\Delta G]E^+ = (jK_c + K_d)E^- + F_{se}^+ \tag{3.17}$$

$$[j\Omega - \frac{1}{2}(1+j\alpha)\Delta G]E^- = (jK_c + K_d)E^+ + F_{se}^- \tag{3.18}$$

In absence of the spontaneous emission noise, multiplying equations (3.17) and (3.18) results into :

$$[j(\Omega - \frac{1}{2}(\alpha)\Delta G] - \frac{1}{2}\Delta G = +(jK_c + K_d) \tag{3.19}$$

$$[j(\Omega - \frac{1}{2}(\alpha)\Delta G] - \frac{1}{2}\Delta G = -(jK_c + K_d) \tag{3.20}$$

Comparing real and imaginary parts of equation (3.19) gives ΔG = -2K_d and Ω = K_c - αK_d while from equation (3.20) $\Delta G = 2K_d$ and Ω = -K_c +αK_d is obtained. The difference between angular frequencies equals to 2(K_c - αK_d). Under the

condition $K_c >> K_d$, the difference between the freqencies will be equal to K_c/π and will appear as a peak in RF spectrum.

Only the mode at $\Omega = K_c - \alpha K_d$ will be lasing since it has lower $\Delta G = G - \tau_p^{-1}$ as compared to the mode at $\Omega = -K_c + \alpha K_d$. Spectral variation around $\Omega = -K_c + \alpha K_d$ can be given as :

$$\Omega = \Delta\omega - K_c + \alpha K_d \tag{3.21}$$

Now in presence of noise and with $\Delta G = -2K_d$, equation (3.17) can be written as:

$$E^+ = \frac{(jK_c + K_d)E^- + F_{se}^+}{j(\Omega + \alpha K_d) + K_d} \tag{3.22}$$

Substitution of equation (3.22) in (3.18) yields:

$$E^- = \frac{(jK_c + K_d)F^+ + [j(\Omega + \alpha K_d) + K_d]F^-}{j(\Omega + \alpha K_d - K_c)[j(\Omega + \alpha K_d + K_c) + 2K_d]} \tag{3.23}$$

After substitution of Ω from equation (3.21), under the condition $\Delta\omega << K_c$ and by ignoring the small value terms; equation (3.32) can be rewritten as:

$$E^- = \frac{(jK_c + K_d)F^+ + [j(\omega - K_c) + K_d]F^-}{(-2K_c)[j\Delta\omega + 2K_d]} \tag{3.24}$$

Above equation can be transformed to equivalent optical power as written below:

$$P_{opt} \sim \frac{1}{\Delta\omega^2 + (2K_d)^2} \tag{3.25}$$

Equation (3.25) implies that 6dB bandwidth of RF-spectrum of mode beating between CW and CCW modes will correspond to $2K_d/\pi$

The schematic of the experimental set-up employed for beat frequency measurements is shown in Figure 3.3. As the output power of the microdisk laser coupled to the fibre is very low, it is amplified with an erbium doped fiber amplifier (EDFA). An optical isolator is placed in between the microdisk laser and the EDFA to avoid coupling of amplified spontaneous emission noise back to the microdisk laser which can destabilize it. The EDFA is followed by an optical tunable filter, tuned at the wavelength of the microdisk laser output light, to suppress spontaneous emission noise generated by the EDFA. The amplified and noise suppressed light is fed to the HP70810B Light Wave Section of an RF spectrum analyser which converts the optical input into a radio frequency (RF) signal. This RF signal is given as an input to the HP7090 8A. Finally the beat frequency of the CW and CCW modes appears as a resonance in the RF spectrum and is seen on display screen. As an example, the RF spectra of microdisk lasers of two generations G_1 and G_2 measured at different bias currents are presented in figure 3.4. The microdisk lasers of G_1 have high roughness as

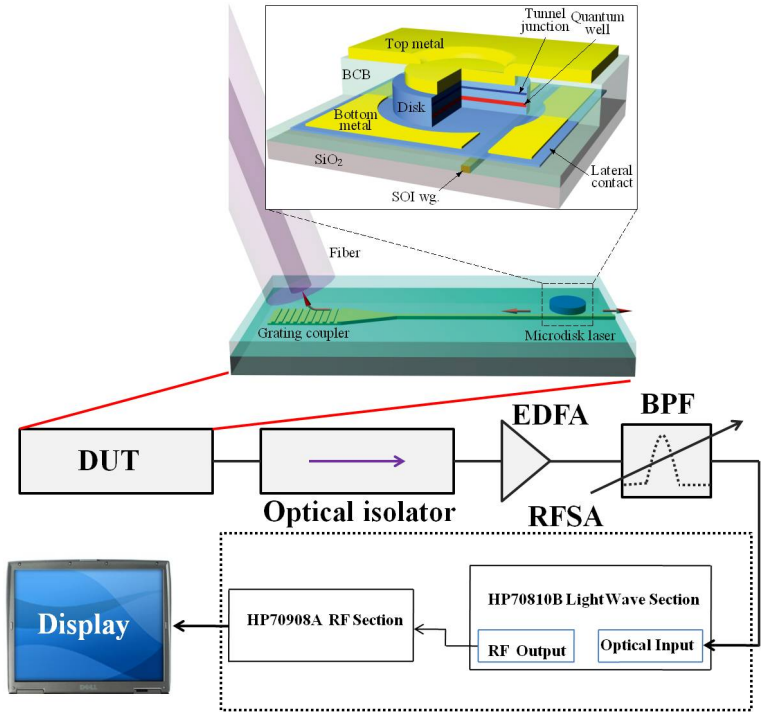

Figure 3.3: Experimental set-up used for characterization of mode coupling. DUT, device under test; RFSA, radio-frequency spectrum analyser; BPF, band pass filter.

compared to that of G_2. Exemplary SEM images of the sidewalls of microdisk lasers of both the generations are shown in figure 3.5 illustrating the difference in the roughness. As can be seen from figure 3.4, the peaks of the RF spectra do not shift to higher frequencies with an increase in the bias current increases. Therefore, it is concluded that the observed resonances are not the relaxation oscillation between the photons and the carriers in the active material, but are due to the beating of the two split lasing frequencies.

In G_1 microdisk lasers, the frequency splitting is large due to the large sidewall surface roughness. As shown in figure 3.4 (a), f =6.0 GHz is normally obtained, corresponding to the conservative coupling coefficient K_c of 1.8 X 10^{10} s^{-1}. This high coupling between the CW and CCW modes prevented achieving the unidirectional operation in G_1 microdisk lasers. In G_2 devices, the sidewall roughness is reduced significantly , and therefore, the resonant frequencies in the RF spectra are now of the order of hundred MHz as shown in figure 3.4(b). While the resonance frequency decreases slightly with increasing bias current as a result of the changing phase of the reflection from the grating couplers,

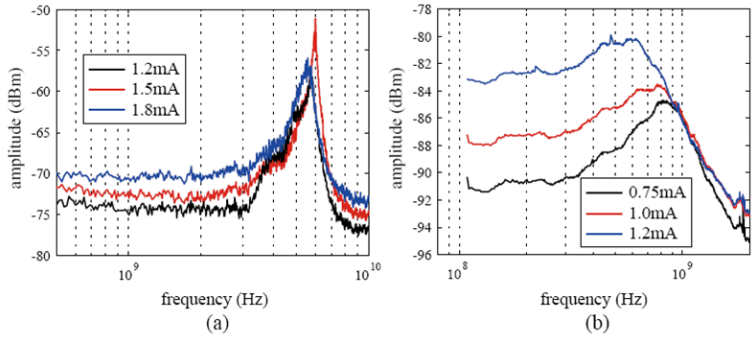

Figure 3.4: Measured RF spectra of the microdisk lasers at different bias currents in (a) first generation [G_1] and (b) second generation [G_2].

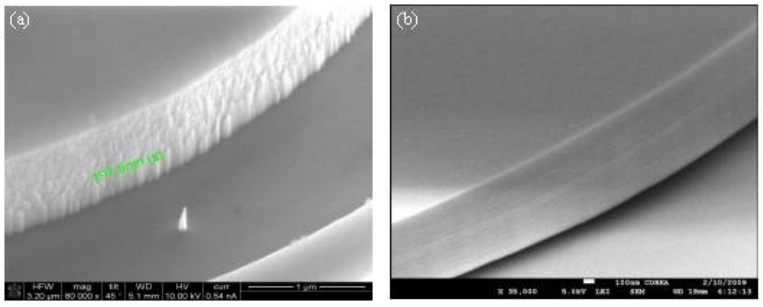

Figure 3.5: The SEM images of the sidewalls of the microdisk cavities in (a) G_1, and (b) G_2 device.

the measurements allowed to conclude that the conservative coupling between CW and CCW modes is K_c = 1.8 X 10^9 s^{-1}. It is difficult to read the dissipative coupling between CW and CCW modes in the results in figure 3.4(b) due to the signal floor from the intensity noise of the laser. The dissipative coupling is of less importance than the conservative coupling concerning the threshold of unidirectional operation [12]

3.5 Lasing characteristics

In this section, the lasing characteristics of microdisk lasers of both generations are presented. As is discussed in the previous section, the mode coupling between CW and CCW modes in G_1 lasers was way too high to achieve bistable behaviour. The same is confirmed by scanning the bias current applied to the microdisk laser and recording the output power from both ends of the wave-

guide.

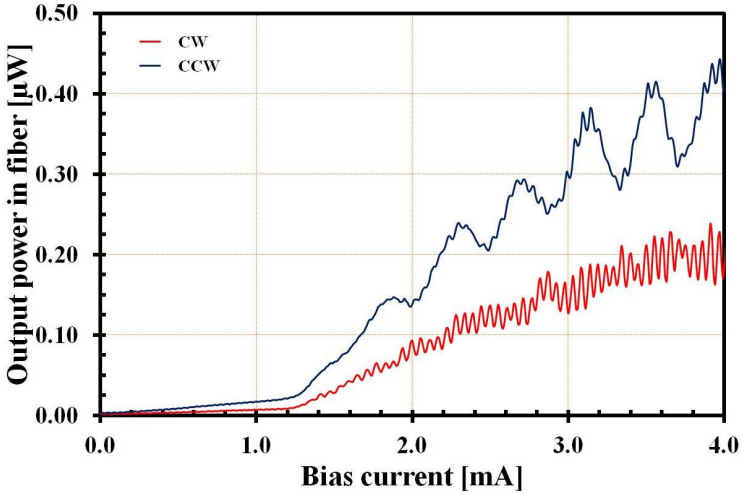

Figure 3.6: The LI curve of a microdisk laser from G_1.

For an illustration, the LI (Light-Current) curve of a microdisk laser from G_1 is plotted in figure 3.6. The diameter of this device was 10 μm. The optical spectrum of the same microdisk measured at 4.3 mA of bias is plotted in figure 3.7. The SMSR (side mode suppression ratio) is > 20 dB and the free-spectral range (FSR) of this laser is 24 nm which is in agreement to theoretical prediction according to the formula: FSR = λ^2/n_gL. Here λ is the peak resonance wavelength while n_g and L are the waveguide group index and the circumference of the microdisk, respectively.

In the LI curve, the ripples are also visible which are due to the Fabry-Perot resonances. The Fabry-Perot cavities are formed in the fiber-optic circuit used for the measurements. For example, the reflections from the fiber-optic connectors, access fibers and grating couplers lead to the formation of Fabry-Perot resonances. As can be seen the output power of these lasers is very low (only few hundreds of nano watts) implying that the photon density in the microdisk cavity is not enough for the occurrence of the bistability.

In figure 3.8 (a) the LI curve of a microdisk laser from G_2 is plotted showing clear bifurcation of power (bistability) between CW and CCW modes for bias current above 1.7 mA. Threshold current is as low as 0.33 mA. The occurrence of the bistable behavior as seen in the LI curve is in agreement with the information of low beat frequency (figure 3.4(b)) obtained by measuring the RF spectrum. The maximum power in the SOI waveguide was 21 μW and is limited by the thermal rollover around 3.8 mA. Figure 3.8(b) presents the lasing spectrum at 3.8 mA bias, showing a single mode operation with SMSR > 40dB. Bistable,

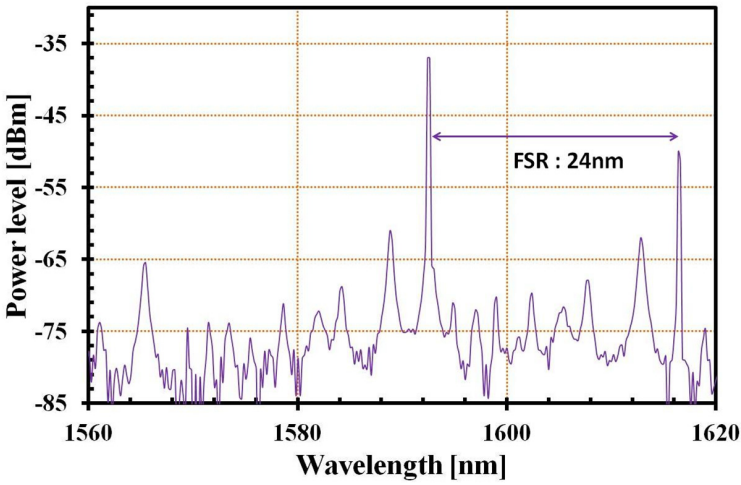

Figure 3.7: The optical spectrum of a microdisk laser from G_1.

unidirectional operation starts at 1.7 mA. Any switching of the lasing direction in the unidirectional regime when increasing the bias current is not observed, which does occur in the large ring lasers [26]. This switching behavior only happens when the laser mode hops to another azimuthal order, i.e., several FSRs away, due to the self heating [26]. Such a mode-hopping is unlikely to happen in this laser, since the microdisk cavity is so small that the FSR is larger than 30 nm as depicted in figure 3.8(b). Periodic oscillations can also be found in the L-I curves, which are an evidence of the reflection feedback from the grating coupler or the fiber facet.

It is to be noted that the epitaxial structure used for G_1 and G_2 microdisk lasers were different. The description of the epitaxial structure used for fabricating the G_1 laser can be found in reference [27] while the epitaxial structure used for fabricating G_2 lasers is provided in chapter 2 (section 2.2). The top contact layer (Au) in the G_2 microdisk laser was made extra thick (600 nm) and served as a heat sink. The heat sink which helped to decrease the thermal resistance to 6.1 K mW^{-1}. The thermal resistance of G_1 microdisk lasers was 10 KmW^{-1}. The diameter of the microdisk cavity was 7.5 μm.

3.6 Dynamic all-optical flip-flop operation

In unidirectional regime, the output power of one of the modes (CW or CCW) is high while that of another is suppressed. The output power of the dominant mode can be suppressed while that of the suppressed mode can be enhanced by

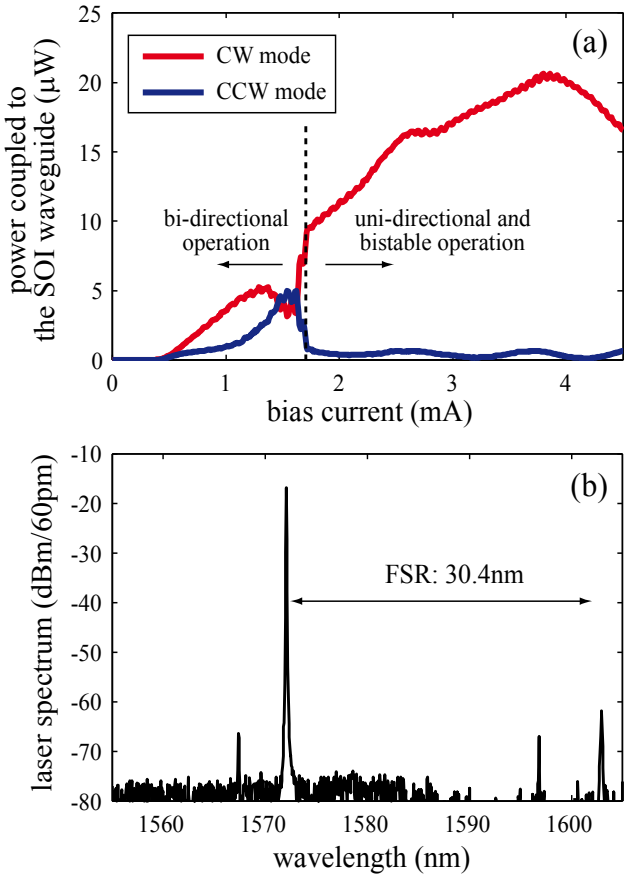

Figure 3.8: (a) The LI curve and, (b) the optical spectrum of a microdisk laser from G_2.

injecting an external optical pulse in the direction of the suppressed mode. This way, depending on the direction of injection of the external optical pulse, the random switching between CW and CCW modes is possible. This phenomenon is equivalent to an electronic set-reset flip-flop (SR-FF). The dynamic measurements were performed to show the all-optical flip-flop operation in a microdisk laser.

The measurement set-up used for testing the dynamic response of the AOFF is outlined in figure 3.9. Two circulators were connected to the access fibres to the sample to separate the injected laser pulses and the output from the microdisk laser. The output laser was detected either by a high-sensitivity, low-speed photodetector (HP 81532A; for the low-speed switching shown in figure

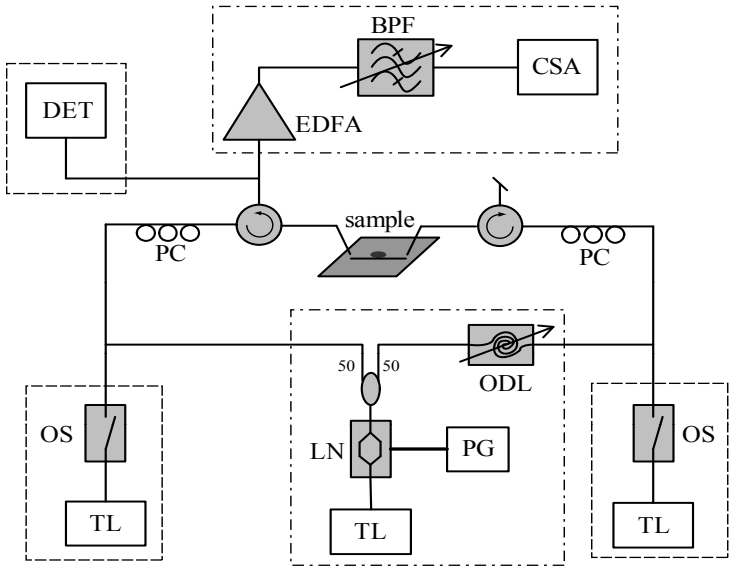

Figure 3.9: Experimental set-up used for dynamic flip-flop operation. The equipments in the dashed frames were used for the low-speed measurements, and those in the dash-dotted frames were used for the high-speed measurements. TL, tunable laser; OS, optical switch; LN, lithium niobate modulator; PG, pattern generator; ODL, tunable optical delay line; PC, polarization controller; DET, high-sensitivity, low-speed detector; BPF, tunable band-pass filter; EDFA, erbium-doped fibre amplifier; CSA, communication signal analyser.

3.10) or by a communication signal analyser (Tektronix CSA8000; for the high-speed switching shown in figure 3.11) with preamplification by an EDFA and filtering by a band-pass filter (FWHM, 0.9 nm). Because the grating couplers give a coupling efficiency of ~ 30 % between the SOI waveguide and the access fibres, ~ 6 μW of the microdisk laser output was normally collected by the fibres.

To achieve a reasonable power level for the communication signal analyser, 25 dB amplification was needed from the EDFA. This high amplification resulted in a large level of spontaneous emission power, which caused a degradation of the extinction ratio of the flip-flop operation when compared to static measurements. For the results shown in figure 3.10, the injected laser pulses were generated by switching on and off an optical switch connected between a tunable laser and the circulator. The typical pulse duration in this scenario was in the order of 100 ms, which was sufficiently long for the microdisk laser to settle. For the high-speed results shown in figure 3.11, the injected pulses were generated

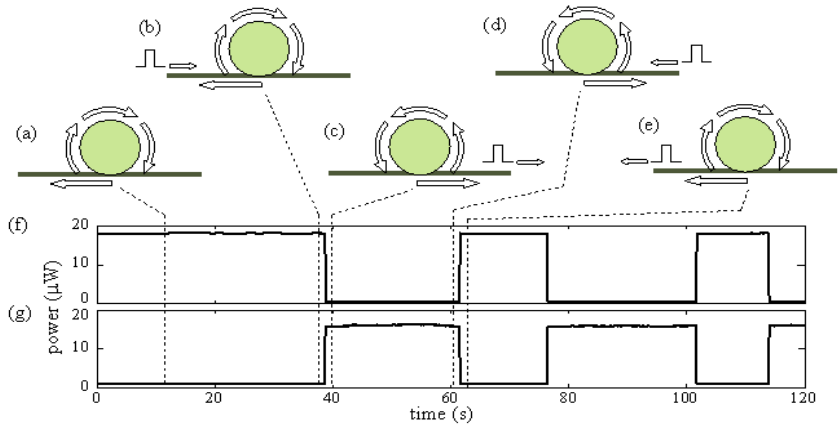

Figure 3.10: Diagrams of the flip-flop operation and measured lasing power at a low switching speed. (a) The microdisk laser (wavelength, 1572.198 nm) initially works in the CW dominant state. (b),(c) An optical pulse (wavelength, 1 572.2 nm) is injected from the left side (b) and switches the laser to the CCW dominant state (c). (d), (e) Similar to (b) and (c), but with injection from the right side. (f),(g) Power measured at the left and right ends of the SOI waveguide, respectively. The vertical dashed lines indicate, approximately, the moments at which the stages in (a)-(e) occurred.

by a lithium niobate modulator (speeds up to 10 Gbits/s) driven by a pattern generator. They were split into two by a 3dB fiber-optic splitter, and then fed to the sample. In one of the arms, a tunable optical delay line was inserted so that the arrival time of the set/reset pulses at the microdisk laser could be adjusted.

A low-speed switching experiment was first performed. The flip-flop operation is presented in figure 3.10. Assume that the microdisk laser works initially in the CW dominant state (figure 3.10 (a)), in which the CCW mode is suppressed and the power measured from the left side of the SOI waveguide is high. At a certain clock period, an optical reset pulse is injected from the left side (figure 3.10(b)). This pulse will couple into the microdisk cavity. If the injected pulse is strong enough, it will invoke the CCW mode. Even after the pulse has passed through, the microdisk laser will stay in the CCW dominant state (figure 3.10(c)). In this case, the power at the left side of the SOI waveguide becomes low. Similarly, the CW dominant state can be recovered by injecting an optical set pulse from the right side (figure 3.10(d) and (e)). Note that this operation is equivalent to a conventional set/reset flip-flop in an electronic circuit. The microdisk laser was biased at 3.5 mA, about twice the threshold current for the unidirectional operation, because self switching due to noise can be observed if working too

close to it. If a continuous-wave light - or a sufficiently long pulse - is injected, reliable switching can be achieved with a power of 360 nW, which is 17 dB below the output power from the microdisk laser. As shown in figure 3.10(f) and(g), power extinction ratios of 13 dB were measured at both sides of the SOI waveguide.

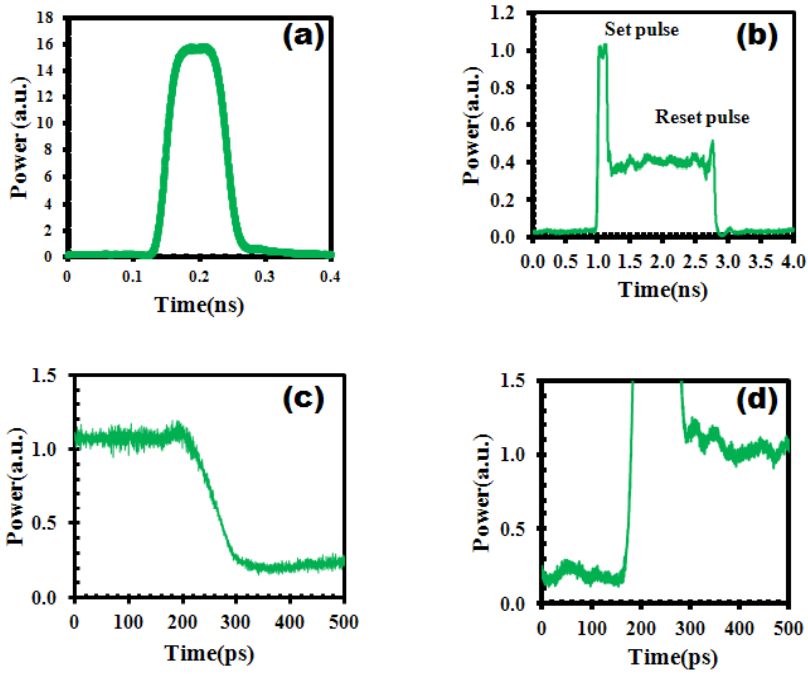

Figure 3.11: High-speed measurements of the switching characteristics. (a) Waveform of the injected optical pulse (central wavelength, 1572.23 nm).(b) Waveform of the measured optical signal at one side of the SOI waveguide. (c),(d)Details of the switch-off (c) and switch-on (d) transients, after applying the index-matching fluid to suppress the appearance of the reset pulses.

To test the switching speed [14] and switching energy, short laser pulses were used as the triggers for flip-flop operation. Figure 3.11 (a) shows the waveform of the triggering pulse, which has a width of 100 ps. As shown in figure 3.11(b), switching between the CW and CCW modes was achieved with a peak power as low as 18 μW measured in the SOI waveguide, corresponding to a pulse energy of 1.8 fJ. An extinction ratio of 11 dB was obtained, slightly less than that observed in the low-speed results shown above, probably due to the spontaneous emission noise from an EDFA used to amplify the relatively weak output

signal from the microdisk laser. Further increasing the peak power of injected pulses induced a strong relaxation oscillation at the switch-on transient, due to the deep depletion of the carriers. The injected set/reset pulses are also visible in 3.11(b). They cover the transient of the microdisk output, which makes it difficult to measure the exact switching time of the flip-flop. The residual reset pulses mainly come from the interface reflection at the cleaved facet of the access fibre. They can be suppressed, to some extent, by using index-matching fluid between the access fibres and the SOI chip. The measured switch-off transient in this case is presented in figure 3.11(b). A switching time of 60 ps was obtained. Any significant improvement of the switch-off time was not observed when increasing the pulse peak power up to the point where the reflected reset pulse started to appear again in the waveform. On the other hand, the set pulses cannot be removed in the current design, because they are at the same wavelength as the microdisk output, and are also propagating in the same direction. Nevertheless, it is obvious from figure 3.11 (d) that the switch-on time should be less than 100 ps. From the above discussions, we can conclude that 10 Gbits/s operation can be supported in the proposed AOFF. In principle, the ultimate switching time is determined by the round-trip time of the cavity. To build up the resonance, the injected photons have to travel over at least several turns inside the laser cavity. Numerical simulations have suggested that a switching time of the order of picoseconds can be achieved in such a small microdisk laser [28-29]. However, to measure such a fast transition, a short triggering pulse is required (to maintain a similar or higher injected energy, the peak power of the pulse should increase [30], which might become even higher than the output laser power from the device), and a smart design to efficiently separate the microdisk laser output from the injected pulses also has to be introduced.

3.7 Discussions and Conclusions

The active device area and the electrical power consumption of the proposed microdisk laser AOFF are the smallest among the AOFFs [32]. The switching energy is similar to that of the VCSEL based AOFF at its lowest speed, and is much better at high speed [29]. It has lower switching energy than the approaches based on ring lasers[27, 29, 33]. The measured switching speed is still less than that of the coupled ring lasers [33], but has the potential for greater speed, as discussed above. The proposed device is also the only electrically pumped AOFF built on SOI so far. This characteristic makes it very suitable as a building block for photonic integrated circuits in various all-optical signal processing applications [34-39], in combination with other ultra-compact functional devices such as optical gates, with ultra-low power consumption. To implement such a system, for example, an optical RAM [37] or shift register [38], requires that the

wavelength of an individual microdisk laser is tuned to within another's injection locking bandwidth. Using deep-ultraviolet (DUV) or electron- beam lithography, the wavelengths of nominally identical microdisk lasers on a single chip vary by 1.0 nm [40]. Thus, on average, tuning of 0.5 nm for each AOFF would be necessary. Accounting for the thermal resistance of the proposed device (6.1 K mW^{-1}) and the temperature sensitivity of the lasing wavelength (0.1 nm K^{-1}), thermally aligning the lasing wavelengths of these lasers requires about 0.8 mW of extra heating power per disk. The overall power consumption can thus be estimated to be 6 mW for storing one bit (3.5 mA X 1.5 V + 0.8 mW), which is close to that of state-of-the-art optical buffering technology with re-circulating delay lines (3.1 mW bit^{-1}; ref.[41]). Although such arrangements may have advantages over AOFFs in terms of the scalability of the data rate and the data format, the fibre or silica-on-silicon based delay lines occupy at least two orders of magnitude larger area. Even with a densely packed SOI waveguide [2], the footprint is still more than ten times higher. Using slow-light based delay lines, the footprint may be reduced to the level of the proposed AOFF. However, the high losses in this technology limit the buffer scale and energy efficiency [42-43]. The AOFF-based optical buffer is also capable of providing a longer and more flexible buffering time, as well as full random access. The threshold current (and thus the power consumption) at which the microdisk laser becomes unidirectional can be further decreased by further reducing the coupling between the CW and CCW modes (for example, by eliminating or reducing the reflections from the grating couplers and by improving the surface roughness of the disk even more) and by reducing the disk diameter or improving the current injection into the disk. Microdisk lasers with a threshold current as low as 40 μA under continuous operation have already been demonstrated in a similar platform [44], and it is therefore estimated that AOFF operation should be possible with an average power consumption of 0.5 mW. Including thermal tuning, the average power consumption per AOFF is then 1.3 mW. Assuming operation at 10 Gbits/s, this corresponds to 0.13 pJ energy consumption per bit over one bit duration. Comparing CMOS buffers, the energy consumption of, for example, an electronic dynamic RAM is projected to be 0.1 pJ bit^{-1} in the next decade, this mainly arising from interconnections and I/O interfaces [45]. Further optimization of the speed of the microdisk AOFF to allow operation at 40 Gbits/s will result in an energy consumption that is very competitive with CMOS solutions. This is even more the case after taking into account the extra opto-electronic conversion that is required for CMOS buffers, which would typically need tens of femtojoules to 0.1 pJ per bit using future optical-interconnect technology [5,45]. Optical buffers can also yield a much smaller access time or latency, although the footprint of CMOS will always be much smaller than that of optical buffers. It is, however, worth noting that the energy consumption in a

CMOS memory does not scale with buffering time [46]. Optical buffering will be a preferable approach in scenarios that require high-speed switching and high data throughput.

References

[**1**] R. Langenhorst, M. Eiselt, W. Pieper, G. Grosskopf, R. Ludwig, L. Kuller, E. Dietrich, and H. G. Weber. *Fiber loop optical buffer.* Journal of Lightwave Technology, 14(3): 324-335, 1996.

[**2**] H. Park, J. P. Mack, D. J. Blumenthal and J. E. Bowers. *An integrated recirculating optical buffer.* Optics Express, 16(15):11124-11131, 2008.

[**3**] E. Tangdiongga, X. Yang, Z. Li, Y. Liu, D. Lenstra, Member, G.-D. Khoe and H. J. S. Dorren. *Optical flip-flop based on two-coupled mode-locked ring lasers.* IEEE Photonics technology Letters, 17(1):208-2011, 2005.

[**4**] H.J.S. Dorren, M. T. Hill, Y. Liu, N. Calabretta, A. Srivatsa, F. M. Huijskens, H. de Waardt and G. D. Khoe. *Optical packet switching and buffering by using all-optical signal processing methods.* Journal of Lightwave Technology, 21(1):2-12, 2003.

[**5**] H.J.S. Dorren, N. Calabretta and O. Raz. *Scaling all-optical packet routers : how much buffering is required? [Invited].* Journal of Optical Networking, 7(11):936-946, 2008.

[**6**] See datasheet *Sierra Monolitcs SMI4026/4036 OC-768 Mux/demux chipset*, http://monolithics.com/wb/pages/products/optical-communication.php.

[**7**] See datasheet *Vitesse VSC8021/VSC8022 OC-48 8 bit 2.5 Gb/s Mux/demux chipset*, http://doc.chipfind.ru/vitesse/vsc8021.htm.

[**8**] See datasheet *CTI communication techniques CR-9000/CR9500 clock recovery modules*,
http://www.omecon.de/cd/pdf/cti/cti_datenblatt_35_38.pdf.

[**9**] E.F. Burmeister, D.J. Blumenthal and J.E. Bowers. *A comparison of optical buffering technologies.* Optical Switching and Networking, 5:10-18, 2008.

[**10**] W. E. Lamb, Jr. *Theory of an optical maser.* Physical Review , 134(6A):A1429-A1450, 1964.

[**11**] C.L. Tang, A. Schremer and T. Fujita. *Bistability in two mode semiconductor lasers via gain saturation.* Applied Physics Letters, 51(18):1392-1394, 1987.

[**12**] M. Sorel, G. Giuliani, A. Scirè, R. Miglierina, S. Donati, and P.J.R. Laybourn. *Operating egimes of GaAs-AlGaAs semiconductor ring lasers: experiment and model.* IEEE Journal of Quantum Electronics, 39(10):1187-1195, 2003.

[**13**] Y. De Koninck. *Niet-lineaire dynamica van enkelvoudige en gekoppelde microschijflasers.* Master's thesis, Ghent University, 2009.

[**14**] K. Huybrechts. *Digital photonics using single laser diodes for all-optical network nodes.* PhD theis, Chapter 4, Uinversiteit Gent, 2010.

[**15**] E. J. D'angelo, E. Izaguirre, G. B. Mindlin, G. Huyet, L. Gil, and J. R. Tredicce. *Spatiotemporal dynamics of lasers in the presence of an imperfect O2 symmetry.* Physical Review Letters, 68(25):3702-3705, 1992.

[**16**] M. Sargent. *Theory of a multimode quasi-equilibriumsemiconductorlaser.* Physical Review A, 48(1):717-726, 1993.

[**17**] M. Sorel, P. J. R. Laybourn, A. Scire, S. Balle, G. Giuliani, R. Miglierina, and S. Donati. *Alternate oscillations in semiconductor ring lasers.* Optics Letters, 27(22):1992-1994, 2002.

[**18**] M. Sorel, P. J. R. Laybourn, G. Giuliani, and S. Donati. *Unidirectional bistability in semiconductor waveguide ring lasers.* Applied Physics Letters, 80(17):3051-3053, 2002.

[**19**] B. E. Little, J. Laine and S.T. Chu. *Surface-roughness-induced contradirectional coupling in ring and disk resonators.* Optics Letters, 22(1):4-6, 1997.

[**20**] B. Li and P. Liu. *Numerical analysis of microdisk lasers with rough boundaries.* IEEE Journal of Quantum Electronics, 33(5):791-795, 1997.

[**21**] D. Rafizadeh, J.P. Zhang, R.C. Tiberio and S.T. Ho. *Propagation loss measurements in semiconductor microcavity ring and disk resonators.* Journal of Lightwave Technology, 16(7):1308-1313, 1998.

[**22**] V. Van, P.P Absil, J.V. Hryniewicz and P.T. Ho. *Propagation loss in single-mode GaAs-AlGaAs microring resonators: measurement and model.* Journal of Lightwave Technology, 19(11):17341739, 2001.

[**23**] K.K. Lee, D.R. Lim, H. Luan, A. Agarwal, J. Foresi and L. C. Kimerling. *Effect of size and roughness on light transmission in a Si/SiO2 waveguide: experiments and model,* Applied Physics Letters, 77(11):1617-1619, 2000.

[**24**] M. Borselli, K. Srinivasan, P.E. Barclay and O. Painter. *Rayleigh scattering, mode coupling, and optical loss in silicon microdisks.* Applied Physics Letters, 85(17):3693-3695, 2004.

[**25**] R. Kumar, L. Liu, G. Roelkens, G. Morthier and R. Baets. *Simple and accurate measurements to characterize microdisk lasers for all-optical flip-flop operation,* Annual Symposium of the IEEE Photonics Benelux Chapter, Belgium, p.81-84, 2009.

[**26**] H.A. Haus, H. Statz and I.W. Smith. *Frequency locking of modes in a ring laser*. IEEE Journal of Quantum Electronics, QE21(1):78-85, 1985.

[**27**] G. Mezosi, M.J. Strain, S. Furst, Z. Wang, and M. Sorel. *Unidirectional bistability in AlGaInAs microring and microdisk semiconductor lasers*. IEEE Photonics Technology Letter, 21(2):88-90, 2009.

[**28**] J.Van Campenhout, P.R. Romeo, P. Regreny, C. Seassal, D. Van Thourhout, S. Verstuyft, L. Di Cioccio, J.-M. Fedeli, C. Lagahe and R. Baets. *Electrically pumped InP-based microdisk lasers integrated with a nanophotonic silicon-on-insulator waveguide circuit*, Optics Express, 15(11):6744-6749, 2007.

[**29**] M.T. Hill, H.J.S. Dorren, T.de Vries, X.J.M. Leijtens, J.H. den Besten, B. Smalbrugge, Y.-S. Oei, H. Binsma, G.-D. Khoe and M.K. Smit. *A fast low-power optical memory based on coupled micro-ring lasers*. Nature, 432:206-209, 2005.

[**30**] G. Yuan, Z. Wang and S. Yu. *Dynamic switching response of semiconductor ring lasers to NRZ and RZ injection signals*. IEEE Photonics Technology Letters, 20(10):785-787, 2008.

[**31**] T. Katayama, T. Kitazawa and H. Kawaguchi *All-optical flip-flop operation using 1.55 μm polarization bistable VCSELs*. Conference on Lasers and Electro-Optics/Quantum Electronics and Laser Science Conference, p.CME5, 2008.

[**32**] L. Liu, R. Kumar, K. Huybrechts, T. Spuesens, G. Roelkens, E.-J. Geluk, T. de Vries, P. Regreny, D. Van Thourhout, R. Baets and G. Morthier. *An ultra-small, low-power, all-optical flip-flop memory on a silicon chip*. Nature Photonics, 4(3):182-187, 2010.

[**33**] A. Trita, G. Mezosi, F. Bragheri, J. Yu; S. Furst, W. Elsasser, I. Cristiani, M. Sorel and G. Giuliani. *Dynamic operation of all-optical flip-flop based on a monolithic semiconductor ring laser*. European Conference on Optical Communication(ECOC), p.We2C3 (2008).

[**34**] H. Kawaguchi. *All-optical signal processing using ultrafast polarization bistable VCSELs*. 2002 International Topical Meeting on Photonics in Switching, p.TuB3, 2002.

[**35**] B. Li, M.I. Memon, G. Mezosi, Z. Wang, M. Sorel and S. Yu. *Characterization of all-optical regeneration potentials of abistable semiconductor ring laser*. Journal of Lightwave Technology, 27(19):4233-4240, 2009.

[**36**] F. Prati, M. Travagnin and L.A. Lugiato. *Logic gates and optical switching with vertical-cavity surface-emitting lasers.* Physical Review A 55(1):690-700, 1997.

[**37**] N. Pleros, D. Apostolopoulos, D. Petrantonakis, C. Stamatiadis and H. Avramopoulos. *Optical static RAM Cell.* IEEE Photonics Technology Letters, 21(2):73-75, 2009.

[**38**] H. Kawaguchi, S. Mori, Y. Sato, Y. Yamayoshi. *Optical buffer memory using polarization-bistable vertical-cavity surface-emitting lasers.* Japanese Journal of Applied Physics, 45:L894-L897, 2006.

[**39**] D. Apostolopoulos, P. Zakynthinos, L. Stampoulidis, E. Kehayas, R. McDougall, R. Harmon, A. Poustie, G. Maxwell, R. Van Caenegem, D. Colle, M. Pickavet, E. Tangdiongga, H.J.S. Dorren, H. Avramopoulos. *Contention resolution for burst-mode traffic using integrated SOA-MZI gate arrays and self-resetting optical flip-flops.* IEEE Photonics Technology Letters, 20(24):2024-2026, 2008.

[**40**] J. Van Campenhout, L. Liu, P.R. Romeo, D. Van Thourhout, C. Seassal, P. Regreny, L Di Cioccio, J.-M.Fedeli and Roel Baets. *A compact SOI-integrated multiwavelength laser source based on cascaded InP microdisks.* IEEE Photonics Letters, 20(16):1345-1347, 2008.

[**41**] J.P. Mack, E.F. Burmeister, H.N. Poulsen, J.E. Bowers and D.J. Blumenthal. *Synchronously loaded optical packet buffer.* IEEE Photonics Technology Letters, 20(21):1757-1759, 2008.

[**42**] Y.A. Vlasov, M.O'Boyle, H.F.Hamann and S.J. McNab. *Active control of slowlight on a chip with photonic crystal waveguides.* Nature, 438:65-69, 2005.

[**43**] F.N. Xia, L. Sekaric and Y. Vlasov. *Ultracompact optical buffers on a silicon chip.* Nature Photonic 1(1):6571, (2007).

[**44**] M. Fujita, R. Ushigome and T. Baba. *Continuous wave lasing in GaInAsP microdisk injection laser with threshold current of 40 μA.* Electronics Letters, 36(9):790-791, 2000.

[**45**] R.S.Tucker. *The role of optics and electronics in high-capacity routers.* Journal of Lightwave Technology, 24(12):4655-4673, 2006.

[**46**] D.A.B. Miller. *Device requirements for optical interconnects to silicon chips.* Proceedings of the IEEE, 97(7):1166- 1185, 2009.

4

Microdisk resonator as an all-optical gate and wavelength converter

An optical gate is a device in which an optical probe signal output is controlled by the control signal. The control signal can be in the electrical or optical domain. In an electrically controlled gate, the applied voltage decides the output level of the optical probe signal. While in an optically controlled optical gate, the probe as well as the control signal both are in the optical domain. An integrated all-optical gate was reported by Lattes et.al. in 1983 [1]. Using the CMOS compatible platform, all-optical control of light by light was reported by Almeida et.al. in 2004 [2]. Afterwards, all-optical gates or modulators on III-V or Si based platforms have been reported by different research groups, e.g. [3-5]. In this chapter, the experimental demonstrations of all-optical gating realized in the microdisks are presented. In the second part of this chapter, the concept of all-optical gating is exploited to realize the all-optical wavelength conversion. Results described in section 4.1.3 and 4.2 of chapter 4 and all the results described in chapter 5 were obtained using molecularly bonded III-V-on-silicon devices fabricated by colleagues at LETI in France.

4.1 All-optical gate using a microdisk

4.1.1 Concept

An all-optical gate can be realized in the microdisk resonator in a pump-probe configuration [3]. When a high-intensity pump beam is tuned to one of the transmission resonances of the microdisk, the change in the transmittance allows to switch a continuous wave (CW) probe beam tuned to the next resonance as shown in figure 4.1. For a given band gap of the active material used for fab-

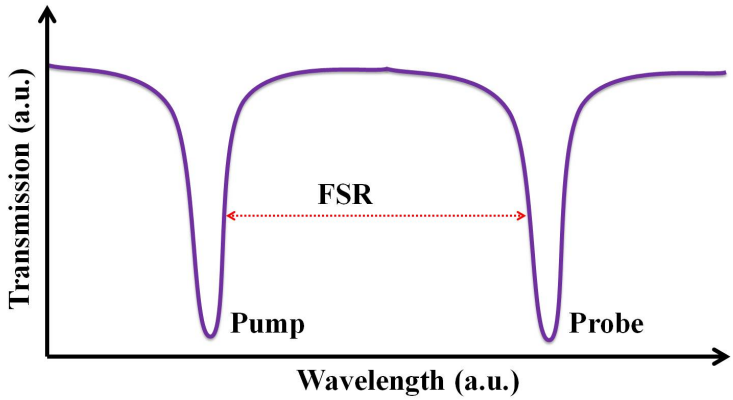

Figure 4.1: Transmission resonance characteristics of a microdisk and the selection of pump and probe wavelengths.

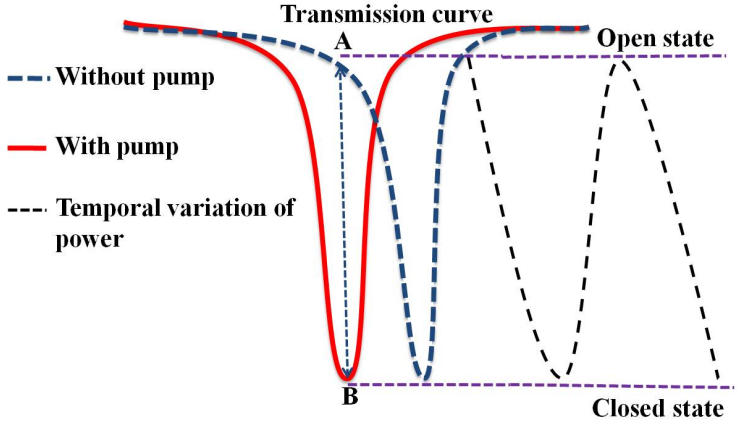

Figure 4.2: Illustration of the concept of an all-optical gate.

ricating the resonator, the switching can be achieved by exploiting either single

photon absorption (SPA) or two photon absorption (TPA) depending upon the wavelength chosen for of the pump. In SPA, each absorbed photon generates an electron-hole pair and these generated carriers change the absorption coefficient and the refractive index of the active layer of the microdisk. Figure 4.2 illustrates the gating concept in a pictorial way. The dotted blue curve shows the transmission dip of the microdisk around the probe wavelength. When pump light is injected into the microdisk at another resonance of the microdisk, free carriers are generated which causes a blue shift in the transmission dip as shown by the solid red curve. Using a pulse train as a pump results in high or low output of the probe beam due to a periodic shifting of the resonance around the probe wavelength. If the probe wavelength is slightly blue tuned off the transmission dip then in the absence of the pump pulse the output is high and the gate is said to be in the open state. In the presence of the pump pulse, due to blue shift of the resonance, the output will be low and the gate is said to be in the closed state. In this way, the power level varies between points A and B in the time domain as represented by the dotted black line. During this whole process, the variation in the power level of the output of the gate follows the pattern of the pump pulses.

4.1.2 Gating with BCB bonded microdisks

First experiments on gating were carried out using the microdisk resonators from generation G_2. In G_2 devices, III-V material was bonded on top of an SOI waveguide circuit using adhesive bonding process as described in section 2.4.1. For more information on G_2 devices, please refer to chapter 3 (page 49, 52). A particular microdisk used for the experiments reported here had a diameter 10 μm. The microdisk had an add-drop configuration of the waveguides. The offsets of the two waveguides were different with respect to the microdisk edge. This was due to a small registration error in the definition of the III-V microdisk. This offset is an important parameter which determines the coupling of light from the waveguide to the microdisk and vice-versa. The FIB-SEM image is shown in figure 4.3 highlighting this offset. The drop-port waveguide has a negative offset off-set of 320 nm (figure 4.3(a)) while the throughport waveguide has a positive off-set of 150 nm (figure 4.3(b)).

4.1.2.1 Transmission characteristics

To find the microdisk resonances, the transmission spectra at the through and drop port were measured with transverse electric (TE) polarized light from a continuous-wave (CW) tunable laser. A good transmission characteristic was observed only at the through port, which is shown in figure 4.4 with the green curve along with a fit (black curve) for the light coupling efficiency of the grating

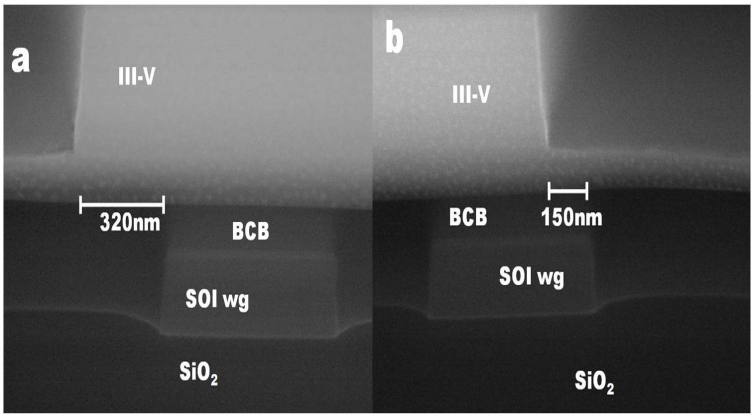

Figure 4.3: Cross section of III-V microdisk and the SOI waveguides showing the off-set of (a) drop port and (b) through port waveguide, respectively.

couplers [6]. This is attributed to the better alignment of the through port SOI waveguide with respect to the disk edge [see figure 4.3(b)]. Since the whispering gallery modes propagate along the edge of the microdisk, the light which couples into the microdisk from the input port does not couple well to the drop port due to the position of the drop port SOI waveguide away from the microdisk edge and more to the center of the disk as is clear from figure 4.3(a). Two resonances, one at 1563.9 nm and another at 1586.5 nm, were observed.

The ripples in the spectral response of the microdisk are due to a Fabry-Pérot resonance formed between the two grating couplers used for coupling light from the tunable laser to the waveguide through single-mode fiber, and reflections from fiber facets, connectors, etc. A large change in the resonance behavior(extinction ratio, Q-factor) at two wavelengths is seen due to the fact that the shorter wavelength (1563.9 nm) has higher absorption as it lies far away from the bandgap wavelength, which is 1600 nm, while the longer wavelength (1586.5 nm) lies closer to the bandgap wavelength of the microdisk [7].

4.1.2.2 Dynamic all-optical gating operation

Dynamic all-optical gating measurements according to the concept explained in section 4.1.1 were performed. The experimental setup used is sketched in figure 4.5. A tunable laser (TL) provides the probe beam while a short pulse source provides a pulse train which acts as a pump. The repetition rate of the short pulse source was set by the frequency of an RF output signal from the RF generator. The gate output was collected at the drop port of a circulator. The gate

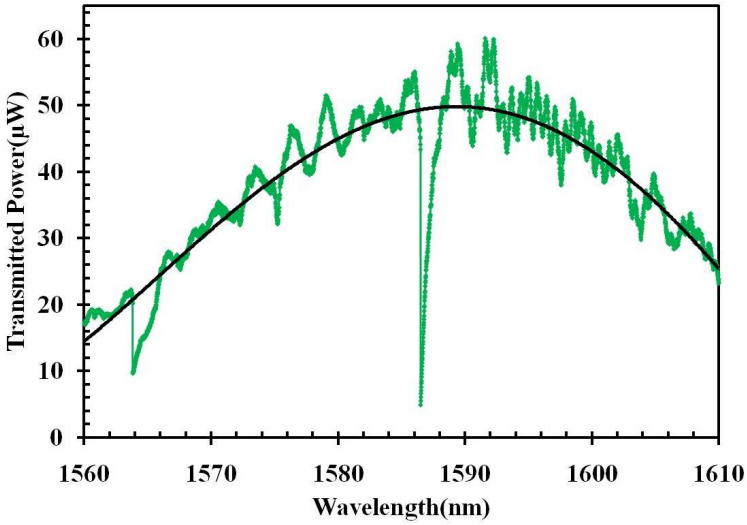

Figure 4.4: Transmission spectrum (green curve) of the microdisk, and a fit (blackcurve) for the light coupling efficiency of the grating couplers.

output was amplified using an L band EDFA. A band pass filter (BPF) followed the EDFA to suppress the amplified spontaneous emission noise generated in the EDFA. The gate output was finally fed to a high speed photodetector (HSPD) connected to a scope. The trigger signal to the scope was provided from the RF generator using a 3 dB RF splitter whose one output was connected to the short pulse source as shown in figure 4.5. The wavelength of the pump light injected at the through port was set at the lower resonance (1563.9 nm), while the wavelength of the probe light injected at the input port was set slightly below the longer resonance (1586.5 nm).

The pump light was a pulse train of 10 GHz repetition rate with each pulse of 7.5 ps duration, extinction ratio of more than 20 dB, and Gaussian in shape as shown in figure 4.6(a). Probe and average pump power in the SOI waveguide were 170 μW and 4 mW, respectively. While carrying out the measurements, the microdisk was kept under a reverse bias of -1 V to reduce the fall time by sweeping away the generated carriers from the active region [8].The gate output corresponding to the pulse train [figure 4.6(a)] is plotted in figure 4.6(b). When the pump pulse has a high/low power level, the gate is in the closed/open state as discussed in Section 4.1.1. The extinction ratio between the closed state and the open state was 4.5 dB. To estimate the gating speed of the device under investigation, transient responses were measured and are plotted in figure 4.7. The rise time and fall time were 8.5 and 41.5 ps, respectively, which suggest that this device can operate up to 20 GHz. The low dynamic extinction ratio, as compared

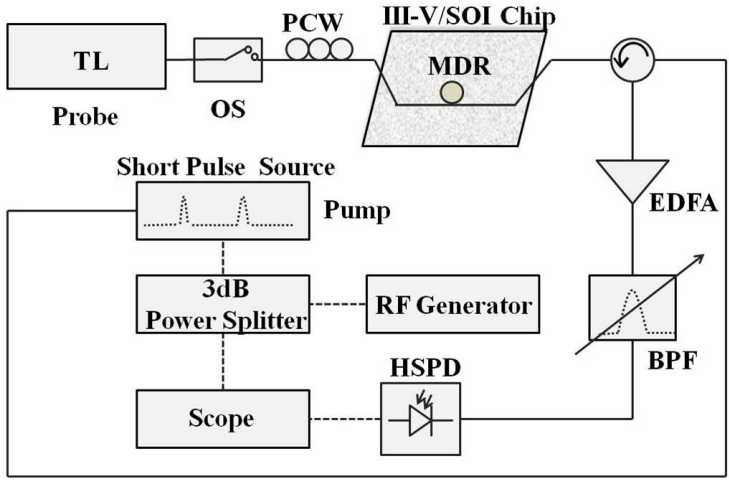

Figure 4.5: Schematic of the experimental setup used for dynamic all-optical gating measurements. MDR, microdisk resonator; OS, optical switch; PCW, polarization controlling wheels.

to the static extinction ratio (~ 10 dB (figure 4.4)), can be attributed to the spontaneous emission noise generated in the erbium-doped fiber amplifier (EDFA) used to amplify the gate output before feeding it to the oscilloscope.

The high speed of the gate is believed to be due to the surface-state recombination at the side walls of the microdisk, along with a contribution from the reverse bias. It seems that by increasing the pump power, the rise time can be reduced but it also requires increasing the reverse bias (e.g., to - 2 or - 3 V) to compensate the increased fall time. Under the same pump power and increasing the reverse bias to -2 V, no improvement in the fall time was seen. This can be explained by the saturation of drift velocity as a function of the applied electrical field. When microdisk is biased at -2V, it is in drift velocity saturation regime [9].The bandwidth of the pump pulse used is 1 nm while the bandwidth of the transmission resonance at 1563.9 nm is 0.4 nm. This implies that the pump power can be further reduced by matching the bandwidth of the pump signal to that of the microdisk resonance.

4.1.3 Gating with molecularly bonded microdisks

As described in the previous section, 10 GHz all-optical gating in a 10 μm diameter microdisk from G_2 was demonstrated but the use of reverse bias was necessary to achieve this speed, and the extinction ratio was only 4.5 dB. Using the same concept as in the previous section, a new set of experiments was car-

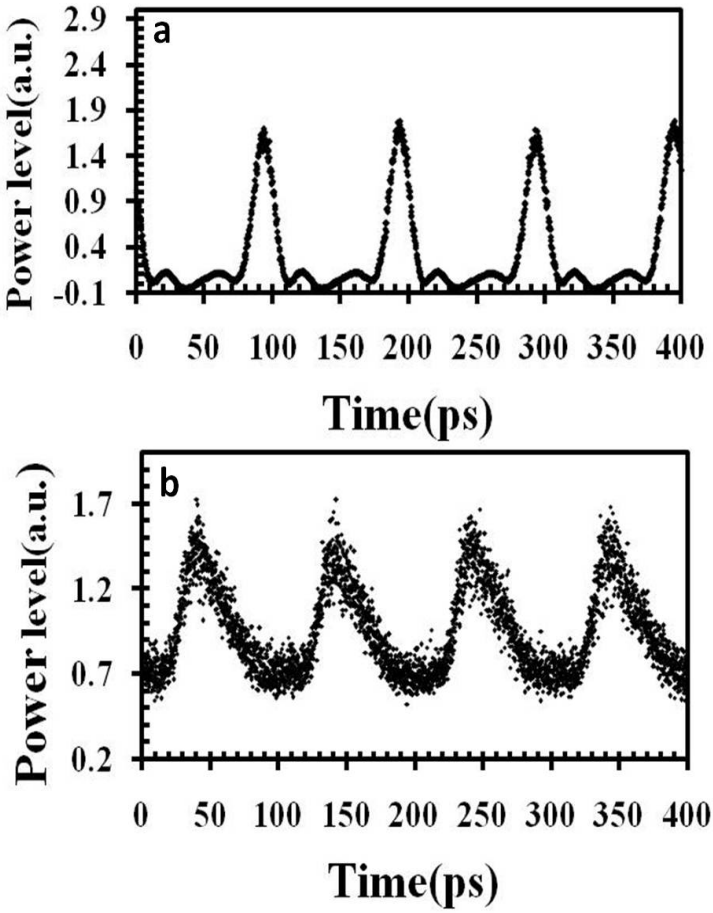

Figure 4.6: All-optical gating output :(a) Pattern of the pulse train and (b) corresponding gate output.

ried out with the microdisks of a new batch G_3. The G_3 microdisks were fully fabricated in a CMOS pilot line. The III-V material was bonded on top of the SOI waveguide circuit using a SiO_2 molecular bonding process resulting into a 130 nm thick bonding layer. The width and the thickness of the silicon waveguide was 600 nm and 220 nm respectively. Unlike microdisks from G_1 and G_2, the microdisks in G_3 were also defined by 193 nm deep ultraviolet lithography (DUV). A particular III-V microdisk used for the experiments reported here, was etched such that the periphery of the microdisk overlaps with the silicon waveguide covering a width of 500 nm. A full description on the fabrication can be found in reference [10].

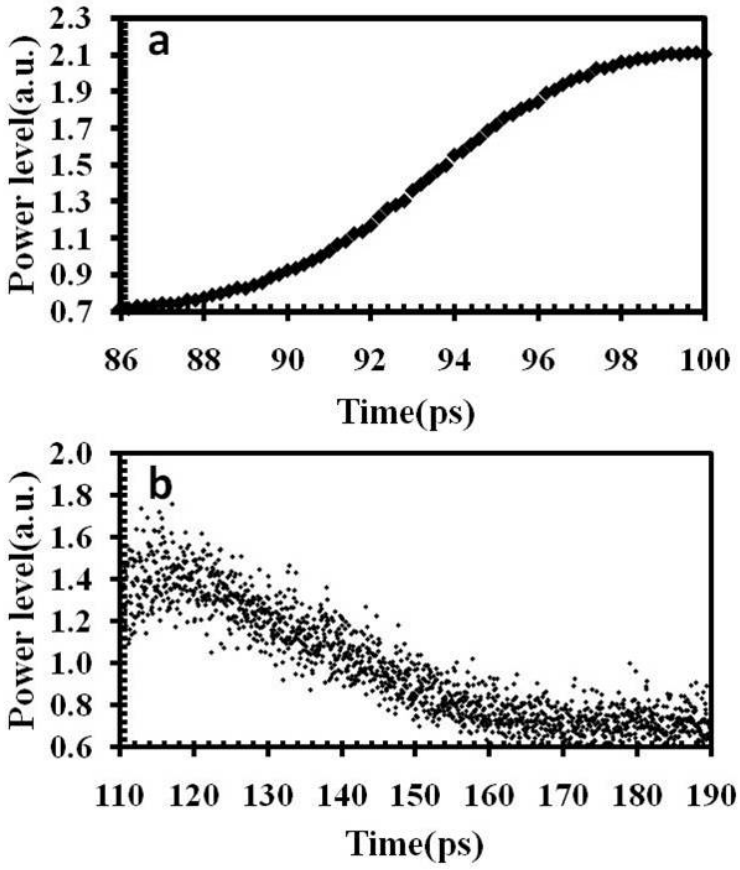

Figure 4.7: Transient response of the gate output: (a) rise and (b) fall edge.

4.1.3.1 Static characteristics

Like in section 4.1.2, the microdisk resonator was characterised statically to locate the transmission resonances. Two resonances corresponding to two azimuthal modes separated by an FSR of 30.8 nm, one around 1550.1 nm and another around 1580.9 nm, were located. The transmission response of the microdisk is plotted in figure 4.8. A higher extinction ratio was seen at the longer wavelength resonance since it lies closer to the band gap of the active material of the microdisk and hence has less absorption compared to that of the shorter wavelength resonance.

Measurements of the influence of the power on the extinction ratio were carried out to identify the critical coupling around 1580.9 nm. Near critical coupling [11] in continuous wave was obtained for -4.25 dBm coupled optical

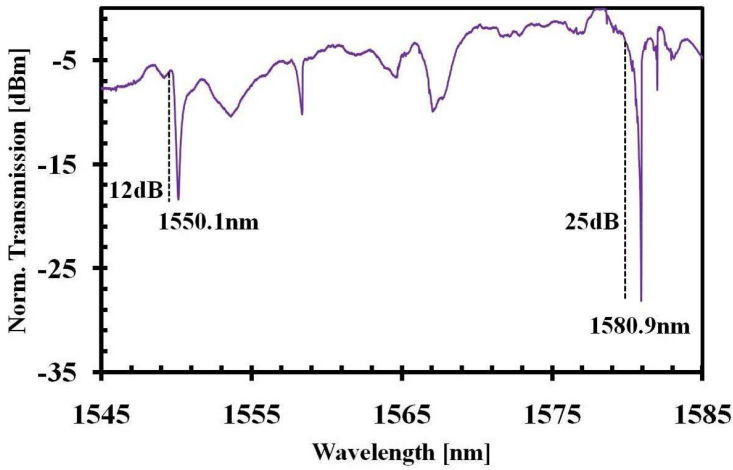

Figure 4.8: Transmission response of the microdisk resonator.

power with an extinction ratio of ~ 25 dB. By fitting the resonator transmission spectrum, the power coupling coefficient from the SOI waveguide to the disk was found to be ~ 6 %. Taking the resonance position of this mode for -13 dBm of power in the SOI waveguide as a reference, the relative change in the resonance position as a function of relative change in the power is plotted in figure 4.9, which shows the spectral shift due to the generation of free carriers and heat generated in the device (thermo-optic effect). It's clear from figure 4.9 that initially there is a blue shift due to the generation of free carriers and as the power increases, the carrier heating effect starts to take over. With 12dB change in the power, the blue shift is completely cancelled by the red shift and the red shift dominates for further power increase.

4.1.3.2 Dynamic characteristics

The dynamic gating measurements were performed for all-optical gating in a pump-probe configuration keeping the probe wavelength around the longer wavelength resonance and nearly critically coupled. The reason to choose the higher wavelength resonance as a probe was that it had a higher static extinction ratio as compared to that of the shorter resonance wavelength and will give higher extinction ratio in the output. A pump with 1.5 mW average power in the SOI waveguide was tuned around the shorter wavelength resonance and was essentially a pulse train of 10 GHz repetition rate. Every pulse was Gaussian in shape and had a duration and the extinction ratio of 8 ps (FWHM) and 22 dB respectively. The pump occupies 1 nm spectral width (FWHM). It is important

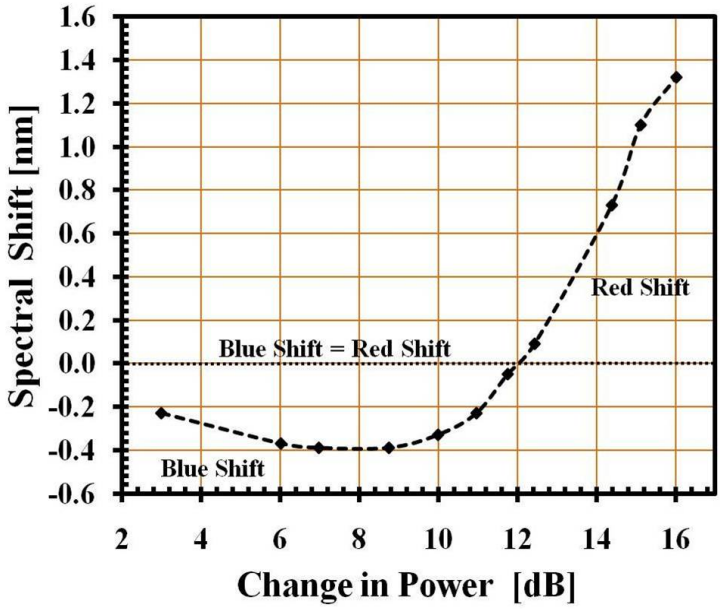

Figure 4.9: Spectral shift as a function of power change in the SOI waveguide.

to note here that unlike in the previous case (section 4.1.2.2), no electrical bias was applied to the microdisk during the measurements.

The gating input and output is shown in figure 4.10(a) and 4.10(b) respectively [12]. Figure 4.11(a) and (b) detail the transient responses. It can be seen that the extinction ratio is more than 12 dB and the rise and fall time are 18.6 and 26.4 ps respectively, implying an achievable gating speed beyond 20 GHz. The fast switch-off time is due to fast recombination of free carriers owing to the high surface to volume ratio and rough side walls of the microdisk. Use of a smaller diameter (7.5 μm) for the microdisk here as compared to that in the previous work (10 μm) contributes to a faster switch-off time. The light propagating along the sidewall of the microdisk (WGM) sees more effect of sidewall roughness in case of 7.5 μm diameter as compared to that in case of 10 μm diameter microdisk. At the same time we believe that the probe beam also acts as a seeding beam [13-15] and contributes to a faster response. In case of experiments with 10 μm diameter microdisk, the probe power was 170 μW while in the present case it was 375 μW. It was observed that the extinction ratio increases with increasing pump power but the switch-off time also becomes larger. Figure 4.12 shows the variation in extinction ratio and falltime as a function of pump power. The switching energy (which is 150 fJ in the SOI waveguide) can still be optimized further by properly choosing a pump source which matches the res-

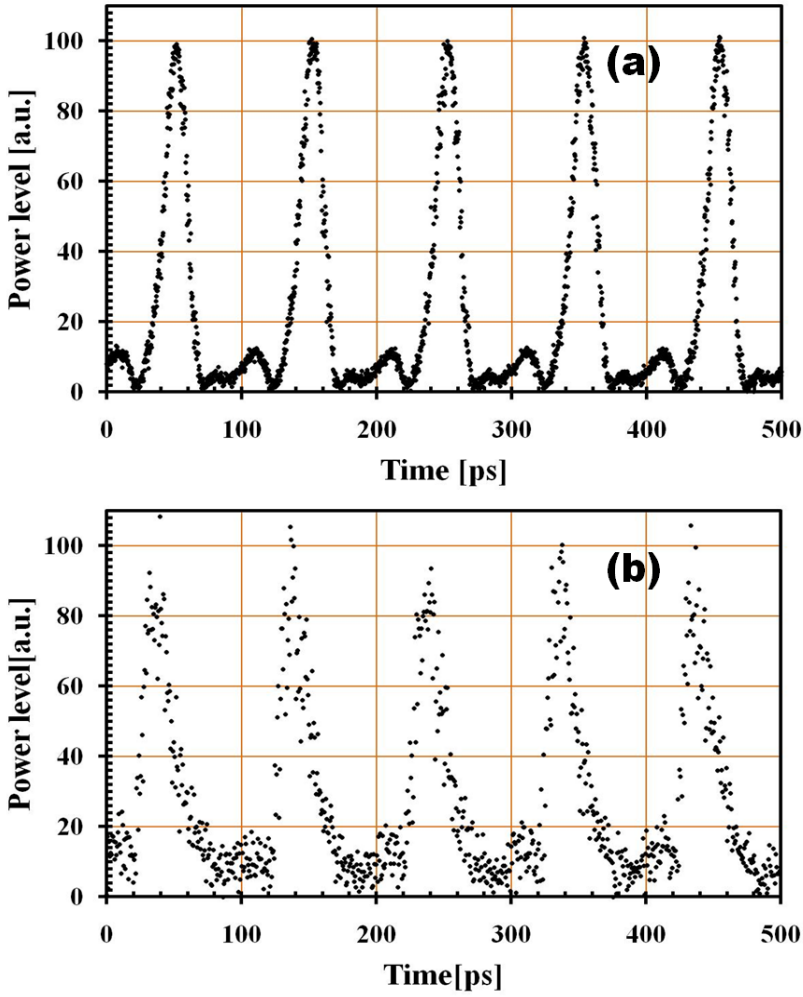

Figure 4.10: Waveform of gating (a) input and (b) output.

onance width of the microdisk pump resonance (which is ~ 0.52 nm wide at FWHM). The reduction in the extinction ratio in the dynamic case (more than 12 dB for the dynamic case while about 25 dB in static measurements) is due to a partial shift of the resonance and a change in the absorption in the presence of the pump pulses.

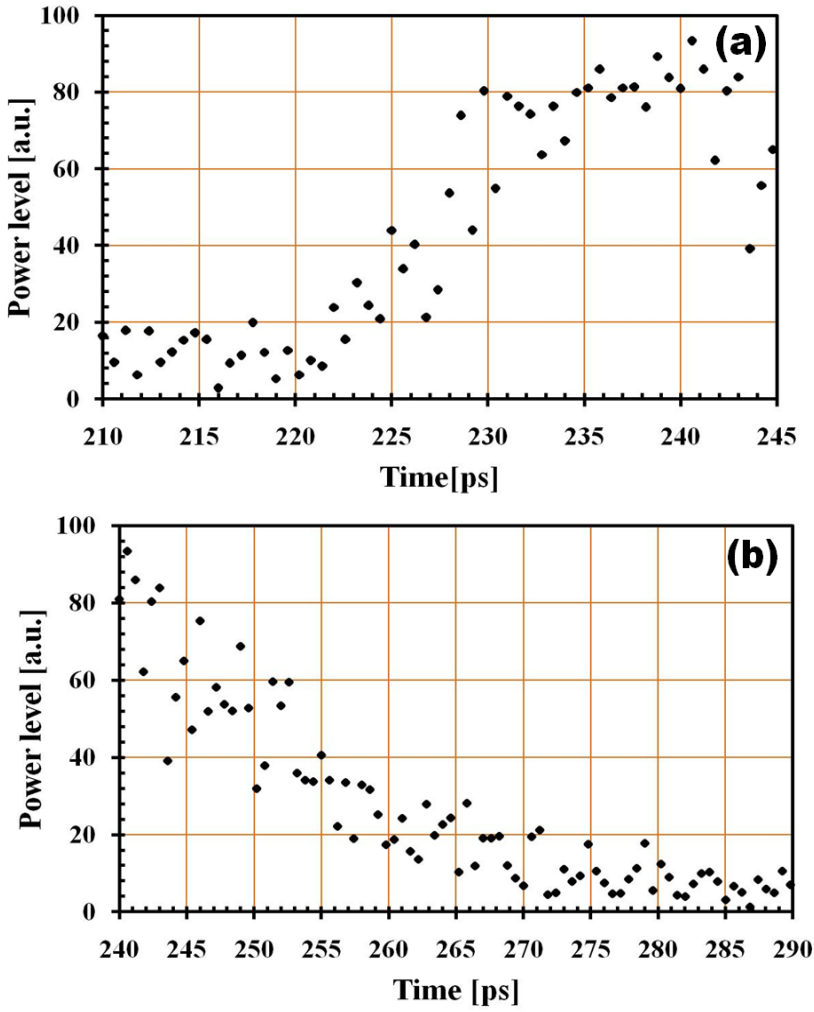

Figure 4.11: Transient details of gating output(a) rising and (b) falling edge.

4.2 All-optical wavelength conversion

4.2.1 Motivation for wavelength conversion

The motivation for wavelength conversion is to increase the flexibility and reduce the blocking probability in wavelength division multiplexing (WDM) networks [16]. In fact, wavelength conversion has been shown to reduce the blocking probability in both circuit switching [17-18] and packet switching wavelength routed optical networks (WRONs) [19-20].

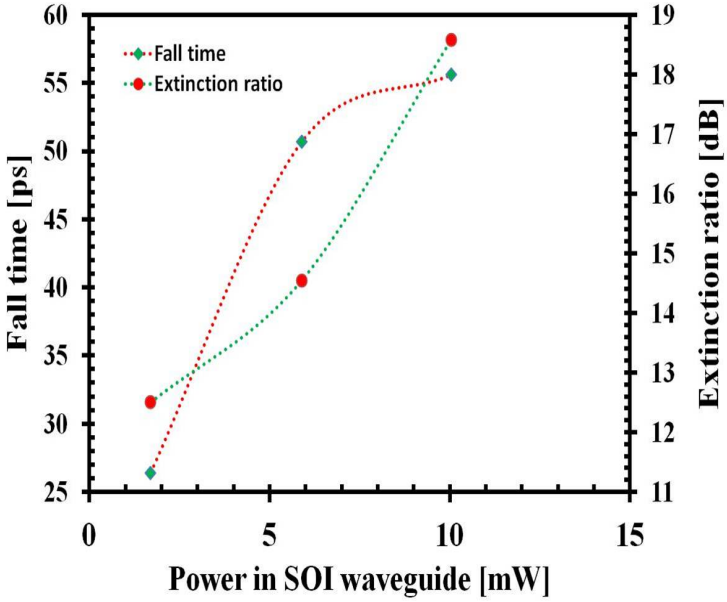

Figure 4.12: Extinction ratio and fall time as a function of pump power in SOI waveguide.

In a wavelength routed optical network (WRON) employing photonic packet switching, if a given output port for certain wavelength channel is occupied by an earlier data traffic, other succeeding data traffic with the same wavelength can not be routed to the output port untill the earlier data traffic has left the given port. Such a blocking problem is usually handled by buffering the packets [21]. If the buffers available are insufficient then the packet is either dropped or deflected. Wavelength conversion is another way to handel blocking in multi-wavelength optical networks. If the correct output for the wavelength on which the packet is coming is not available, the packet can be converted to another wavelength for which the output port is available.

4.2.2 Techniques for all-optical wavelength conversion

A variety of all-optical wavelength converters have been proposed and investigated so far. Various kinds of optical nonlinearity can be exploited to realize all-optical wavelength conversion, although there is a significant problem of trade-off between required optical power and response speed. For example, the Kerr effect induced in silica fiber has a subpicosecond response time, but its efficiency is quite low and it requires several hundreds mW of optical pump power to induce a phase shift large enough to be utilized for wavelength conver-

sion [22-23]. Most of the wavelength conversion schemes reported so far exploit the non-linear phenomenon discussed below :

(a) Four wave mixing

The IM, DPSK, DQPSK, or QAM signals; all can be wavelength converted by means of FWM [24]. The FWM is amongst the most widely used parametric processes employed for all-optical wavelength conversion. Mathematically, in the frequency domain, it can be expressed as -

$$\omega_C = 2\omega_P - \omega_{Pr}$$

where ω_C is the wavelength of the converted signal while ω_P and ω_{Pr} represent the degenerate pump and probe signals. FWM happens due to the Kerr nonlinearity and has been widely investigated using SOAs, e.g. [25-26], nonlinear fibers, e.g.[24]. The FWM has a huge potential for high operational speed, with demonstrations exceeding 100 Gbits/s in IM RZ signals [27].

(b) Cross-Gain Modulation

The Cross-gain modulation (XGM) was among the first effects to be exploited in order to accomplish all-optical wavelength conversion [24]. The XGM based wavelength conversion is usually realized in an SOA device, where a strong input signal at λ_S and a weaker continuous wave (CW) lightwave pump at λ_P are simultaneously injected. As both the signals are within the gain band of the device and the SOA is saturated, the modulation of the overall intensity turns out into a fast modulation of the SOA gain, which is directly transferred to the pump at λ_P [28]. The optimum frequency tuning of the signal, saturation effects, and the use of longer/optimized SOAs has led to conversion speeds up to 40 Gbit/s [28-30].

(c) Cross-Phase modulation

The Cross-phase modulation (XPM) is a nonlinear optical effect where one wavelength of light can affect the phase of another wavelength of light through the optical Kerr effect. Various all-optical wavelength conversion schemes using XPM have been demonstrated [31-34]. The effect of XPM does not simply result into all-optical wavelength conversion. In order to achieve wavelength conversion, the XPM has to be combined with an interferometric structure, where the nonlinear phase change is transformed into an amplitude modulation. All-optical wavelength conversion using XPM has been mostly demonstrated using either a fiber or an SOA as nonlinear material. In case of the fibers, the most popular all-optical wavelength conversion scheme is by means of the nonlinear optical loop mirror (NOLM)[31]. The SOA based wavelength convertors using XPM are similar to the NOLM where in each arm of interferometer an SOA device is inserted [32-34].

4.2.3 Wavelength conversion using a microdisk resonator

Owing to their smaller achievable size and enhanced nonlinearity originating from the resonant behavior along with high optical confinement, microdisks/rings are considered to be promising for compact and integrated wavelength conversion devices along with many other applications. Wavelength conversion in III-V microdisk using FWM was reported by Absil et.al [35]. On a pure silicon platform, the same was reported by Xu et.al. [36] using all-optical modulation. Wavelength conversion in III-V-on-silicon microdisks can be achieved with or without application of an electrical bias. Using electrically biased III-V-on-silicon microdisk, the working principle is based on the fact that the natural lasing from the microdisk can be suppressed when an external control beam is injected into the microdisk cavity. Therefore, the information carried on the injected beam will be copied inversely to the natural lasing wavelength of the microdisk [37-39].

4.2.3.1 Concept

The concept of wavelength conversion in III-V-on-silicon microdisk without using any electrical bias is illustrated in figure 4.13. The information at a wavelength (say, λ_1) can be transferred to another wavelength (say, λ_2) if λ_1 and λ_2 correspond to the transmission resonances of the microdisc resonator. This concept is based on the refractive index and hence transmission modulation of the resonance, to which the probe beam is tuned, in response to the logic level of data (pump) stream tuned at another resonance.

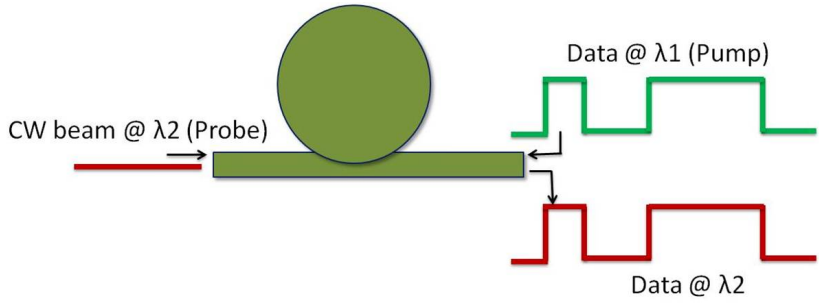

Figure 4.13: Illustration of wavelength conversion concept in a microdisk resonator using pump-probe configuration.

4.2.3.2 Dynamic operation

All-optical wavelength conversion was done for 10 Gbits/s PRBS data having a pattern length of 2^7 - 1 as the control (pump) signal. The sketch of the experi-

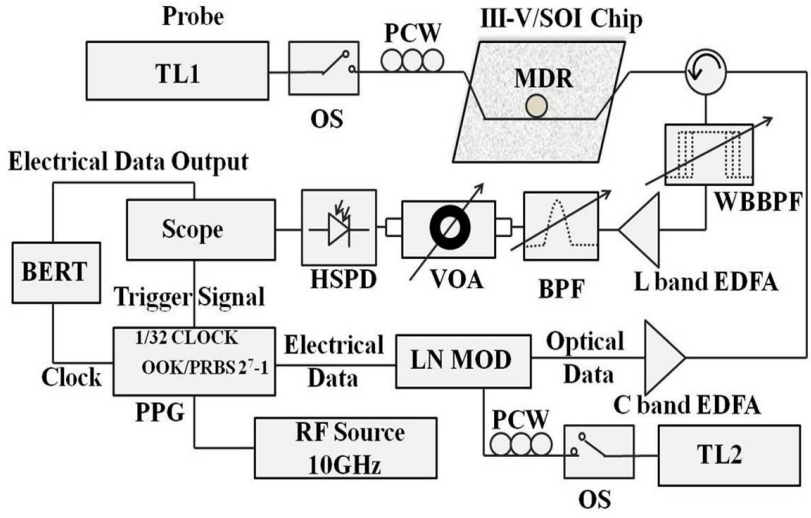

Figure 4.14: Schematic of the experimental setup used for all-optical wavelength conversion. TL1 and TL2, tunable lasers; OS, optical switch; PCW, polarization controlling wheels; MDR, microdisk resonator; WBBPF, wideband bandpass filter-it has a passband of 10-15nm and is used to suppress the backreflection of the original control signal from the fiber facets and grating couplers making sure that only the probe signal is seen on the scope; BPF, bandpass filter-it has a bandwidth of 1:2nm (FWHM) and is used to suppress the amplified spontaneous emission noise from the EDFA; HSPD, high-speed photodiode (30 GHz); LN MOD, lithium niobate Mach-Zehnder modulator; PPG, pulse pattern generator; VOA, variable optical attenuator.

mental setup used for these measurements is shown in figure 4.14. TL1 was used to provide a probe signal and it had the same specifications as described in the section 4.1.3.2. Electrical PRBS data at the speed of 10 Gbits/s generated from the pulse pattern generator driven by a RF source at 10 GHz were converted into optical PRBS data using an electro-optic LiNbO3 Mach-Zehnder modulator and a cw optical signal from TL2 tuned at the shorter wavelength resonance. In this way, the generated optical PRBS control signal had an extinction ratio of 14 dB and an average power ~ 9 mW (in the SOI waveguide). The pulse duration was 85 ps (FWHM) for a logic 1 level. A circulator was used to collect the probe signal. The backreflected control signal was suppressed by a wideband bandpass optical filter tuned to pass the probe signal. Afterward, the probe signal was amplified and the ASE was removed with a sharp filter before being detected by the photodiode connected to a scope. A variable optical attenuator was used to

control the received optical power into the high speed photodiode. The electrical output of the scope was connected to a bit error rate tester for carrying out the bit error rate (BER) measurements.

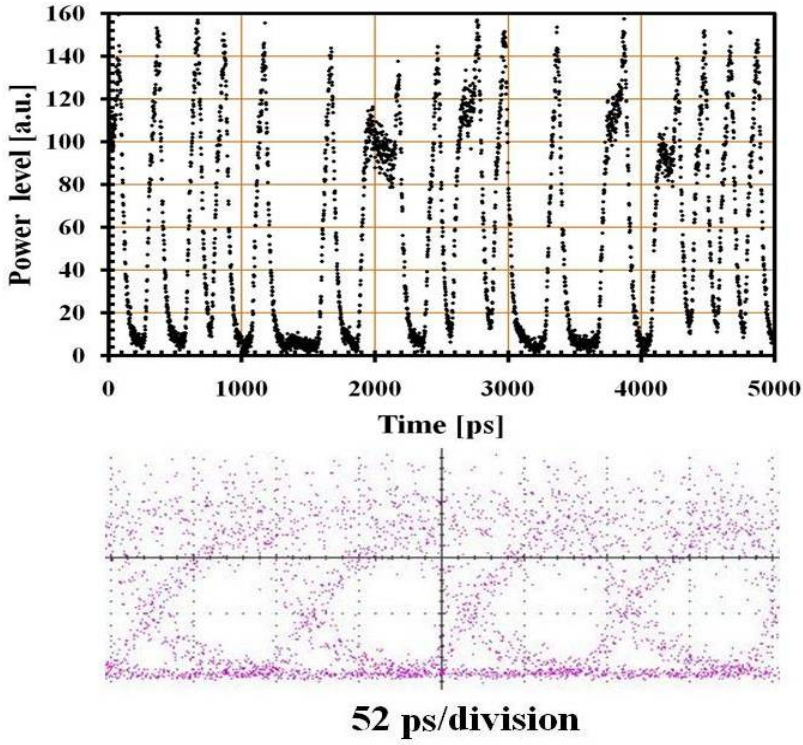

Figure 4.15: Waveform of the wavelength converted signal (top) and the corresponding eye diagram(bottom).

The information contained in the control signal at the lower resonance wavelength was transferred to the higher resonance wavelength (cw probe beam) and is plotted in figure 4.15. The eye diagram corresponding to the wavelength converted signal is shown in the same figure (below) and has an ER of 11.7 dB. To evaluate the system performance, bit error rate measurements were done. BER curves are plotted in figure 4.16. These curves show that the error free wavelength conversion at 10 Gbits/s is possible with a power penalty of ~3.5 dB.

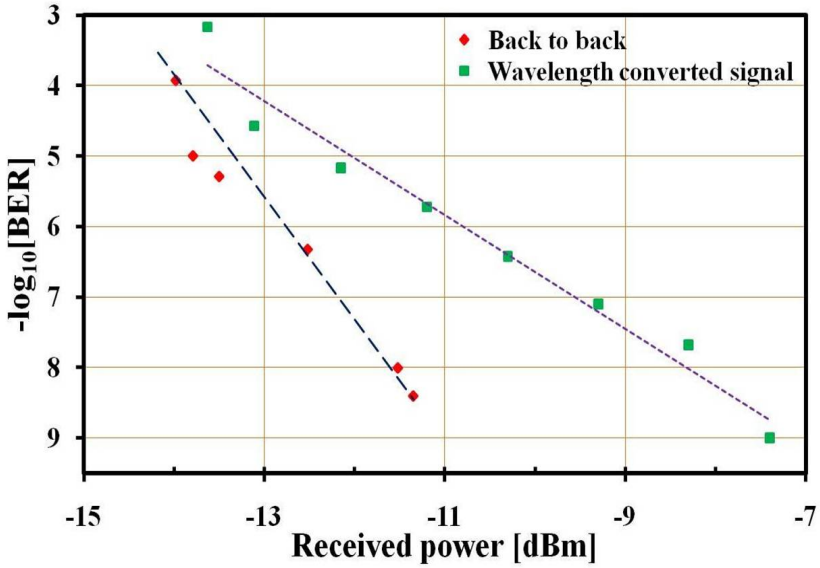

Figure 4.16: BER curves corresponding to the wavelength-converted signal and back-to-back measurements taken after the C band EDFA. The dashed lines are the linear fits to their respective data points.

4.3 Conclusions and discussions

In the first part of this chapter, demonstration of fast all-optical gating in pump-probe configuration is presented when the microdisk of 10 μm diamter was reverse biased. In the second set of experiments, electrical bias-free all-optical gating in a 7.5 μm diamter microdisk was demonstrated. In second part of this chapter, the demonstration of high-extinction ratio and bias-free all-optical wavelength conversion at a speed of 10 Gbits/s with a NRZ-OOK PRBS control data signal in a 7.5 μm diameter microdisk resonator is presented. This is the first bias-free demonstration of all-optical wavelength conversion using a PRBS data on III-V-on-silicon platform. All-optical gating measurements show that it is possible to achieve bias-free wavelength conversion beyond 20 Gbits/s. The devices which can be operated without electrical bias do not need top and bottom metal contacts and therefore the number of processing steps during the fabrication are reduced. The concept of gating presented here can be used to realize logic functions such as AND and NAND. In that case, two optical pump signals will control the transmittance of probe signal. The logic level of two pumps together will decide the logic level of AND or NAND gate. For the realization of AND gate, initially the probe beam wavelength will be needed to be

tuned at the dip of the probe resonance. In the case of a NAND gate, initially the probe beam wavelength needs to be placed at the left side shoulder (shorter wavelength side) of the probe resonance.

References

[**1**] A. Lattes, H. Haus, F. Leonberger and E. Ippen. *An ultrafast all-optical gate.* IEEE Journal of Quantum Electronics. 19(11):1718-1723, 1983.

[**2**] V.R. Almeida, C.A. Barrios, R.R. Panepucci and M. Lipson. *All-optical control of light on a silicon chip.* Nature, 431:1081-1084, 2004.

[**3**] V. Van, T.A. Ibrahim, K. Ritter, P.P. Absil, G.G. Johnson, R. Grover, J. Goldhar and P.-T.Ho. *All-optical nonlinear switching in GaAs-AlGaAs microring resonators.* IEEE Photonics Technology Letters, 14(1):74-76, 2002.

[**4**] T.B.-Jones, M. Hochberg and Axel Scherer. *All-optical modulation in a silicon waveguide based on a single-photon process.* IEEE Journal of Selected Topics in Quantum Electronics, 14(5):1335-1342, 2008.

[**5**] M. Först, J. Niehusmann, T. Plötzing, J. Bolten, T. Wahlbrink, C. Moormann and H. Kurz. *High-speed all-optical switching in ion-implanted silicon-on-insulator microring resonators.* Optics Letters, 32(14):2046-2048, 2007.

[**6**] G. Roelkens, D. Vermeulen, S. Selvaraja, R. Halir, W. Bogaerts and D. Van Thourhout. *Grating-based optical fiber interfaces for silicon-on-insulator photonic integrated circuits.* IEEE Journal of Selected Topics in Quantum Electronics, 17(13):571-580, 2011.

[**7**] R. Kumar, L. Liu, G. Roelkens, E.-J.Geluk, T. de Vries, F. Karouta, P. Regreny, D. Van Thourhout, R. Baets and G. Morthier. *10GHz All-Optical Gate Based on a III-V/SOI Microdisk.* IEEE Photonics Technology Letters, 22(13):981-983, 2010.

[**8**] S.F. Preble, Q. Xu, B.S. Schmidt and M. Lipson. *Ultrafast all-optical modulation on a silicon chip.* Optics Letters, 30(21), 2891-2893, 2005.

[**9**] J. M. T. Pereira. *Frequency response analysis of InGaAs/InP photodiodes.* Conftele 2007-6th Conference on Telecommunications, Peniche (Portugal), pp. 287-290, 2007.

[**10**] T. Spuesens, D. Van Thourhout, P. Rojo-Romeo, P. Regreny and J.-M. Fedeli. *CW operation of III-V microdisk lasers on SOI fabricated in a 200 mm CMOS pilot line.* IEEE conference on Group IV photonics, p.ThC, 2011.

[**11**] A. Yariv. *Universal realtions for coupling of optical power between microresonators and dielectric waveguides.* Electronics Letters, 36(4): 321-322, 2000.

[**12**] R. Kumar, T. Spuesens, P. Mechet, P. Kumar, O. Raz, N. Olivier, J.-M. Fedeli, G. Roelkens, R. Baets, D. Van Thourhout and G. Morthier. *Ultrafast and bias-free all-optical wavelength conversion using III-V-on-silicon technology.* Optics Letters, 36(13):2450-2452, 2011.

[**13**] R.J. Manning and D.A.O. Davies. *Three-wavelength device for all-optical signal processing.* Optics Letters, 19(12):889-891, 1994.

[**14**] L. Zhang, I. Kang, A. Bhardwaj, N. Sauer, S. Cabot, J. Jaques and D.T. Neilson. *Reduced recovery time semiconductor optical amplifier using p-type-Doped multiple quantum wells.* IEEE Photonics Technology Letters, 18(22):2323-2325, 2006.

[**15**] M.T. Hill, E. Tangdiongga, H. de Waardt, G.D. Khoe and H.J.S. Dorren. *Carrier recovery time in semiconductor optical amplifiers that employ holding beams.* Optics Letters, 27(18):1625-1627, 2002

[**16**] J. M. Wiesenfield. *Wavelength conversion in WDM networks.* Lasers and Electro-optics Society Annual Meeting, 1:88-89, 1997.

[**17**] R. A. Barry and P.A. Humblet. *Models of blocking probability in all-optical networks with and without wavelength changers.* IEEE Journal on Selected Areas in Communication, 14(5)858-867, 1996.

[**18**] S. Subramaniam, M. Azizoglu and A.K. Somani. *All-optical networks with sparse wavelength conversion.* IEEE/ACM Transactions on Networking, 4(4):544-557, 1996.

[**19**] S. L. Danielsen, B. Mikkelsen, C. Joergensen,T. Durhuus and K.E. Stubkjaer. *WDM packet switch architectures and analysis of the influence of tunable wavelength converters on the performance.* Journal of Lightwave Technology, 15(2):219-227, 1997.

[**20**] G. A. Castanon, O.K. Tonguz and A. Bononi. *Benefits of wavelength translation in datagram all-optical networks.* Electronics Letters, 33(18):1567-68, 1997.

[**21**] H. J. S. Dorren, M.T. Hill, Y. Liu, N. Calabretta, A. Srivatsa, F.M. Huijskens, H. de Waardt and G. D. Khoe. *Optical packet switching and buffering by using all-optical signal processing methods.* Journal of Lightwave Technology, 21(1):2-12, 2003.

[**22**] B.-E. Olsson, P. Ohlen, L. Rau, and D. J. Blumenthal. *A simple and robust 40-Gb/s wavelength converter using fiber cross-phase modulation and optical filtering.* IEEE Photonics Technology Letters, 12(7): 846-848, 2000.

[**23**] Y. Jianjun and P. Jeppesen. *80-Gb/s wavelength conversion based on cross-phase modulation in a high-nonlinearity dispersion-shifted fiber and optical filtering*. IEEE Photonics Technology Letters, 13(8):833-835, 2001.

[**24**] E. Ciaramella. *Wavelength conversion and all-optical regeneration: achievements and open issues*. Journal of Light Wave technology, 30(4):572-582, 2012.

[**25**] M.C. Tatham, G. Sherlock and L.D. Westbrook. *20-nm optical wavelength conversion using nondegenerate four-wave mixing*. IEEE Photonics Technology Letters, 5(11):1303-1306, 1993.

[**26**] A. D'Ottavi, E. Lannone, A. Mecozzi, S. Scotti, P. Spano, R. Dall'Ara, G.Guekos and J. Ekkner. *Frequency conversion by four-wavemixing on a frequency range of 8.6 THz*. European Conference on Optical Communication, 25-29, 1994.

[**27**] A.E. Kelly, A.D. Ellis, D. Nesset, R. Kashyap and D.G. Moodie. *100 Gbit/s wavelength conversion using FWM in a MQW semiconductor optical amplifier*. Electronics Letters, 34(20):1955-1956, 1998.

[**28**] B. Glance, J.M. Wiesenfeld, U. Koren, A. H. Gnauck, H. M. Presby and A. Jourdan. *High performance optical wavelength shifter*. Electronicsd Letters, 28(18):1714-1715, 1992.

[**29**] J.M. Wiesenfeld, J.S. Perino, A.H. Gnauck and B. Glance. *Bit error rate performance for wavelength conversion at 20 Gbit/s*. Electronics Letters, 30(9):720-721, 1994.

[**30**] S.L. Danielsen, C. Joergensen, M. Vaa, B. Mikkelsen, K. E. Stubkjaer, P. Doussiere and F.L. Pommerau. *Bit error rate assessment of 40 Gbit/s all-optical polarisation independent wavelength converter*. Electronics Letters, 32(18):1688-1689, 1996.

[**31**] K. A. Rauschenbach, K.L. Hall, J.C. Livas and G. Raybon. *All-optical pulsewidth and wavelength conversion at 10 Gb/s using a nonlinear optical loop mirror*. IEEE Photonics Technology Letters, 6(9):1130-1132, 1994.

[**32**] T. Durhuus, C. Joergensen, B. Mikkelsen, R.J.S. Pedersen and K.E. Stubkjaer. *All optical wavelength conversion by SOA's in a Mach-Zehnder configuration*. IEEE Photonics Technology Letters, 6(1):53-55, 1994.

[**33**] F. Ratovelomanana, N. Vodjdani, A. Enard, G. Glastre, D. Rondi, R. Blondeau, C. Joergensen, T. Durhuus, B. Mikkelsen, K.E. Stubkjaer, A. Jourdan,

and G. Soulage. *An all-optical wavelength-converter with semiconductor optical amplifiers monolithically integrated in an asymmetric passive Mach-Zehnder interferometer.* IEEE Photonics Technology Letters, 7(9):992-994, 1995.

[**34**] B. Mikkelsen, S. L. Danielsen, C. Joergensen, R. J. S. Pedersen, H. N. Poulsen and K. E. Stubkjaer. *All-optical noise reduction capability of interferometric wavelength converters.* Electronics Letters, 32(6):566-567, 1996.

[**35**] P. P. Absil, J. V. Hryniewicz, B. E. Little, P.S. Cho, R.A. Wilson, L.G. Joneckis and P.-T. Ho. *Wavelength conversion in GaAs micro-ring resonators.* Optics Letters, 25(8):554-556, 2000.

[**36**] Q. Xu, V. R. Almeida and M. Lipson. *Micrometer-scale all-optical wavelength converter on siliocn.* Optics Letters, 30(20):2733-2735, 2000.

[**37**] L. Liu, J. Van Campenhout, G. Roelkens, D. Van Thourhout, P. Rojo-Romeo, P. Regreny, C. Seassal, J.-M. Fédéli and R. Baets. *Ultralow-power all-optical wavelength conversion in a silicon-on-insulator waveguide based on a heterogeneously integrated III-V microdisk laser.* Applied Physics Letters, 93(6):061107(1)-061107(3), 2008.

[**38**] O. Raz, L. Liu, R. Kumar, G. Morthier, D. Van Thourhout, P. Regreny, P. Rojo-Romeo, T. de Vries and H.J.S. Dorren. *Compact, low power and low threshold electrically pumped micro disc lasers for 20Gb/s non return to zero all optical wavelength conversion.* The Optical Fiber Communication Conference and Exposition (OFC) and The National Fiber Optic Engineers Conference (NFOEC), p.OMQ5, 2010.

[**39**] J. Hofrichter, O. Raz, L. Liu, G. Morthier, F. Horst, P. Regreny, T. de Vries, H.J.S Dorren and B.J. Offrein. *All-optical wavelength conversion using mode switching in InP microdisc laser.* Electronics Letters, 47(16):927-929, 2011.

5

All-optical time domain demultiplexing and format conversion

Ultra-high-speed time-division multiplexing-demultiplexing (MUX/DEMUX), where the channels of the lower digital hierarchy signals are multiplexed to those of the higher hierarchy signals (MUX) and vice versa (DEMUX) in the time-domain, is one of the key functions to achieve high speed optical transmission. The basic principle of time-division multiplexing and demultiplexing is that each of the baseband data streams is allocated a series of time slots on the multiplexed channel. A MUX assembles the data streams at higher bit rates from the baseband streams and a DEMUX reconstructs the original data streams at lower bit rates. The techniques for this purpose are well established in the electronic domain but are power hungry due to OEO conversions. In the optical domain these techniques are emerging and the pace of progress is quite fast. As an example, all-optical demultiplexing of 640-to-10 Gbits/s has been demonstrated in a 5 cm long chalcogenide waveguide using FWM effect [1].

All-optical demultplexing has been realized on a silicon [2-3] as well as on III-V [4] platform. In silicon material based devices; FWM is used for all-optical demultiplexing, but the power requirements are high. Resonant structures in III-V-on-silicon material can reduce the power requirements for the realization

of all-optical demultiplexers. In addition, the III-V-on-silicon devices provide a size advantage in comparison to the devices investigated so far for all-optical demultiplexing. In this chapter, a proof-of-concept demonstration of all-optical demultiplexing using a microdisk of 7.5 μm is presented. The details about the transmission resonance characteristics, which are used for demonstration of all-optical demultiplexing, of this microdisk have been described in chapter 4 (section 4.1.3.1). In the second part, a format converter from NRZ to RZ signal is presented. The working principle of NRZ to RZ conversion is similar to all-optical demultiplexing. But it differs from demultiplexing by the fact that the pulse width (in the time domain) of the output signal is reduced. All the experiments reported in this chapter were done without application of an electrical bias to the microdisk.

5.1 All-optical demultiplexing using a microdisk resonator

5.1.1 Concept

The effect of refractive index modulation caused by the free carrier generation in a pump-probe configuration can be exploited to realize an all-optical demultiplexer in a microdisk resonator. The modulation of the refractive index results in the modulation of the transmission characteristics of the microdisk resonator. In a pump-probe configuration, a probe is tuned to one resonance wavelength while the pump is tuned to another. For the implementation of the demultiplexer in microdisk resonators an optical clock is used as a pump and the optical data signal is used as a probe. If the wavelength of the optical data signal is chosen to be on-resonance of the microdisk resonator then in the absence of the optical clock pulses, the optical data signal will be coupled into the microdisk. In the presence of the optical clock pulses, free carriers will be generated which will result in a blue shift of the resonance and the optical data will become off-resonance for the duration of the optical clock pulses. This way the optical data output from the microdisk will be high or low depending upon the presence or absence of the optical clock pulses. This is illustrated in figure 5.1. The combination of the input optical data rate and the optical clock rate will decide the data rate of the demultiplexed output [5-7].

5.1.2 Dynamic measurements on all-optical demultiplexing

The all-optical demultiplexing experiments were carried out using the set-up as shown in figure 5.2. A 10 Gbits/s NRZ optical data signal was generated using a pulse pattern generator (PPG), a first electro-optic LiNbO3 modulator (LN

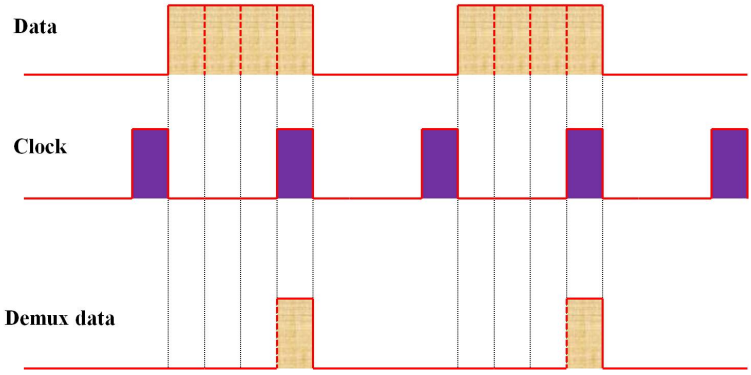

Figure 5.1: Illustration of the concept of all-optical de-multiplexing.

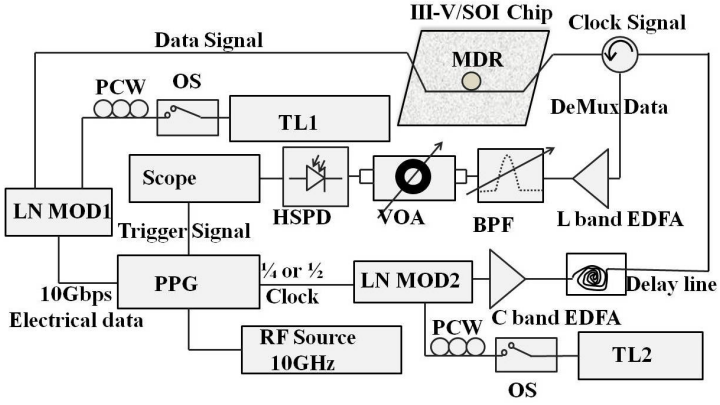

Figure 5.2: Schematic of experimental set-up used for all-optical demultiplexing.

MOD1) and a first tunable laser (TL1) tuned around a longer wavelength (1580.9 nm) resonance of the microdisk. An optical clock signal having a repetition rate of 2.5 GHz and 5 GHz was generated using a second tunable laser (TL2) tuned around a shorter wavelength (1550.1 nm) resonance, a second electro-optic LiNbO3 modulator (LN MOD2) and the electrical clock from the PPG. An optical delay line was used for the synchronization of the optical clock with the optical data signal. A circulator was used to collect the demultiplexed data and an EDFA was used to amplify the demultiplexed data. A band pass filter (BPF) was used to suppress the ASE noise generated from the EDFA. A variable optical attenuator (VOA) was used to control the input power to the high-speed

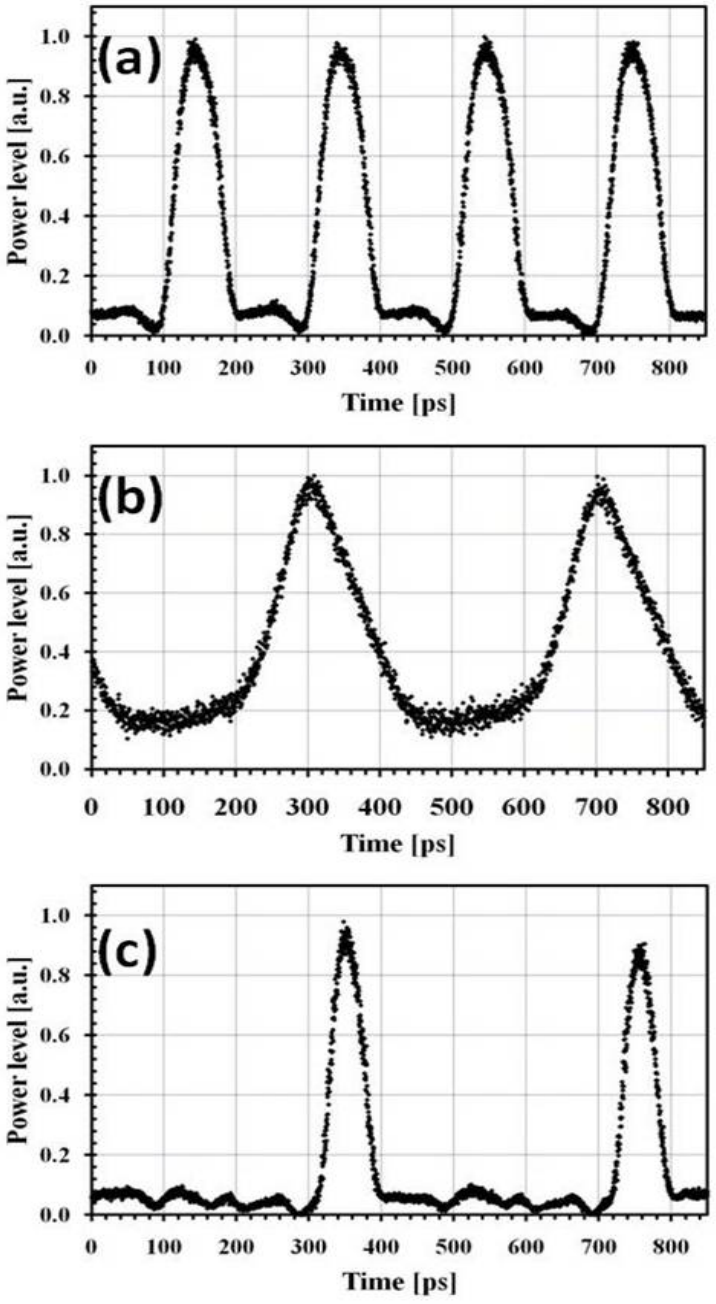

Figure 5.3: Waveforms of (a) 10 Gbits/s 01010..optical input data, (b) 2.5 GHz optical clock, (c) Demultiplexed output as a result of (a) and (c).

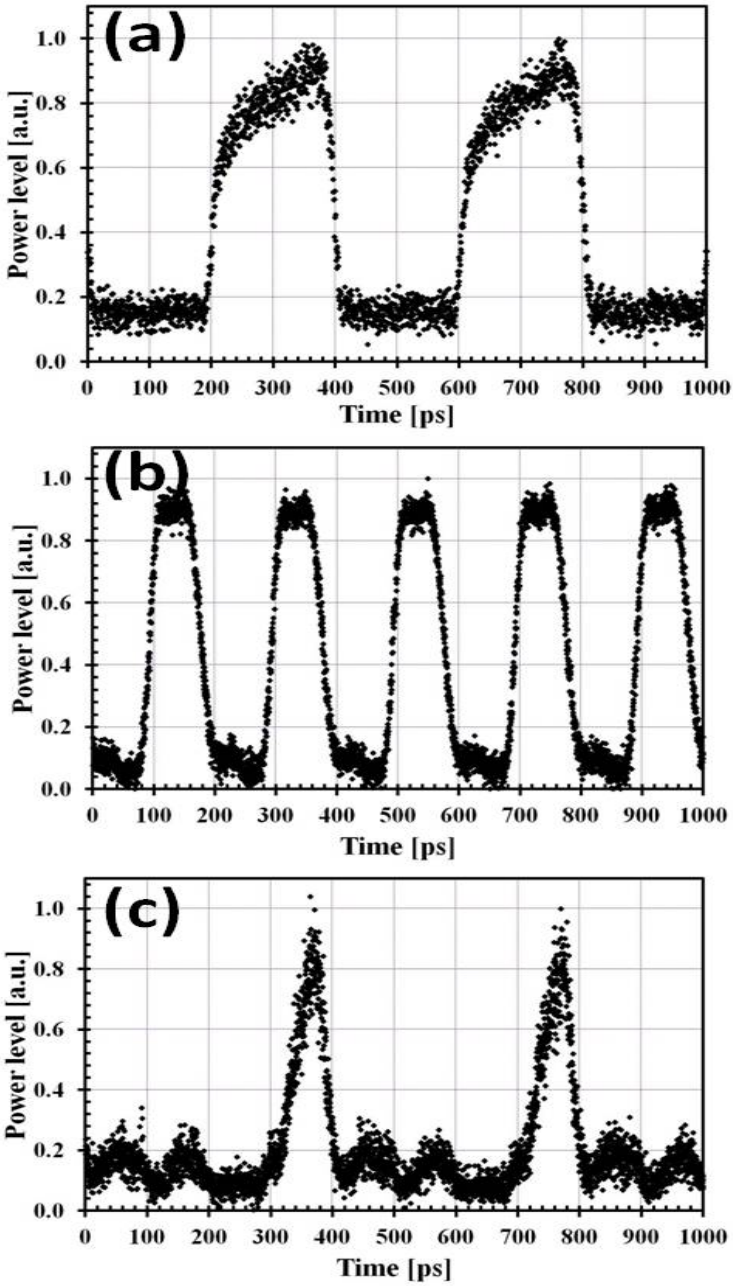

Figure 5.4: Waveforms of (a) 10Gbits/s 001100..optical input data, (b) 5 GHz optical clock and (c) Demultiplexed output as a result of (a) and (b).

photodiode (HSPD) connected to the scope. The waveform of the optical data signal at 10 Gbits/s with alternate 0s and 1s is shown in figure 5.3(a) while 5.3(b) shows the waveform of the optical clock signal at 2.5 GHz.

To demultiplex the optical data signal, the wavelength of the data signal was tuned to the longer resonance wavelength while the wavelength of the clock signal was tuned to the shorter resonance wavelength. In the absence of the clock signal, the data signal remained coupled into the microdisk and a low dc power level was seen on the scope. In the presence of the clock, the resonance of the microdisk shifts, because of the plasma-dispersion effect due to generated free carriers, causing the data signal to go out of resonance and therefore the demultiplexed data was seen on the scope for the duration when the clock level is high. Figure 5.3(c) shows the demultiplexed output. Comparing the figures 5.3(a) and 5.3(c), it can be seen that the logic 1 levels which are originally separated by 200 ps become separated by 400 ps after demultiplexing. The experiment was repeated for the data pattern of 001100..and an optical clock at the rate of 5 GHz. Figure 5.4(a) and 5.4(b) shows the waveform of the optical data and the optical clock respectively. The output after demultiplexing is plotted in figure 5.4(c).

5.2 All-optical format conversion

5.2.1 Motivation

All-optical format conversion is important for connecting different all-optical networks. Two basic modulation formats known as non-return-to-zero(NRZ) and return-to-zero (RZ) have found extensive use in fiber communication systems. Depending upon the size and requirements of the network, either an NRZ or RZ modulation format can be selected for use in future optical networks [8]. The RZ data format is widely employed in optical time-division multiplexing (OTDM) systems due to its tolerance for polarization mode dispersion and fiber nonlinearities [9]. The NRZ format is preferred in wavelength division multiplexed (WDM) networks owing to its high spectral efficiency and tolerance to timing-jitter. Format conversion from NRZ to RZ and vice-versa becomes important to add to the flexibility and scalability of optical networks. To perform the format conversion from NRZ to RZ all-optical e.g. [10-23] as well as optoelectronic e.g. [24-28] approaches have been explored. Most of the investigated all-optical approaches employed semiconductor optical amplifiers (SOAs) and very few used other devices such as periodically poled lithium niobate waveguides [29], silicon waveguides [10], III-V waveguides [23] and III-V ring lasers [30]. All-optical data format conversion devices based on SOAs have a large footprint with the cavity length of a single SOA varying from several hundreds of micrometers to a few tens of millimeters, e.g. the SOA used in reference [19]

had a cavity length of 20.83 mm [31]. Moreover the SOA based format convertors need a DC bias of several hundreds of mAs which results into extra power consumption. Likewise other kinds of format converters [10], [23], [24-31] have large footprints which reduce their potential for compact integration and make them less suitable for practical applications.

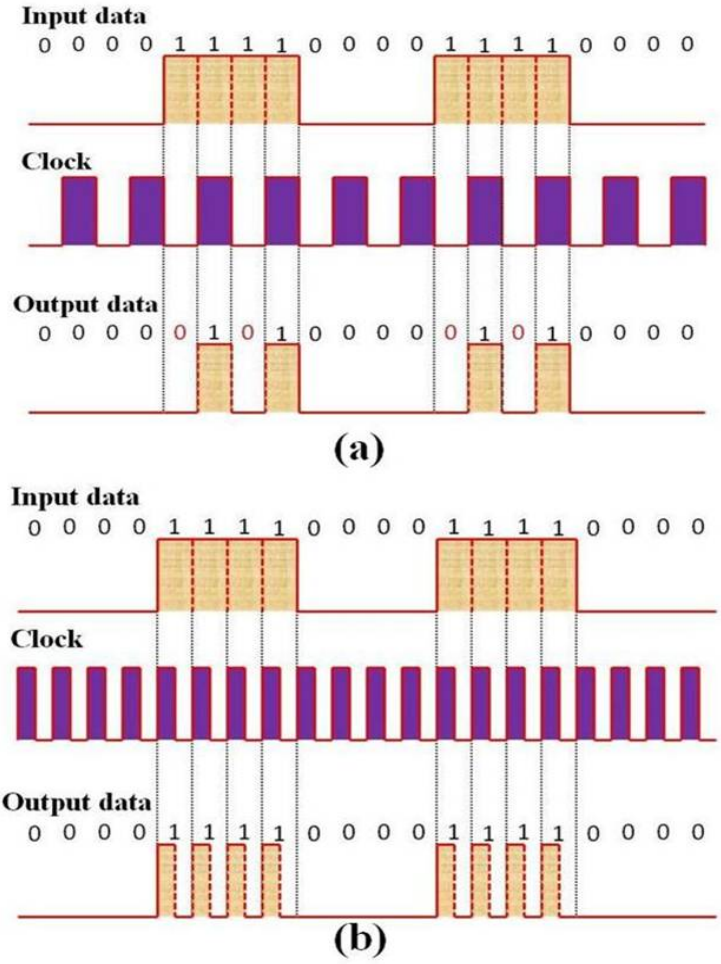

Figure 5.5: Illustration of (a) data output as a function of level (high /low) of the clock, (b) format conversion from NRZ to RZ.

5.2.2 Concept of NRZ-OOK to RZ-OOK format conversion

Using the effect of refractive index modulation caused by the free carrier generation in a pump-probe configuration, the transmission characteristics of the microdisk/ring resonators can be changed in real-time [32-33]. In the pump-probe configuration, a probe is tuned to one resonance wavelength while the pump is tuned to another. If an optical pulse train (clock, here after) is used as a pump and the data signal as a probe, then the pattern as well the format of the data signal can be changed. If the wavelength of the data signal is chosen to be on- resonance then in the absence of the clock pulses, the data signal will be coupled into the microdisk. In the presence of the clock pulses, free carriers will be generated resulting in a blue shift of the resonance and the data will become off-resonance for the duration of the pulses. This way the data output from the microdisk will be high or low depending upon the presence or absence of the clock pulses. If the clock pulse duration is shorter than the bit duration of the data then the format of the NRZ signal becomes RZ. Figure 5.5 illustrates the concept by taking an example of data pattern and clock signal.

In figure 5.5(a) the clock pulse duration is chosen equal to the bit duration. If the data pattern 0000111100001111....is imprinted on a resonance wavelength of the microdisk, then only for the duration for which the clock as well as the input data is high, the output data will be high. Therefore, the data pattern at the output becomes 0000010100000101.... . If we consider the consecutive four 1s to be a single pulse; we can say it has been carved into two smaller pulses. As illustrated in figure 5.5(b), if the duration of the clock pulse is less than that of a bit and both the clock as well as data are high, in the output each '1'occupies the time of the clock pulse. This is effectively the conversion of the data format from NRZ to RZ.

5.2.3 Dynamic measurements for format conversion

Experiments were done first to verify the concept of pulse carving, as illustrated in figure 5.5(a), using a 10 Gbit/s NRZ-OOK signal and 5 GHz clock. The schematic of the experimental set-up used is shown in figure 5.6. Using a pulse pattern generator (PPG), a 10 Gbit/s NRZ electrical data pattern of four consecutive 1s followed by four consecutive 0s, and there after repeating periodically, was generated. The electrical data pattern was converted into the optical domain by using the first electro-optic LiNbO3 modulator (MOD1) and the first tunable laser (TL1). Use of polarization controlling wheels (PCWs) ensures that the generated optical data is TE polarized. Using the 1/2 clock output of the PPG, a second electro-optic LiNbO3 modulator (MOD2) and the second tunable laser (TL2); an optical clock with a repetition rate of 5 GHz was generated. The tunable lasers TL1 and TL2 were tuned to the resonant wavelengths 1580.9

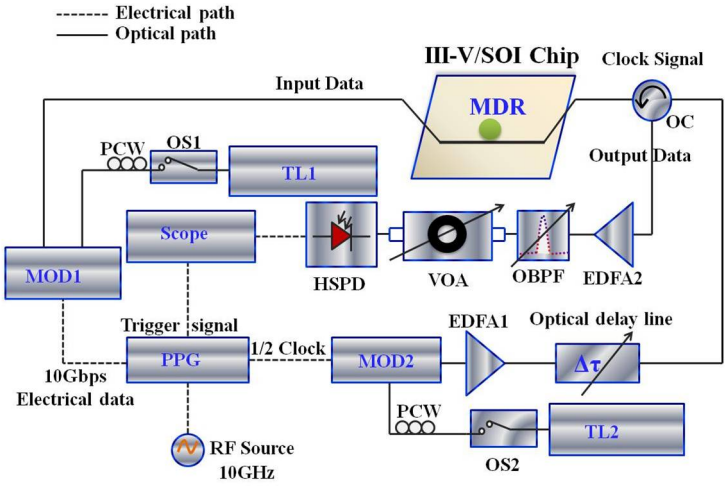

Figure 5.6: Schematic of the experimental setup for pulse carving measurements.

nm and 1550.1 nm respectively. Output of the MOD2 was amplified using a C band erbium-doped fiber amplifier (EDFA1) and was followed by an optical delay line to synchronize the optical clock with the optical input data. The output data was collected at the drop-port of an optical circulator (OC) and was amplified using an L band erbium-doped fiber amplifier (EDFA2). An optical band pass filter (OBPF) followed the EDFA2 to suppress the ASE noise. A variable optical attenuator (VOA) was used to control the input power to the high-speed photodiode (HSPD) connected to the scope. The waveform of the optical data and the optical clock is shown in figure 5.7(a) and 5.7(b) respectively. The average power of the input optical data and the optical clock in the SOI waveguide was estimated to be ~ -2 and ~ +1 dBm respectively. In the absence of the optical clock, the optical data signal remained coupled into the microdisk and a low power level was seen on the scope. Injection of the optical clock pulses into the microdisk results into the generation of the free carriers causing a blue-shift of the resonance. This causes the input optical data to go out of resonance. Therefore, output optical data had a high power level only when both the input optical data as well as the optical clock were high as illustrated in figure 5.7(c). It is clear from these plots that a 400ps input data pulse, which is formed as a result of four consecutive 1s, has been divided into two pulses and first and third 1s have been converted to 0s due to the low level of the optical clock in this time interval. This way the data pattern has changed from 0000111100001111....to 0000010100000101....as discussed in section 5.2.2. Secondly, by choosing the

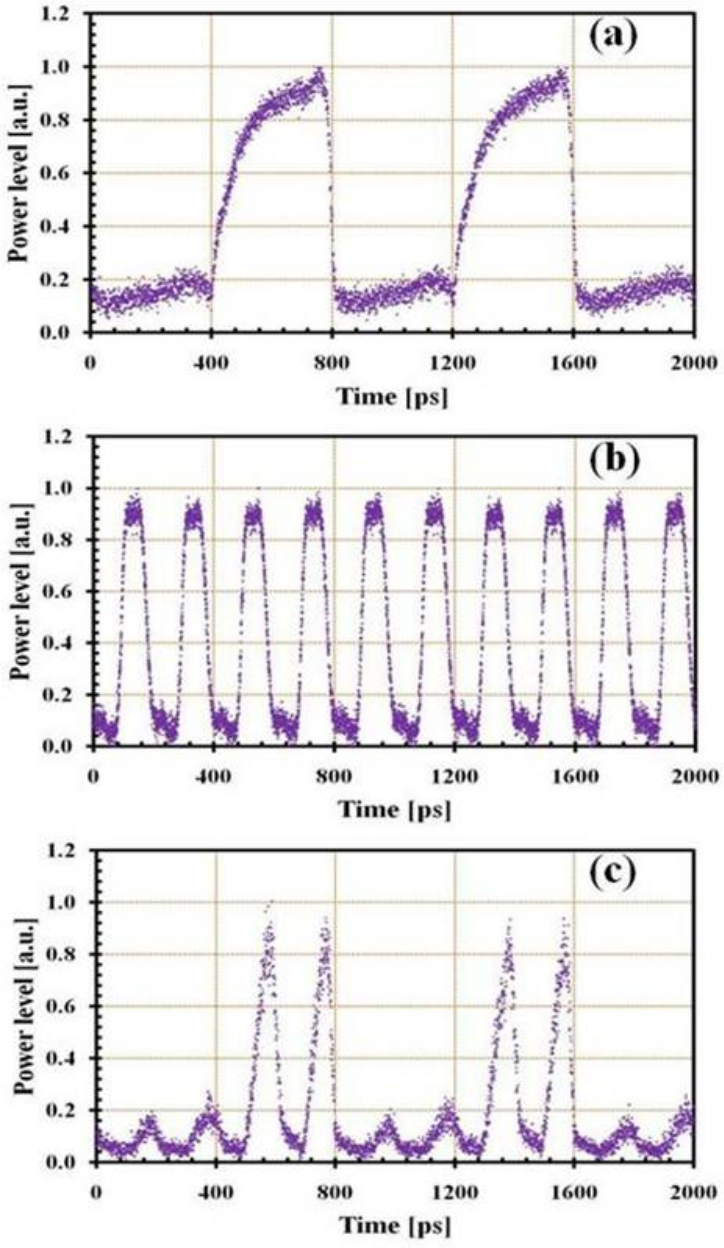

Figure 5.7: Waveform of (a) optical input data, (b) optical clock and (c) optical output data.

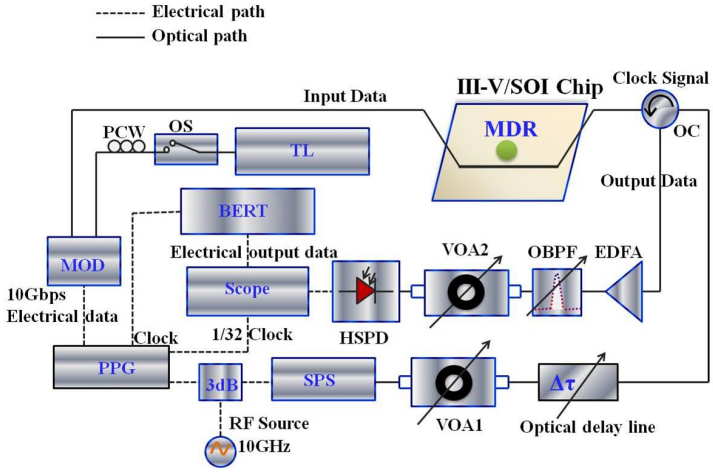

Figure 5.8: Schematic of the experimental set-up used for the format conversion.

clock pulses shorter than the bit duration, format conversion experiments were performed and the system performance in terms of the bit-error-rate and Q factor of the eye diagrams was evaluated. The sketch of the experimental set-up used for this purpose is drawn in figure 5.8. The method of generating the optical input data remained the same as in the first experiment. To generate the optical clock signal, a short pulse source (SPS) was used. It was driven by the same RF source, using a 3dB RF splitter, which drived the PPG. The optical clock at 10 GHz had a pulse width (FWHM) of ~ 8 ps. A variable optical attenuator (VOA1) was used to regulate the output power of the optical clock. The procedure of detecting the optical output data was the same as in the first part. For the bit-error-rate measurements, the electrical output data from the scope was fed to a bit-error-rate tester (BERT).First a 10 Gbit/s NRZ-OOK optical input data pattern of alternate 1s and 0s was used. The input optical data waveform consisting of alternate 1s and 0s and the optical clock is shown in figure 5.9(a) and 5.9(b) respectively. In figure 6(b), the pulse width looks much wider than its actual width (FWHM 8ps) due to the limited bandwidth of the photodiode (~ 30GHz). Figure 5.9(c) shows the format converted optical data output pattern. The 1 bit of the optical output data occupies a time slot of ~ 50 ps although the clock duration is much shorter than this time slot. This is due to the slower dynamics of the photo-generated carriers in the microdisk. For the system performance measurements, the optical input data signal is changed to a PRBS pattern of length 2^7-1. Figure 5.10(a) shows a part of the waveform of the format converted PRBS signal from NRZ to RZ. Figure 5.10(b) shows the bit-error measurement curves of the input NRZ and the output RZ data.

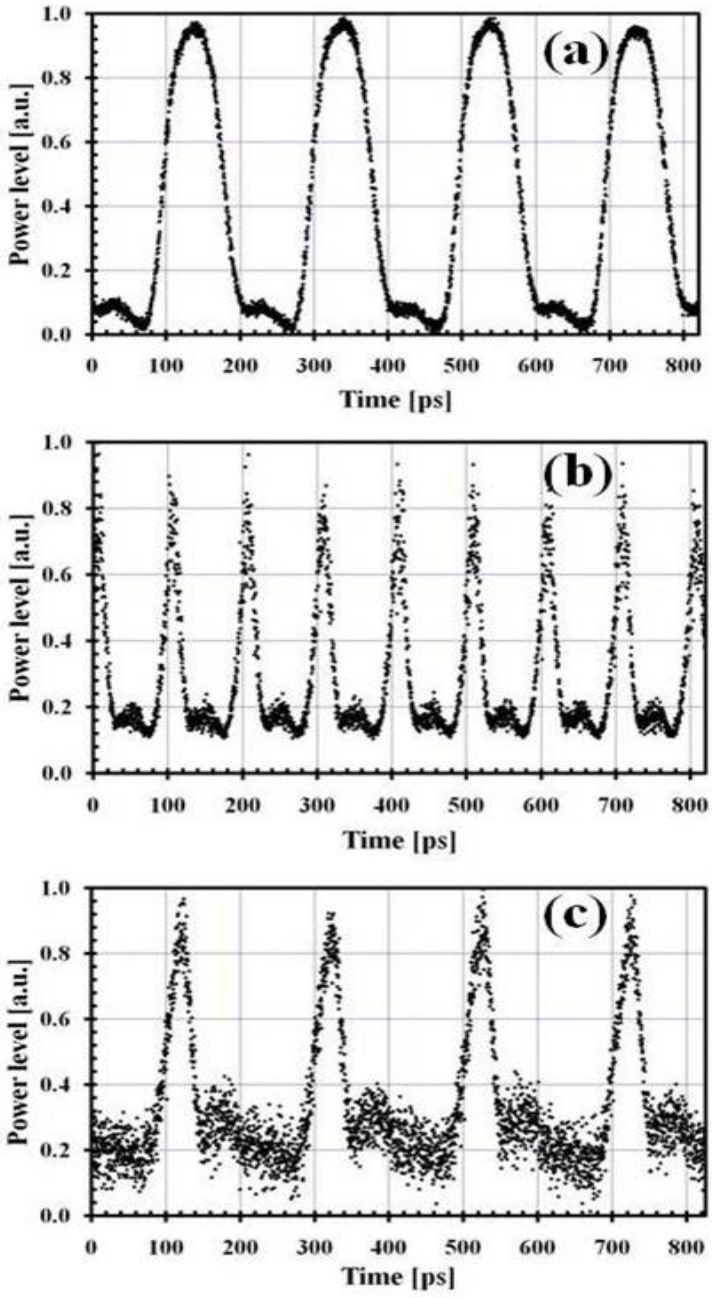

Figure 5.9: Waveform of (a) optical input data, (b) optical clock and (c) optical output data.

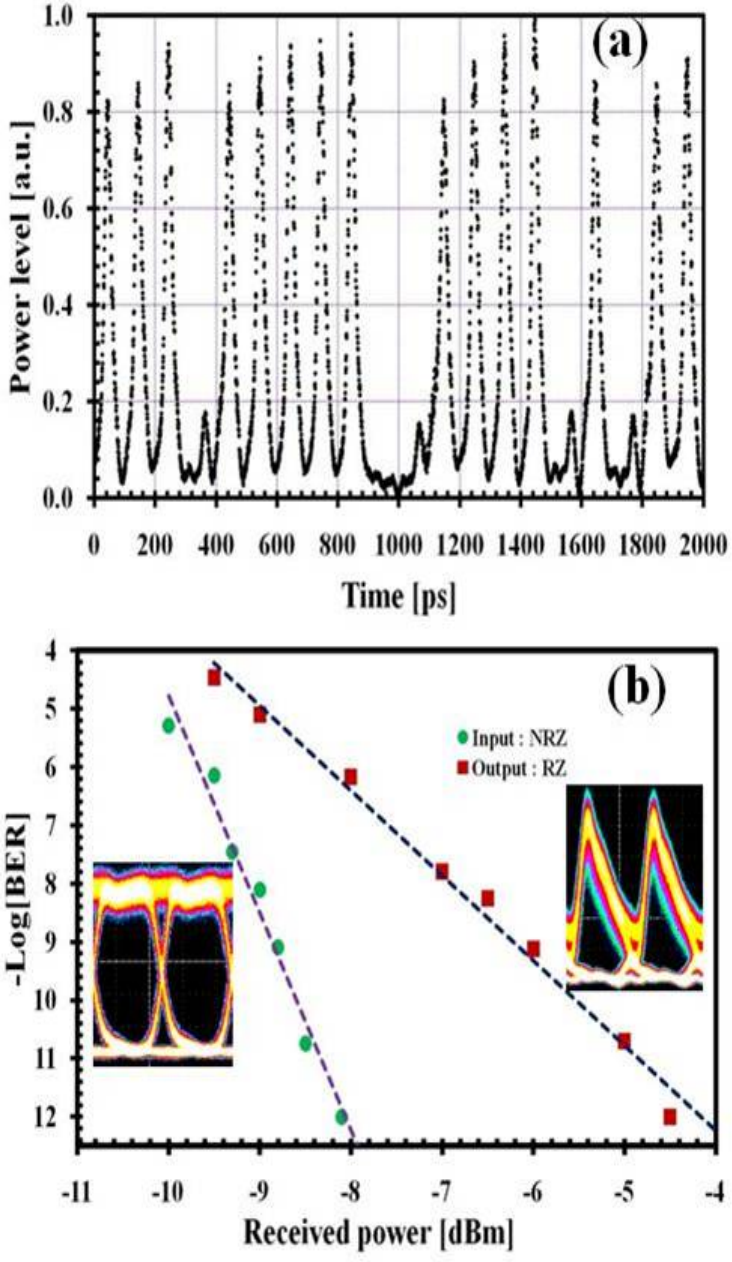

.5

Figure 5.10: Waveform of a part of the format converted PRBS data and (b) System performance: BER and eye diagram before (left) and after (right) format conversion. The time scale for both the eye diagrams is 48ps/division.

It is to be noted that the BER measurements for the input NRZ data was performed by keeping it off-resonance of the microdisk. An error free (BER ~10^{-12}) format conversion was achieved with a power penalty of 3.6 dB. The ASE noise added due to the amplification of the format converted signal results into the power penalty. The patterning effect is another possible source of signal degradation and the power penalty. The amplification was required for the format converted signal because it had half the power of the original signal due to the basic procedure and principle of the format conversion involved here. It was found that the Q factor of the format converted signal matches very well to the measured BER. For example, at a received power of ~ -6dBm, the Q factor is ~6 which correspond to a BER ~ 10^{-9} [34] and the same is found from the BER measurements as can be seen from figure 5.10(b). As an illustration, the eye diagram of the format converted signal and that of the original signal is shown in figure 5.10(b).

5.3 Conclusions and discussion

In conclusion, in the first part of this chapter, demonstration of all-optical time domain demultiplexing with different combinations of 1s and 0s for a 10 Gbit-s/s NRZ optical signal and for optical clocks at 2.5 GHz and 5 GHz has been described. This concept is elaborated further for pulse carving as described in second part of this chapter. The time domain demultiplexing will work for a PRBS pattern too. This was proved by the fact that format conversion was possible for a PRBS data pattern. The concept of pulse carving led to demonstration of NRZ to RZ format conversion. An error free 10Gbit/s NRZ-OOK to RZ-OOK format conversion in a 7.5 μm III-V-on-silicon microdisk completely processed in a CMOS pilot line was demonstrated. The format conversion was achieved with a moderate power penalty and relatively low average power consumption in a pump-probe configuration. The wavelength of the data signal remains preserved after the format conversion. The speed of the format conversion can be further increased by (a) applying a reverse bias, (b) use of a holding beam, and (c) ion-implantation in the active region of the microdisk resonator to improve the carrier dynamics. Use of a holding beam will increase the total power consumption as an extra optical source will be required to provide the holding beam. Also, ion implantaion will result into higher propagation loss of microdisk and hence will increase the total power consumption.

References

[**1**] M. Galili, J. Xu, H.C. Mulvad, L.K. Oxenløwe, A.T. Clausen, P. Jeppesen, B.L.-Davies, S. Madden, A. Rode, D.-Y. Choi, M. Pelusi, F. Luan and B.J. Eggleton. *Breakthrough switching speed with an all-optical chalcogenide glass chip: 640 Gbit/s demultiplexing.* Optics Express 17(4):2182-2187, 2009.

[**2**] B. Corcoran, M.D. Pelusi, C.Monat, J. Li, L. O'Faolain, T.F. Krauss and B.J. Eggleton. *Ultracompact 160 Gbaud all-optical demultiplexing exploiting slow light in an engineered silicon photonic crystal waveguide.* Optics Letters, 36(9):1728-1730, 2011.

[**3**] F. Li, M. Pelusi, D-X. Xu, A. Densmore, R. Ma, S. Janz and D.J. Moss. *Error-free all-optical demultiplexing at 160Gb/s via FWM in a silicon nanowire.* Optics Express 18(4):3905-3910, 2010.

[**4**] I. Cestier, A. Willinger, V. Eckhouse, G. Eisenstein, S. Combrié, P. Colman, G. Lehoucq and A. De Rossi.*Time domain switching/demultiplexing using four wave mixing in GaInP photonic crystal waveguides.* Optics Express 19(7):6093-6099, 2011.

[**5**] R. Kumar, T. Spuesens, P. Mechet, P. Regreny, J.- M. Fedeli, N. Olivier, G. Roelkens, D. Van Thourhout and G. Morthier. *All-optical de-multiplexing using III-V/SOI microdisk resonators.* European Semiconductor Laser Workshop (ESLW), p.C2, 2011.

[**6**] R. Kumar, T. Spuesens, P. Mechet, J.-M. Fedeli, N. Olivier, P. Regreny, G. Roelkens, D. Van Thourhout and G. Morthier. *Proof-of-concept Demonstration of an all-optical De-multiplexer using III-V/SOI microdisk resonator fabricated in a CMOS pilot Line.* IEEE Photonics Conference, p.127-128, 2011.

[**7**] R. Kumar, T. Spuesens, P. Mechet, J.-M. Fedeli, N. Olivier, P. Regreny, G. Roelkens, D. Van Thourhout and G. Morthier. *All-optical de-multiplexing of 10 Gbps data using III-V/SOI microdisk resonators.* Annual Symposium of the IEEE Photononics Benelux Chapter, p.89-92, 2011.

[**8**] D. Norte, E.Park and A.E. Willner. *All-optical TDM-to-WDM data format conversion in a dynamically reconfigurable WDM network.* IEEE Photonics Technology Letters, 7(8):920-922, 1995.

[**9**] D. Breuer and K. Petermann. *Comparison of NRZ- and RZ-modulation format for 40-Gb/s TDM standard fiber systems.* IEEE Photonics Technology Letters, 9(3):398-400, 1997.

[**10**] W. Astar, J.B. Driscoll, X. Liu, J.I. Dadap, W.M.J. Green, Y.A. Vlasov, G.M. Carter and R.M. Osgood, Jr. *Conversion of 10Gb/s NRZ-OOK to RZ-OOK utilizing XPM in a Si nanowire.* Optics Express, 17(15):12987-12999, 2009.

[**11**] L.-S. Yan, A.-L Yi, W. Pan, B. Luo and J. Ye. *Simultaneous NRZ-to-RZ format conversion and one-to-six error-free channel multicasting using a single pump in a highly nonlinear fiber.* Optics Express, 18(20):21404-21409, 2010.

[**12**] X. yang, A.K. Mishra, R.J. Manning, R.P. Webb and A.D. Ellis. *All-optical 42.6Gbit/s NRZ to RZ format conversion by cross-phase modulation in a single SOA.* Electronics Letters, 43(16):890-892, 2007.

[**13**] X. yang, A.K. Mishra, R.J. Manning and R. Giller. *All-optical 40 Gbit/s NRZ to RZ format conversion by nonlinear polarization rotation in SOAs.* Electronics Letters, 43(8),469-471, 2007.

[**14**] J. Dong, X. Zhang, F. Wang, Y. Yu and D. Huang. *Single-to-dual channel NRZ-to-RZ format conversion by four-wave mixing in single semiconductor optical amplifier.* Electronics Letters, 44(12):763-764, 2008.

[**15**] X. Zhao and C. Lou. *Investigation of all-optical nonreturn-to-zero-to-return-to-zero format converter based on a semiconductor optical amplifier and a reconfigurable delayed interferometer.* Applied Optics, 49(7):1158-1162, 2010.

[**16**] J. Dong, X. Zhang, J. Xu, D. Huang, S. Fu and P. Shum. *40Gb/s all-optical NRZ to RZ format conversion using single SOA assisted by optical bandpass filter.* Optics Express 15(6):2907-2914, 2007.

[**17**] H.N. Tan, M. Matsuura and N. Kishi. *Transmission performance of a wavelength and NRZ-to-RZ format conversion with pulsewidth tunability by combination of SOA- and fiber-based switches.* Optics Express 16(23):19063-19071, 2008.

[**18**] C.G. Lee, Y.J. Kim, C.S. Park, H.J. Lee and C.-S. Park. *Experimental demonstration of 10-Gb/s data format conversion between NRZ and RZ using SOA-loop-mirror.* Journal of Lightwave Technology, 23(2):834-841, 2005.

[**19**] S. Fu, W.-D. Zhong, P.P. Shum and Y.J. Wen. *All-optical NRZ-OOK-to-RZ-OOK format conversion with tunable duty cycles using nonlinear polarization rotation of a semiconductor optical amplifier.* Optics Communications, 282(11):2143-2146, 2009.

[**20**] G.-R. Lin, K.-C Yu and Y.-C. Chang. *10Gbit/s all-optical non-return to zero-return-to-zero data format conversion on a backward dark-optical-comb injected semiconductor optical amplifier.* Optics Letters. 31(10):1376-1378, 2006.

[**21**] J. Yu, G.K. Chang, J. Barry and Y. Su *40Gbit/s signal format conversion from NRZ to RZ using a Mach-Zehnder interferometer.* Optics Communications, 248(4-6):419-422, 2005.

[**22**] T. Kurosu, S. Namiki, R. Akimoto, S. Sekiguchi, N. Yasuoka, K. Morito, T. Hasama and H. Ishikawa. *Demonstration of 172-Gb/s optical time domain multiplexing and demultiplexing using integrable semiconductor devices.* IEEE Photonic Technology Letters, 22(19):1416-1418, 2010.

[**23**] P. Apiratikul, W. Astar, G.M. Carter and T.E. Murphy. *10-Gb/s wavelength and pulse format conversion using four-wave mixing in a GaAs waveguide.* IEEE Photonics Technology Letters, 22(12):872-874, 2010.

[**24**] S. Pan and J. Yao. *Optical NRZ to RZ format conversion based on a frequency-doubling optoelectronic oscillator.* IEEE LEOS annual meeting, p.797-798, 2009.

[**25**] X. Zhao, C. Lou, H. Zhou, D. Lu and L. Huo. *Optical regenerative NRZ to RZ format conversion based on cascaded lithium niobate modulators.* Optics Express, 18():23657-23663, 2010.

[**26**] L. Huo, Y. Dong, C. Lou and Y. Gao. *Clock extraction using an optoelectronic oscillator from high-speed NRZ signal and NRZ-to-RZ format transformation.* IEEE Photonics Technology Letters, 15(7):981-983, 2003.

[**27**] Y. Yu, X. Zhang, J.B.R.-Fernandez, D. Huang, R. V. Pemty and I.H. White. *Simultaneous multiple DWDM channel NRZ-to-RZ regenerative format conversion at 10 and 20 Gb/s.* Optics Express 17(5):3964-3969, 2009.

[**28**] G. Lu, L. Chen and C. Chan. *Novel NRZ-to-RZ Format Conversion with Tunable Pulsewidth Using Phase Modulator and Interleaver.* Optical Fiber Communication Conference(OFC) and Exposition and The National Fiber Optic Engineers Conference(NFOEC), p.JThB32, 2006.

[**29**] J. Wang, J. Sun, Q. Sun, X. Zhang, D. Huang and M. M. Fezer. *First demonstration of PPLN +RSOA-based tunable all-optical NRZ-to-RZ format conversion.* European Conference on Optical Communication(ECOC), p.1-2, 2007.

[**30**] B. Li, M.I. Memon, G.Mezosi, Z. Wang, M. Sorel and S. You. *All-optical logic gates using bistable semiconductor ring lasers.* Journal of Optical Communications, 30(4):190-194, 2009.

[**31**] See data sheet, *CIP SOA(SOA-L-OEC-1550)*on web address: http://www.coretk.com/CataLog/cata_img/FILE/963076829/CIP/166_167_1139895559.pdf

[**32**] V. Van, T.A. Ibrahim, P.P. Absil, F.G. Johnson, R. Grover and P.-T. Ho. *Optical signal processing using nonlinear semiconductor microring resonators.* IEEE Journal of Selected Topics in Quantum Electronics, 8(3):705-713, 2002.

[**33**] S.F. Preble, Q. Xu, B.S. Schmidt and M. Lipson. *Ultrafast all-optical modulation on a silicon chip.* Optics Letters, 30(21):2891-2893, 2005.

[**34**] G.P. Agrawal. *Fiber-Optic Communication Systems*, Chapter 4, John Wiley & Sons, 2002.

6

Towards the complex PICs with III-V-on-silicon microdisks

As described in the preceding chapters (3, 4 and 5), a number of optical functionalities, namely set-reset flip-flops, gates, demultiplexers, wavelength converters and format converters have been demonstrated using III-V microdisks integrated on top of SOI waveguide circuits. The demonstrated functionalities have a promise of serving as building blocks for the realization of PICs with increased complexity level. The foot-prints of PICs which can be realized using the functionalities demonstrated here will be significantly less as compared to any other approach investigated so far. In this chapter, a description of some of the complex PICs, which can be constructed on the basis of demonstrated functionalities, is presented. The feasibility of complex PICs at conceptual level is explored. Many designs of complex PICs were made and a brief description of those designs is presented highlighting the SOI access waveguides and the routing paths. This is complemented by the designs needed, in particular the electrical probe pads, for processing III-V microdisks. So far, complex PICs have not been measured as the fabrication work is still in progress. Details about the designs of different layers of III-V microdisks have been presented in chapter 2. As the complexity level increases, many issues need to be resolved which can be tackled at fabrication or post fabrication (characterization) level. A number of such problems are identified during the course of the research work presented

here and possible solutions are explored.

6.1 The data flip-flops

A data flip-flop can be constructed using an all-optical gate and a set-reset flip-flop as described in chapters 4 and 3 respectively. The output of the gate serves as a control input for changing the state of the set-reset flip-flop. A simplified diagram of a data flip-flop formed as a result of cascading the optical gate and set-reset flip-flop is drawn in figure 6.1. The optical data is tuned to one resonance wavelength of the gate while the optical clock is tuned to another resonance wavelength. The optical clock is chosen to be weaker than the optical data in terms of optical power. It passes to the upper waveguide coupled to the set-reset flip-flop when the data has low (logic 0) level. This combination of clock and low level of data acts as set input to set-reset flip-flop. When the data has a high level (logic 1), it blue shifts the transmission resonance of the gate and the clock becomes off-resonance to the gate and it directly couples to the set-reset flip-flop. This combination of the clock and high level of data serves as a reset input to set-reset flip-flop. The design of the SOI waveguide circuit and the III-

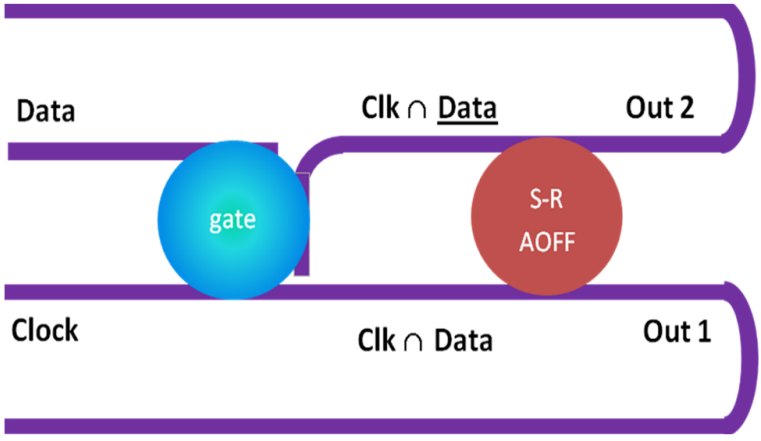

Figure 6.1: Simplified diagram of a data flip-flop .

V contact lithography mask for the data flip-flop in accordance to figure 6.1 was made using the IPKISS and PICAZZO software [1]. While designing the waveguide circuit and the III-V contact mask special emphasis was given to solve the possible difficulties which could arise during the measurements. Since access fibers will be needed at different inputs and outputs, input and output waveguides were ended with the grating couplers at a pitch of 127 μm corresponding to the pitch of an standard fiber array. A multiple number of electrical probes

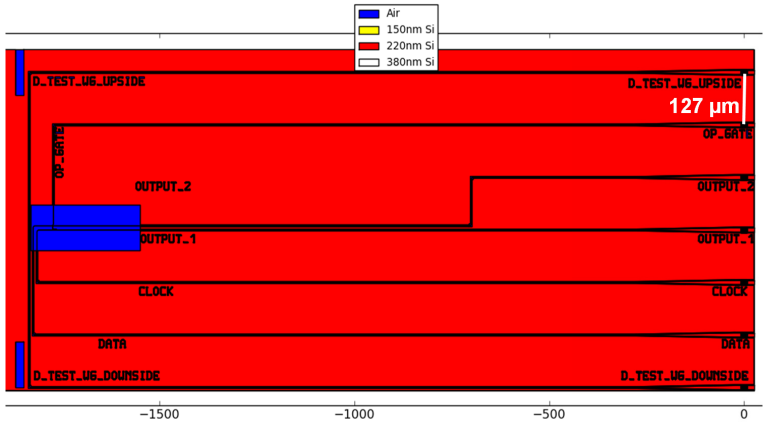

Figure 6.2: SOI waveguide circuit for the data flip-flop .

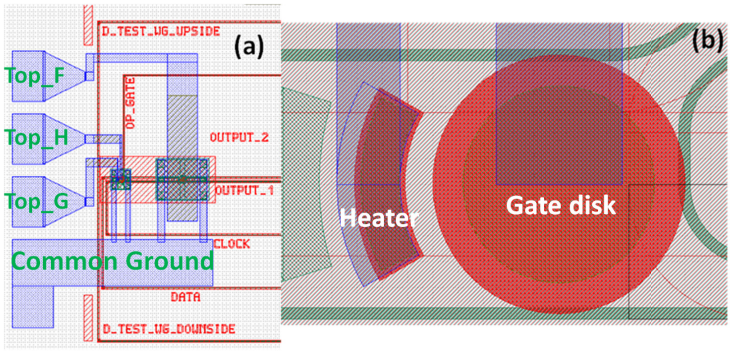

Figure 6.3: III-V and metal design layers on top of SOI waveguide circuit, (b) zoom-in view showing the waveguides, heater, microdisk and metal layers for the gate disk.

will be required and hence the contact pads were designed with a pitch of 150 μm. The bottom metal contact was designed in a contour shape encircling the microdisks to ensure uniform electrical injection. A virtual fabrication picture showing the SOI waveguide circuit is shown in figure 6.2. As can be seen from this figure, in addition to the input and output waveguides, test waveguides (uppermost and lowermost) are also designed for a better alignment of the access fibers to the input and output waveguides . Figure 6.3 shows the area of the design with III-V and contact metal layers on top of the SOI waveguide circuit. The role of the heater will be explained in section 6.5. Its clear from figure 6.1 and 6.3(b) that the microdisk acting as a gate needs to be aligned to three waveguides which implies that the definition of the microdisk needs to be done us-

ing either DUV or e-beam lithography. Photolithography can not be used as the alignment uncertainty is hundreds of nanometers. More than the waveguide alignment issue, the stringent requirement that the transmission resonance of the gate should match the lasing resonance of the microdisk laser makes it necessary to use DUV or e-beam lithography for the definition of microdisks.

6.2 Multichannel demultiplexers

In chapter 5, all-optical time domain demultiplexing experiments using a single microdisk are described. In the device used there, only one channel was possible and it had only one access waveguide underlying the microdisk. By having two access waveguides beneath the microdisk, the data can be demultiplexed at the drop-port. A demultiplexer with multiple channels can be made by properly adjusting the delays such that the input signal couples to each microdisk with a predecided interval of time. For example, for a four channel 40-to-10 Gbits/s demultiplexer the input data signal should couple to each subsequent microdisk by a time interval of 25 ps. In the case of a four channel 20-to-5 Gbits/s demultiplexer, this time gap will correspond to 50 ps.

The SOI waveguide circuits and the III-V microdisk designs were made for a four channel 40-to-10 Gbits/s demultiplexer and a 20-to-5 Gbits/s demultiplexer. At the same time it's also a must that the clock is synchronised with the input of each microdisk. The SOI waveguide spirals were used for delay lines. The length of spiral delay lines was chosen such that the data signal reaches each microdisk at a defined delay. According to the specifications of the epixfab technology platform [2], a length of 1717 μm is required to get a delay of 25 ps. The MMI based 3dB power splitters were placed to have power division. A screenshot of the design for a 40-to-10 Gbits/s demultiplexer is shown in figure 6.4. At the bottom of the figure are the zoom-in views of the microdisk and the power splitters. As can be seen in the zoom-in view of power splitters, the first 3dB splitter (rightmost) divides the data power into two equal parts and then two 3dB splitters further divide the data power, same way as the first one. Ultimately the data power is divided into four parts and each part is an input to one of the microdisks. In the zoom-in view of the microdisk, split-heaters can be seen. These split-heaters are designed with a purpose of transmission resonance matching of the microdisks in case there is a mismatch in the transmission resonances of the microdisk resonators . Figure 6.5 shows the electrical probe pads connected to the microdisks and the heaters. Here again, the SOI waveguides for coupling the data and clock in and out are designed with a pitch of 127 μm to match the fiber array pitch.

Looking at the time response of all-optical gating [3] in 7.5 μm diameter microdisk, 20-to-5 Gbits/s demultiplexers are possible. But for 40-to-10 Gbits/s

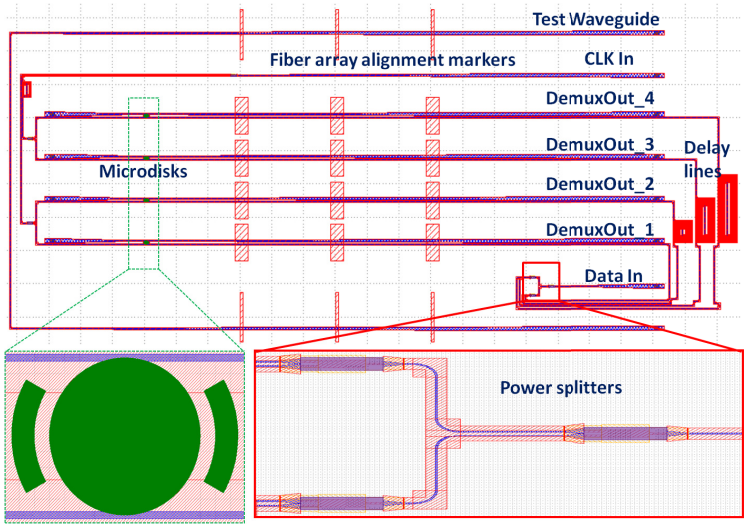

Figure 6.4: Four channel demultiplexer based on III-V-on-silicon microdisks.

demultiplexers, further reduction in carrier life time is necessary. In order to do so, at least one of the following techniques will be needed- (a) ion-implantation [4], (b) use of seeding beam [5] and (c) application of reverse bias [6-7]. To form an N channel demultiplexer, N number of microdisks will be required.

6.3 Shift registers

A register is a memory device that is used for storing several bits of digital data. It basically consists of a set of flip-flops, with each flip-flop meant for storing one bit of the register. Thus, an N bit register has N number of flip-flops. A special type of register, called the shift register, is used to pass or transfer bits of data from one flip-flop to another. This process of transferring data bits from one flip-flop to the next one is known as *shifting*. Shift registers are useful for transferring data in a serial manner while allowing parallel access to the data. A shift register is basically a set of flip-flops interconnected in such a way that the input to a flip-flop is the output of the one just before it. Clocking all the flip-flops at the same time causes the bits of data to shift to the right in one direction i.e. towards the last flip-flop.

In the past, the shift registers in the optical domain have been demonstrated using fiber buffers [8], self-electro-optic effect devices [9] and serially connected flip-flops, where each flip-flop consisted of two ring lasers sharing a single active element [10]. In all of these shift registers, the foot-print as well as the power

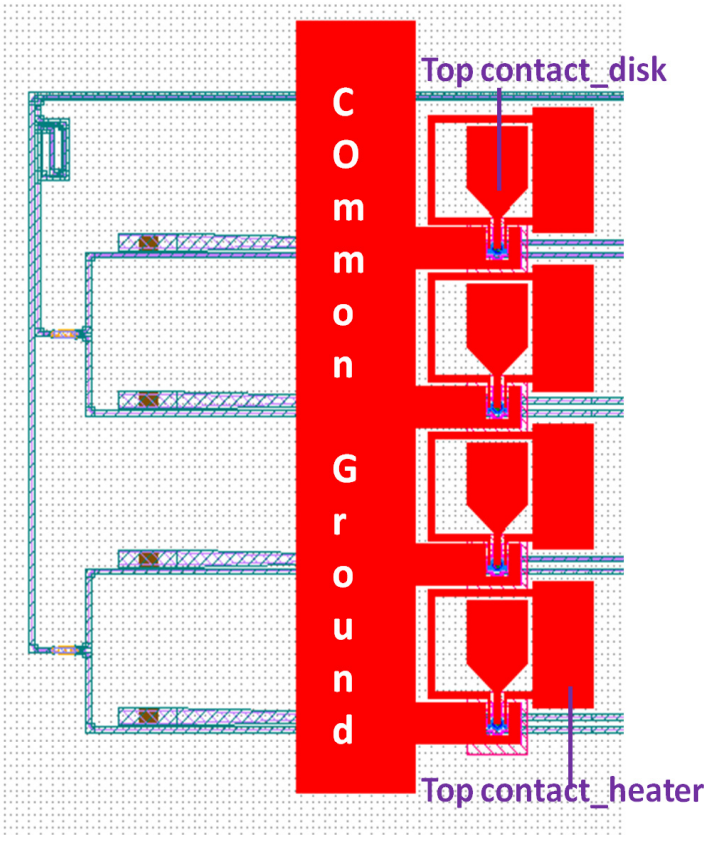

Figure 6.5: Electrical probe pads for a four channel demultiplexer .

consumption were many times higher than what can be achieved using III-V-on-silicon microdisks. The shift registers in optical domain can be constructed using the microdisks after the data flip-flops can be realized. The data flip-flops form the building blocks for the realization of the shift registers. An N bit shift register will need N+1 number of data flip-flops. Since one data flip-flop will need two microdisks, an N bit shift register will make use of 2(N+1) number of microdisks.

A simplified diagram of a one bit shift register based on the microdisks is shown in figure 6.6. It consists of two data flip-flops. The description of data flip-flops based on the microdisks has been presented in section 6.1. The output of the first data flip-flop (DFF1) acts an input for the second data flip-flop (DFF2). The idea of a one bit shift register as represented in figure 6.6 is translated into an SOI waveguide circuit and III-V microdisk design. The SOI waveguide circuit corresponding to the proposed shift register is shown in figure 6.7

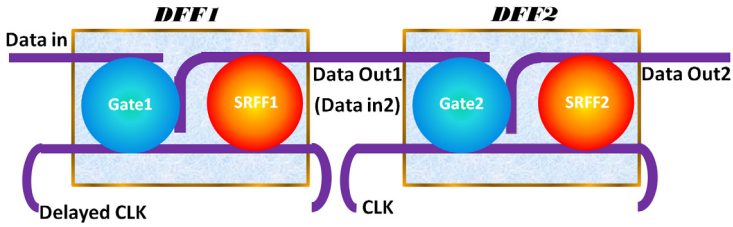

Figure 6.6: Simplified diagram of one bit shift register based on III-V-on-silicon microdisks.

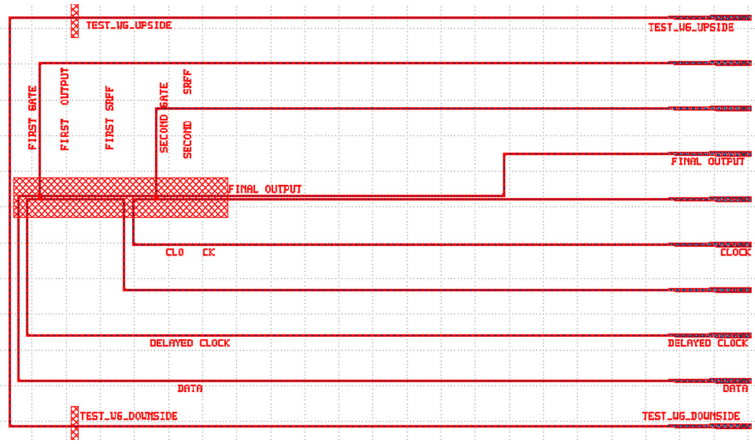

Figure 6.7: The SOI design for one bit shift register.

while figure 6.8 shows an overview of the probe pads needed for electrical probing of such a device. In figure 6.8; CG stands for common ground electrical probe pad while H_G1, G1, SF1, H_G2, G2 and SF2 stands for the top electrical probe pads for the heater around the first gate disk, the first gate disk, the first set-reset flip-flop disk, the heater around the second gate disk, the second gate disk and the second set-reset flip-flop disk respectively. As can be seen from figure 6.8, with the increase in the number of microdisks needed for increased complexity of the optical functions, the electrical probing becomes harder which requires the use of an array of electrical probe needles. In order to understand the working of an optical shift register as described here, an example using 10 Gbits/s data and 10 GHz clock is depicted in figure 6.9.

In this figure, time domain separation between two consecutive vertical lines is 50 ps. It is assumed that the input data is stronger in terms of optical power than the delayed clock. It is also assumed that initially the lasers representing the SRFF1 and SRFF2 have high output power in CCW direction. The

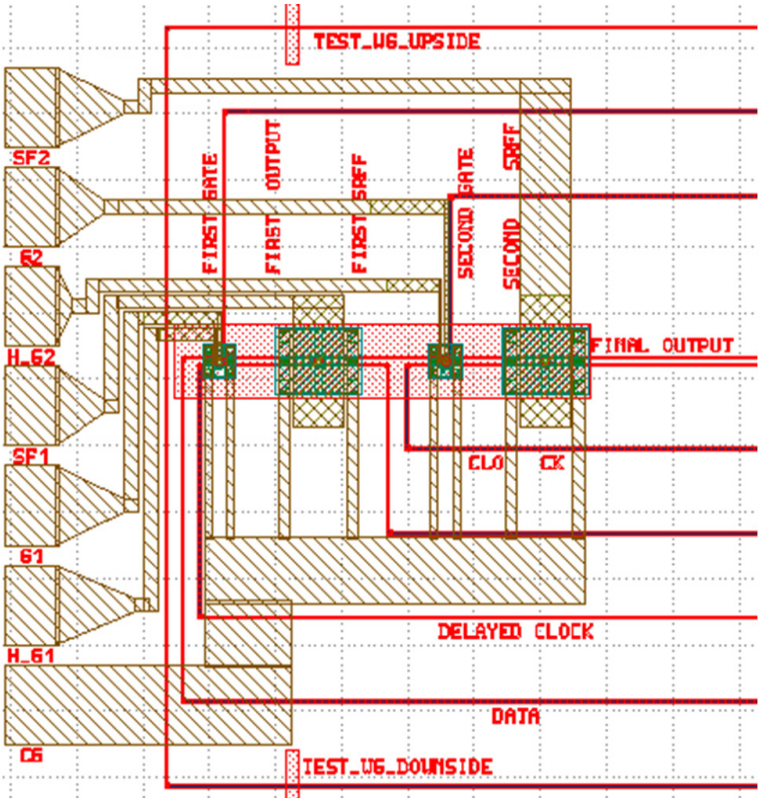

Figure 6.8: Electrical probe pads for one bit shift register.

delayed clock *DCin* and the clock *Cin* both are off-resonance initially to Gate1 and Gate 2 respectively. The input data *Din* is on-resonance to the Gate1 and also the data input to the second gate (DO_1)is on-resonance to Gate2 . When the logic level of *Din* is high the delayed clock *DCin* becomes on resonance to Gate1 and it passes to upperside waveguide of SRFF1 represented by *G1wgup*. When logic level of *Din* is low, the delayed clock *DCin* remains off-resonance to Gate1. The state of SRFF1 is controlled by *G1wgup* and *G1wgdown*. As can be seen from figure 6.9, the output of first data flip-flop -DO_1- is shifted by 50ps as compared to *DCin*. The output after second data flip-flop-DO_2- shifts futher by 50 ps, same way as it happens from *Din* to DO_1. In all, the output after second data flip-flop is shifted by 100 ps as compared to the input data *Din* which corresponds to shifting by 1 bit for a 10 Gbits/s data.

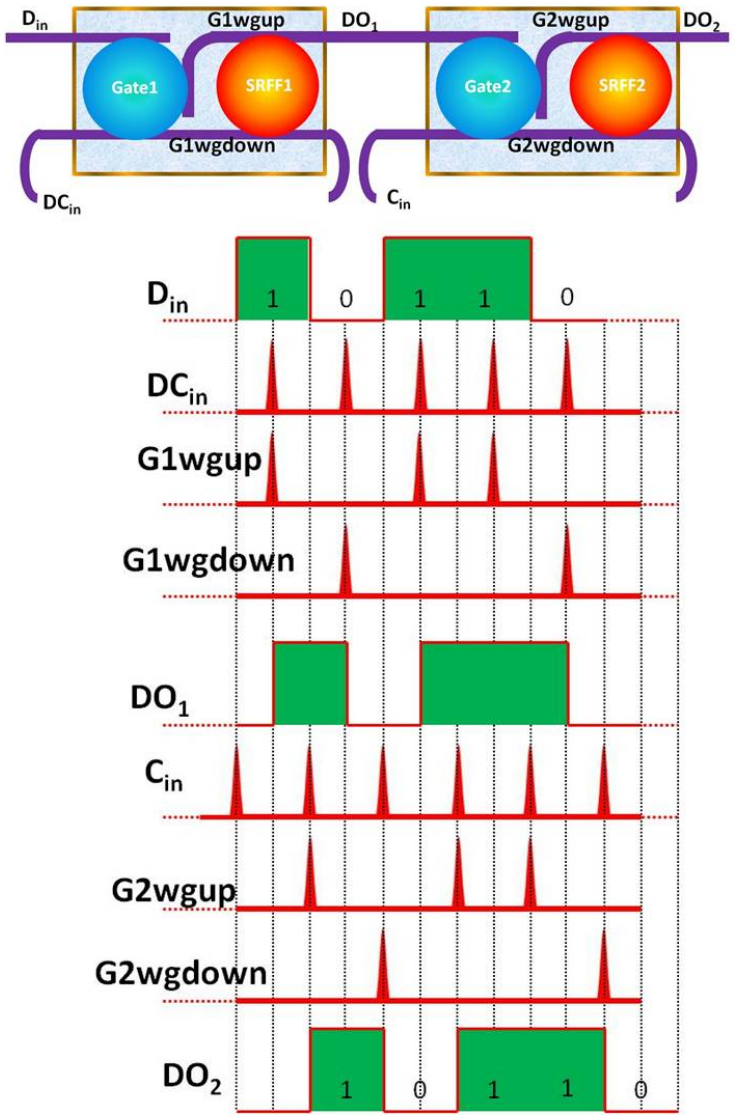

Figure 6.9: Illustration of 1 bit shift register operation using two data flip-flops based on microdisks.

6.4 Complete functional photonic digital blocks

Like an example presented in chapter 1 (figure 1.8), a fully functional digital photonic circuit can be constructed using microdisk lasers and resonators. In the examples taken so far (data flip-flops, demultiplexers and shift registers), waveguide crossings have been avoided. As the complexity level rises, it does not remain possible to avoid the crossing of the waveguides. The waveguide crossing will result into the cross-talk of signals propagating in the waveguides crossing each other. Therefore, novel solutions are required to avoid such a

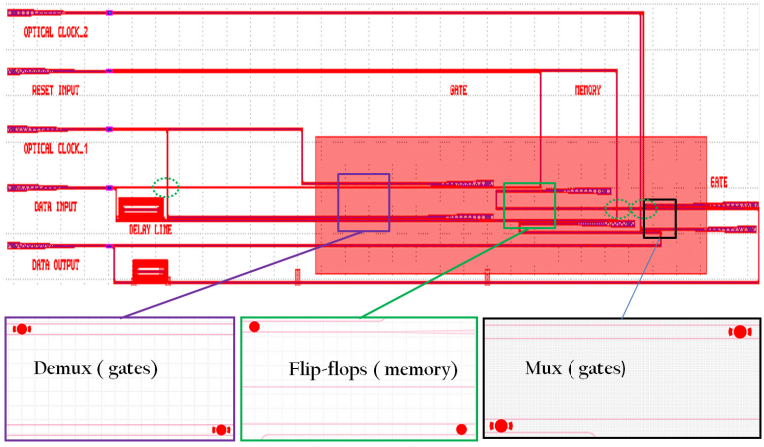

Figure 6.10: The SOI design for complete functional digital photonic block.

cross talks. Authors in reference [11] have described and experimentally demonstrated the low loss and low cross talk waveguide crossing. In the crossing region, straight SOI waveguides were broadened using a 2.85 μm parabolic taper in each arm. The waveguides were expanded from 450 nm to 800 nm. By locally applying a lower index contrast using a double-etch technique, loss of confinement was reduced and 97.5 % transmission was achieved with only -40 dB cross talk. The waveguide crossings as described above were used in design of 2X1 mux/demux with latching memory. Like previous cases, single disk lasers and resonators were meant to act as flip-flops and mux/demux units. So, in all; this design had two flip-flops, two mux and two demux. Figure 6.10 shows the SOI waveguide circuit design of a 2X1 mux/demux with latching memory. In the same figure, dotted green circles show the positions of waveguide crossings. The zoom-in view of one such a waveguide crossing is shown in figure 6.11. As mentioned previously, with the increase in number of the microdisk elements, the complexity of the probe pads for electrical injection increases and an array of electrical probe needles is needed. Accordingly, here also the electrical

probe pads are designed with a pitch of 150 μm. Figure 6.12 shows the design of the electrical probe pads. In this figure DG1_H and DG1_Top represent the electrical probe pads for the heater and the top contact, respectively, for the first demultiplexing gate. The same is represented by DG2_H and DG2_Top for the second demultiplexing gate. At the other end, for multiplexing, MG1_H and MG1_Top represent the electrical probe pads for the heater and the top contact for the first multiplexing gate. Similarly, MG2_H and MG2_Top represent the electrical probe pads for the heater and the top contact for the second multiplexing gate. The FF1_Top and the FF2_Top represent the probe pads for the top electrical contacts for the first and the second SR flip-flop, respectively. At the bottom is the common ground for all the microdisks.

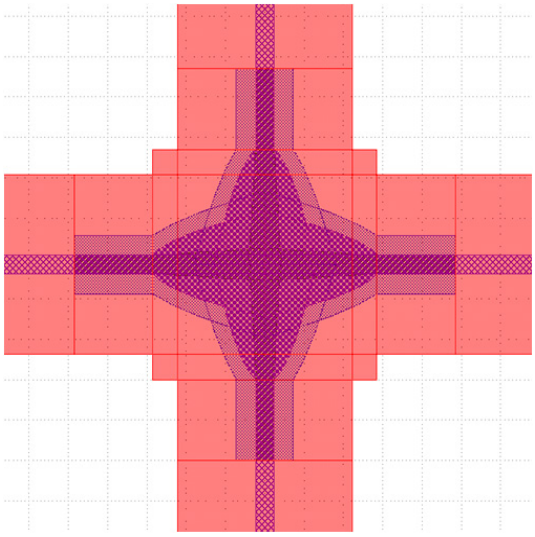

Figure 6.11: Design for SOI waveguide parabolic crossing. Such a crossing was originally designed, fabricated and characterized by Bogaerts et.al. at UGent-imec [11].

6.5 Critical issues and possible solutions

To integrate two or more working microdisks where one requires input from the output of another is quite a challenging work. For the operation of a microdisk laser as a flip-flop, smooth side walls of the microdisk are necessary which been described in detail in the supplementary information of reference [12]. It is possible to fabricate the microdisk with smooth sidewall by an optimized fabrication process. In case of data flip-flops and shift registers, since the optical gates

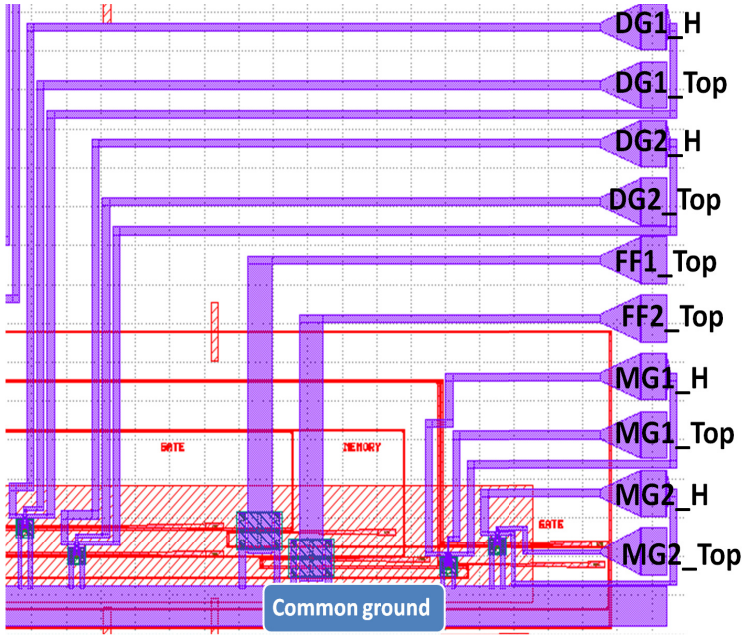

Figure 6.12: The electrical probe pads for complete functional digital photonic block.

drive the set-reset flip-flops, it's necessary that the transmission resonances of the gates match to the lasing resonances of the set-rest flip-flops. In case of multichannel multiplexers/demultiplexers, the transmission resonances of all the microdisks should match. In general, the transmission and lasing resonance matching condition applies to all the complex PICs proposed in this chapter. The microdisk definition by e-beam lithography is required due to its high accuracy in defining the patterns. Several tuning mechanisms have been explored which can be employed to match the transmission resonance of the gate to the lasing resonance of the set-reset flip-flop. These are described in the following subsections.

6.5.1 Thermo-optic tuning

In the designs made for the data flip-flops, shift registers, demultiplexers and the complete functional digital blocks; circular heaters are defined in the III-V material. These heaters can be used to heat the microdisks resulting in the red-shift of the transmission resonances of the gates. The microdisks surrounded by the heaters have been fabricated earlier, as shown in figure 6.13, and were tested to see the influence of heating on the lasing resonance of the microdisk lasers.

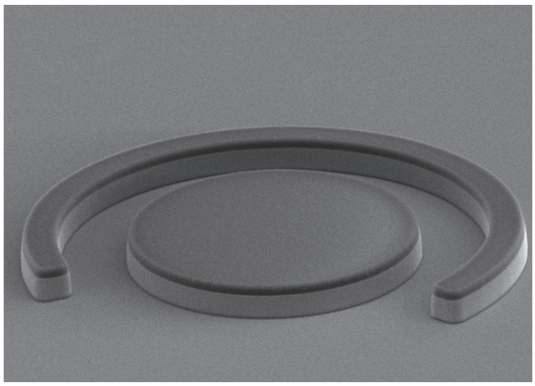

Figure 6.13: SEM image of III-V microdisk surrounded by a III-V heater.

Details about it can be found in reference [13]. For a microdisk laser of 7.5 μm diameter, the tuning efficiency and the tuning range of 0.35 nm/mW and 2 nm respectively have been shown [13]. Similar behaviour can be expected for the transmission resonances of the microdisks.

6.5.2 Tuning by direct bias application

When an electrical bias is applied to the microdisk, it causes the change in the refractive index due to the change in the free carrier concentration in the active layer of the microdisk. This results in blue or red shift of the transmission resonance wavelength depending upon whether the applied voltage is positive or negative respectively. Figure 6.14 shows an example in which a transmission resonance wavelength was shifted by 0.9 nm using a reverse bias of 1 volt. This data was recorded for the microdisk of 10 μm diameter. It is to be noted that the application of reverse bias not only shifts the transmission resonance wavelength but also enhances the speed of operation of an optical gate [6].

6.5.3 Tuning by variation in pump power

Since the amount of the free carriers generated depends upon the pump power absorbed, there is a refractive index decrease leading to the blue shift of the resonance wavelength of the microdisk resonator. For the microdisk of 7.5 μm diameter the resonance characteristics were recorded in a pump probe configuration. The probe was a CW light while the pump was a Gaussian pulse train with a repetition rate of 10 GHz. The power of the probe beam was kept fixed while the power of the pump was varied. The power of probe beam was ~-4.25dBm in the SOI waveguide. The microdisk was nearly critically coupled [14] when

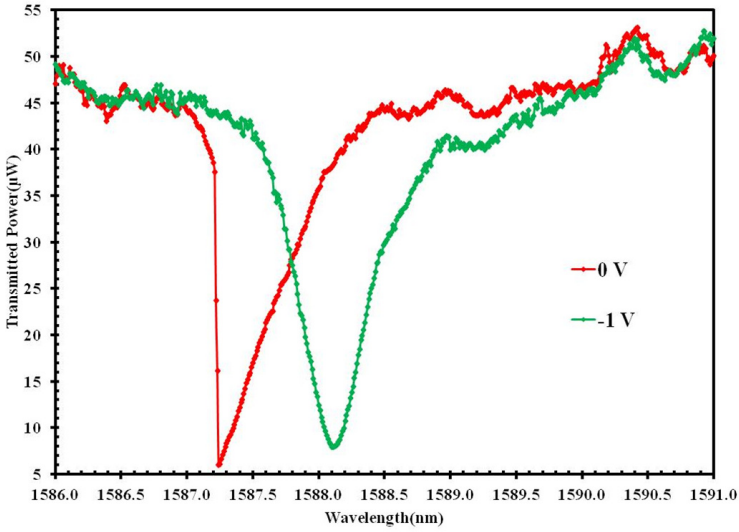

Figure 6.14: Tuning of transmission resonance by application of an electrical bias.

the pump was not present. The transmission characteristics of the microdisk resonator were recorded by scanning the wavelength of the probe light. The results are plotted in figure 6.15. The pump power shown is in the SOI waveguide coupled to the microdisk. As can be seen from this figure, a small blue tuning of the resonance by 0.25 nm was obtained after injecting a pump power of -4.8 dBm. Blue shift of the probe resonance is accompanied by decrease in extinction ratio. The decrease in extinction ratio happens due to the decrease in absoprtion of probe beam in presence of pump. This absorption decreases further as the pump increases. With increase in pump power, the probe beam (which has fixed power) does not remain critically coupled . Injection of a pump power more than -4.8 dBm leads to a red shift and can be as high as 0.77 nm with +5.16 dBm of injected power. Red shift is the result of free-carrier absorption at higher pump power.

6.6 Conclusions and discussions

Digital photonics is in the emerging stage. For the implementation of digital photonic VLSI, there is a need of components or set of components that can be cascaded to implement any digital function. A buliding block should be at least of microscopic size(needless to say that basic building block smaller than

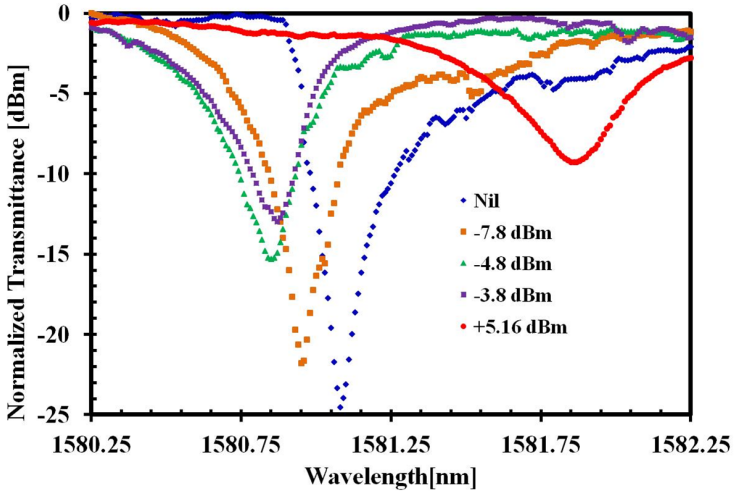

Figure 6.15: Resonance shift as a function of pump power in a pump-probe configuration.

micron scale will be even better) and be densely integrable preferablry using CMOS technology platform. Amongst many basic building blocks investigated so far, SOAs are quite mature but their foot-prints are in centimeters or millimeters and consume several tens or hundreds of milliwatts of power. The ring or disk shape building blocks in silicon have been investigated but are power hungry due to the fact that realized functionalities are based on nonlinear phenomenon such as two-photon absorption. Other than the question of power, indirect bandgap of silicon does not allow its use in active functionalities such as transmitter and memory elements. Microdisk laser and resonator based photonic components, devices and the complex PICs based on them are promising candidates for future photonic signal processing and computing given their small size and realtively low power consumption. By using heterogeneous integration of InP on SOI waveguide circuits, the lasers and resonators can be fabricated in CMOS pilot line. In this chapter, some of the complex PICs based on III-V-on-silicon microdisks have been proposed. The description of the concepts and the designs for different type of PICs are presented. Some issues which could arise in the complex PICs based on III-V-on-silicon microdisk have been addressed and are supported by the experimental findings while working on single microdisk based devices. A large fanout is needed in case of logic applications especially using all-optical flip-flops. The output power of the microdisk laser used for AOFF was 21 μW in the SOI waveguide. This power can provide a fanout of more than 58. An output power of 120 μW (in the SOI waveguide) was recorded later with another microdisk [15]. If this microdisk was unidirectional

then it can provide a fanout of more than 333. With further improvement in the microdisk laser design and improved fabrication processes, it can be envisaged that the fanout will increase further. The use of a resonator, as has been investigated in this work, restricts the use of the all-optical wavelength converter to a few discrete wavelengths. In order to add flexibility in original and target wavelengths larger diameter microdisks can be used.

References

[**1**] Web address: http://www.ipkiss.be/. *The software is developed at INTEC Photonics, Ghent University, Ghent, Belgium.*

[**2**] Web address: http://www.epixfab.eu/

[**3**] R. Kumar, T. Spuesens, P. Mechet, P. Kumar, O. Raz, N. Olivier, J.-M. Fedeli, G. Roelkens, R. Baets, D. Van Thourhout and G. Morthier. *Ultrafast and bias-free all-optical wavelength conversion using III-V-on-silicon technology.* Optics Letters, 36(13):2450-2452, 2011.

[**4**] M. Waldow, T. Plötzing, M. Gottheil, M. Först, J. Bolten, T. Wahlbrink and H. Kurz. *25ps all-optical switching in oxygen implanted silicon-on-insulator microring resonator.* Optics Express, 16(11):7693-7702, 2008.

[**5**] R.J. Manning and D.A.O. Davies. *Three-wavelength device for all-optical signal processing.* Optics Letters, 19(12):889-891, 1994.

[**6**] R. Kumar, L. Liu, G. Roelkens, E.-J. Geluk, T. de Vries, F. Karouta, P. Regreny, D. Van Thourhout, R. Baets and G. Morthier. *10-GHz all-optical gate based on a III-V/SOI Microdisk.* IEEE Photonics Technology Letters, 22(13):981-983, 2010.

[**7**] S.F. Preble, Q. Xu , B.S. Schmidt and M. Lipson. *Ultrafast all-optical modulation on a silicon chip.* Optics Letters, 30(21):2891-2893, 2005.

[**8**] N.A. Whitaker Jr., M.C. Gabriel, H. Avramopoulos and A. Huang. *All-optical, all-fiber circulating shift register with an inverter.* Optics Letters, 16(24):1999-2001, 1991.

[**9**] B. Tian, W. van Etten and W. Beuwer. *Ultrafast all-optical shift register and its perspective application for optical fast packet switching.* IEEE Journal of Selected Topics in Quantum Electronics, 8(3):722-728, 2002.

[**10**] S. Zhang, Z. Li, Y. Liu, G.D. Khoe and H.J.S. Dorren. *Optical shift register based on an optical flip-flop memory with a single active element.* Optics Express 13(24):9708-9713, 2005.

[**11**] W. Bogaerts, P. Dumon, D. Van Thourhout and R. Baets. *Low-loss, low-cross-talk crossings for silicon-on-insulator nanophotonic waveguides.* Optics Letterds, 32(19):2801-2803, 2007.

[**12**] L. Liu, R. Kumar, K. Huybrechts, T. Spuesens, G. Roelkens, E.-J. Geluk, T. de Vries, P. Regreny, D. Van Thourhout, R. Baets and G. Morthier.*An ultra-small, low-power, all-optical flip-flop memory on a silicon chip.* Nature Photonics, 4:182-187, 2010.

[**13**] L. Liu, T. Spuesens, G. Roelkens, D. Van Thourhout, P. Regreny and P. Rojo-Romeo. *A thermally tunable microdisk laser built on a III-V/Silicon-on-insulator heterogeneous integration platform.* IEEE Photonics Technology Letters, 22(17):1270-1272, 2010.

[**14**] A. Yariv. *Universal relations for coupling of optical power between microresonators and dielectric waveguides.* Electronics Letters, 36(4):321-322,2000.

[**15**] T. Spuesens, L. Liu, T. de Vries, P.R.-Romeo, P. Regreny and D. Van Thourhout. emphImproved design of an InP-based microdisk laser heterogeneously integrated with SOI. IEEE International Conference on Group IV Photonics, United States, p.FA3, 2009.

7

Conclusions and outlook

Due to the extensive research being done in the optical technology it is set to revolutionize the short-reach as it has done for the long-reach communication. Silicon photonics is on the forefront to lead the optical technology for on-chip signal processing due to the availability of the mature and cost effective CMOS technology. For the realization of the multi- and fully-functional all-optical chips we need to realize and integrate the active photonic components and devices on a single chip. This has been the main motivation to carry out the research work presented in this thesis. The integration of III-V material on top of SOI waveguide circuits has the promise of realization of multi- and fully-functional optical chips with unprecedented integration density as evident from the description of different PICs proposed in the previous chapter. Smaller, faster and less power consuming are the keywords for next generation optical components, devices and PICs. The heterogeneously integrated III-V microdisks on top of passive optical waveguide circuits have the potential to meet these expectations. In the course of this PhD, a number of optical functionalities have been demonstrated using single microdisks. The results obtained have advanced the state-of-art of microring/disk laser and resonator based devices in terms of combination of energy consumption, switching speed and foot-print. In the first part of this chapter conclusive highlights of different functionalities demonstrated with III-V-on-silicon microdisks are presented while the second part gives an overview of the future scope of this work.

7.1 Conclusions

One of the major weakness in the implementation of all-optical packet switching is the absence of a practically useable all-optical random access memory. In this regard, microdisk laser based flip-flops have set a new set of benchmarks for the combination of speed, power consumption and the footprints. The static power consumption of the microdisk laser based flip-flop for practical applications is calculated to be 6 mW for storing one bit. For changing the state of the flip-flop, only 1.8 fJ of energy was needed. Over-all power consumption is comparable to the electronic counterparts. The footprint of this device was only 7.5 x 7.5 μm^2. There is still much room for improvement of this kind of flip-flops and this will be discussed briefly in the outlook section.

Other than flip-flops, optical gates are fundamental building blocks for several complex PICs. The PICs in which gates serve as a fundamental building blocks can be used for long haul as well as short reach communications. For example, time domain multiplexers and demultiplexers find applications in long haul applications while PICs like shift registers are meant for short reach applications such as computing. The optical gating has been at the heart of many other functionalities such as wavelength converters and the format converters. A significant progress was achived during the PhD in all-optical gating. The all-optical gating was realized in a pump-probe configuration. The pump was a pulse train while the probe was a CW beam of light. The probe was weaker than the pump in terms of optical power. First, all-optical gating at 10 GHz was demonstrated using a microdisk with a footprint of 10 x 10 μm^2. While working with this device, a reverse bias was needed to operate at 10 GHz. In the second attempt, all-optical gates with a footprint of 7.5 x 7.5 μm^2 were demonstrated at 10 GHz. Transient response revealed that the these gates are capable of working up till 20 GHz without use of any electrical bias. The switching energy for these devices was found to be 150 fJ at 10 GHz.

In all-optical packet switching, all-optical wavelength conversion is needed for contention resolution of two signals coming at the same wavelength. A further success of all-optical gating was in realization of an all-optical wavelength converter. The data signal at the wavelength of 1550.1 nm was wavelength converted to 1580.9 nm which is also a band conversion from C to L band. In these experiments, the data is basically a pump signal while the probe has the same role as in all-optical gating. At 10 Gbit/s, an NRZ-OOK PRBS data was wavelength converted with a bit error rate of 10^{-9}. The extinction ratio of the wavelength converted signal was ~ 12 dB and the power penalty was ~ 3.5 dB.

Time domain all-optical demultiplexing is an important functionality needed for the realization of the fully functional photonic digital circuits such as the one presented in chapter 6. The time domain (de)multiplexing also finds applications for increasing the information carrying capacity of an optical channel. Therefore, the microdisk resonators were used for the realization of all-optical demultiplexing. A 10 Gbits/s data was demultiplexed using the optical clocks at 5 and 2.5 GHz. In case of demultiplexing, the microdisk resonator essentially acts as an AND gate. The output of the gate is high only when the data as well as the clock are present in the microdisk. In the absence of the clock, the data remains coupled into the microdisk. In case of all-optical demultiplexing the clock had higher optical power while the data was low power. Here, the clock was a control signal contrary to wavelength conversion where the optical data was a control signal.

All-optical format conversion between non-return-to-zero(NRZ) and return-to-zero (RZ) is an important interface technology for future optical networks that employ both wavelength division multiplexing (WDM) and time division multiplexing (TDM) technologies. Because of their small foot-prints and low power consumption, microdisk resonators are an attractive candidate for this kind of applications. All-optical format conversion, from NRZ-OOK to RZ-OOK, in microdisk resonators was demonstrated using the method of pulse carving. In essence, a big pulse was carved into the smaller pulses to obtain the format conversion. Here again, the optical data was weaker as compared to the optical clock in terms of power and hence the clock was a control signal. The output of the microdisk resonator was high only when the optical clock and the optical data both had high power level inside the microdisk. First the principle of pulse carving was verified by using a bit stream of alternate 1s and 0s and then an NRZ-OOK PRBS data was used for format conversion. An error free operation (BER $\sim 10^{-12}$) at 10 Gbits/s was obtained with a power penalty of $\sim$ 3.6 dB

7.2 Outlook

A number of optical functionalities have been demonstrated using III-V-on-silicon microdisks. Still, there remains a lot of scope to extend this work for many more functionalities. New applications of microdisks with single disks can be found but prospects are more promising with the cascaded microdisks which can make use of the optical functionalities demonstrated so far during the course of this thesis work. Obviously, it will be interesting to improve the performance of the demonstrated functionalities. Some of the efforts which can be made at the fabrication level to improve the performance of demonstrated functionalities are listed below.

1. Since total power consumption is always an issue of concern, the electrical injection efficiency of microdisk lasers needs to be improved. One of the ways to do so is the ion-implantation in the whole microdisk area minus the area where the whispering gallery modes exist.
2. Further reduction in the sidewall roughness can lower the mode-coupling and can reduce the cavity losses. This will result in the reduction of the threshold current as well as in the reduction of the required current for the occurrence of the bistability in the microdisk laser. So far, the smallest microdisk lasers used for the all-optical flip-flop had a diameter of 7.5 μm and the ability to further reduce sidewall roughness will enable the use of microdisk lasers of diameters less than 7.5 μm.
3. The speed of all-optical gates and other functionalities based on gating is limited by the carrier life time. Ion-implantation of the microdisk resonators will result into more defect states in the resonators and hence in reduced carrier life time. This in turn will result in the faster operation of all-optical gates and its derivative functionalities.

Many optical functionalities are proposed in chapter 6. Those functionalities have been explored at the conceptual level and the designs have been made. A substantial work need to be done to experimentally demonstrate such functionalities. Those functionalities once demonstrated experimentally can open the doors for the realization of advanced devices used in computing such as counters. It will be interesting to look at the dynamics of the photonic circuits where the next stage is driven by the previous one. The PICs from chapter 6 can serve as examples for such theoretical investigations.

The format conversion is another area where there is great possibility of using the III-V-on-silicon microdisks. The format conversion from NRZ-OOK to RZ-OOK was demonstrated and there is scope for extending this work for phase modulation formats; for example, from NRZ-OOK to BPSK and QPSK.